Tropical High Cloud Feedback Relationships to Equilibrium Climate Sensitivity

Emma Maxwell Dawson

Charlottesville, VA

B.S. Environmental Sciences, University of Virginia, 2021

A Thesis presented to the Graduate Faculty
of the University of Virginia in Candidacy for the Degree of
Master of Science

Department of Environmental Sciences

University of Virginia

December 2024

Acknowledgements

Portions of this work have been accepted for publication in the *Journal of Climate.* I would like to thank my committee members – Kathleen Schiro, Kevin Grise, and Todd Scanlon – for their support and feedback through the completion of this research. I am deeply grateful for their guidance, and my work has been significantly improved as a result of their input. I would also like to thank the members of the Schiro Lab and Office 296, especially Sayali Kulkarni and David Crowe, for their support, encouragement, and friendship. I would like to express my gratitude towards the UVa Environmental Sciences department for fostering a culture that has been welcoming and supportive from the beginning. I owe a special thanks to the UVa women's soccer team, particularly my teammates, for being my family away from home and keeping me grounded as I have navigated the ups and downs of the last six years. Finally, I'd like to thank my family for their unwavering love and support. None of this would be possible without them.

Table of Contents

Abstract

Clouds constitute a large portion of uncertainty in predictions of equilibrium climate sensitivity (ECS), with tropical high cloud feedbacks exhibiting considerable spread across models. This study applies the cloud radiative kernel technique of Zelinka et al. (2012a; 2013) to 22 models across the CMIP5 and CMIP6 ensembles to survey tropical high cloud feedbacks and analyze their relationship to ECS, mean state properties, and changes to the tropical overturning circulation, precipitation efficiency, and deep convective organization across scales. First, the intermodel spread in tropical high cloud net, altitude, and optical depth feedbacks exhibit significant correlations to ECS in the tropical mean and on convective margins while the spread in the high cloud amount feedback is uncorrelated to ECS, motivating further exploration of physical mechanisms driving the intermodel spread in high cloud feedbacks. Intermodel variability in deep convective organization – at both the mesoscale and planetary scales – relates to the intermodel spread in high cloud feedbacks along convective margins. Most notably, decreases in tropical ascent area and increases in mesoscale organization of deep convection relate to more positive high cloud feedbacks, particularly within weak ascent and weak descent regimes. Increases in mesoscale organization also coincide with a greater weakening of the Pacific Walker circulation. Precipitation efficiency, on the other hand, does not appear to systematically drive much spread in high cloud feedbacks across the tropics. Finally, connections between mean state high cloud properties and high cloud feedbacks are explored in an attempt to place observational constraints on high cloud feedbacks and ECS. High ECS models are cloudier in the upper troposphere but have a thinner high cloud population. Having more thin high clouds in the mean state generally yields more positive high cloud altitude and optical depth feedbacks and it either amplifies or dampens the high cloud amount feedback depending on the large-scale

dynamical regime. A clear link between mean state high cloud characteristics and deep convective onset behavior across the CMIP ensemble highlights how model diversity in convective processes contributes systematically to diversity in mean state high cloud properties. In summary, this analysis highlights the importance of tropical high cloud feedbacks for driving intermodel spread in ECS, underscores the influence of dynamical regime shifts on the response of high clouds to warming, and suggests that mean state high cloud characteristics might provide a unique opportunity for observationally constraining high cloud feedbacks.

1. Introduction

A critical objective for the climate science community is estimating the amount of warming that will occur as a result of anthropogenic greenhouse gas emissions. This is typically quantified as equilibrium climate sensitivity (ECS), a metric defined as the amount of the long-term global average surface temperature change due to a doubling of CO_2 relative to preindustrial levels. One of the earliest assessments of ECS reported a sensitivity range of 1.5 to 4.5 °C (Charney, 1979). Since this initial estimate, global climate models (GCMs) have evolved to become the most comprehensive representation of the climate system and the most useful tool for quantifying climate sensitivity. However, despite improvements in model representation of physical processes, the two most recent generations of GCMs, Coupled Model Intercomparison Project 5 (CMIP5) and CMIP6, contain models with ECS values ranging from 2.1 to 4.7 K (Andrews et al., 2012) and 1.8 to 5.6 K (Meehl et al., 2020), respectively. This demonstrates that even with advancements in modelling and theory, there is a persistent disagreement around the value of climate sensitivity.

Although the initial radiative forcing associated with a doubling of CO_2 varies across models, climate feedbacks have been identified as the dominant driver of uncertainty in climate sensitivity (Roe & Armour, 2011; Webb et al., 2013). Thus, there is a particular focus in the field on understanding how models differentially represent feedbacks in the climate system and how the intermodel variability of these feedbacks is related to the intermodel variability of ECS. The global mean net feedback can be decomposed into additive parts, including the Planck, water vapor, lapse rate, albedo and cloud feedbacks, though decomposition methods vary (Forster et al., 2021). Of these components, cloud feedbacks exhibit the most variability among GCMs across model ensemble generations, notably increasing in spread from CMIP5 to CMIP6

(Zelinka et al., 2020). Clouds represent an important component of the climate system through their fundamental role in the planetary energy budget. They reflect incoming solar radiation and trap and reemit outgoing longwave radiation, resulting in global mean net cooling of about -20 W m^{-2} (Boucher et al., 2013). The radiative effect of clouds is variable, with individual tropical convective systems evolving from strongly cooling deep convective cores to detrained thin cirrus that impart heating on the climate system (Gasparini et al., 2021). Moreover, the predominance of different cloud populations across various regions yields a spatially heterogeneous cloud radiative effect (Hartmann & Berry, 2017; Zelinka et al., 2017). The ways that clouds will change in response to the dynamic and thermodynamic changes to the atmosphere that accompany surface warming are likewise complex, varying spatially and across different cloud species. Variability in the global mean net cloud feedback is closely related to variability in climate sensitivity across GCMs (Wang et al., 2021), so reducing uncertainty in cloud feedbacks among models could help constrain ECS. In sum, understanding how clouds will change under global warming as environmental conditions evolve and estimating the resultant effect of cloud feedbacks on the Earth's radiative balance remain critical questions in climate science.

The purpose of this study is to examine the relationships between intermodel variability in tropical high cloud feedbacks, mean state tropical high cloud characteristics, dynamical responses to warming, and equilibrium climate sensitivity across an ensemble of fully-coupled GCMs. This thesis is organized as follows: Section 2 overviews a background of relevant literature. Section 3 outlines three research questions guiding this study. Sections 4-6 are the data, methods, and results sections, respectively, all divided into three subsections corresponding to each of the three research questions. Section 7 contains a discussion of the results and directions for future work. Section 8 outlines main conclusions.

2. Background

In order to more precisely identify sources of cloud feedback variability, the global mean net cloud feedback is commonly decomposed by climatological region such that tropical, subtropical, and polar cloud feedbacks are considered separately. While the large variability of cloud feedbacks among models arises from a combination of differences in cloud feedbacks across regions (Lutsko et al., 2021), the tropics have been highlighted as making a significant contribution to the intermodel spread of cloud feedbacks (Bony et al., 2006; Webb et al., 2013; Zelinka et al., 2020). For instance, Vial et al. (2013) attribute 55% of the standard deviation of climate sensitivity among an ensemble of CMIP5 models to cloud feedbacks, highlighting that a majority of this variability comes from the shortwave component across a variety of tropical dynamical regimes. Beyond variability of cloud feedbacks among climate models, Sherwood et al. (2020) highlight that the tropical marine low cloud and tropical anvil feedbacks occupy a significant portion of the uncertainty associated with cloud feedbacks by using a combination of historical data, paleoclimate evidence, and process understanding. Consequently, constraining the variability of cloud changes in tropical environments characterized by warm sea surface temperatures, high humidity, and weak temperature gradients, could make significant progress towards constraining climate sensitivity.

In addition to decomposition by region, cloud feedbacks occurring in the boundary layer are often considered separately from cloud feedbacks occurring at higher altitudes in the free troposphere. In the tropics, low cloud feedbacks have garnered significant attention due to the strong cooling effect of marine low clouds (Hartmann et al., 1992) and their sensitivity to changes in sea surface temperatures and inversion strength (Klein et al., 2017; Ogura et al., 2023; Qu et al., 2015). Although there is a general consensus that low clouds will reduce under

warming, resulting in a positive feedback (Ceppi et al., 2017; Sherwood et al., 2020), the magnitude and sign of the low cloud feedback vary among GCMs, and it has been highlighted as the largest contributor of variance to the global cloud feedback (Bony & Dufresne 2005; Caldwell et al., 2016; Zelinka et al., 2016). High cloud feedbacks also exhibit substantial intermodel spread, and the disagreement among models has garnered recent attention in the literature. For example, Zelinka et al. (2022) found that 8 out of 19 GCMs produced tropical high cloud anvil feedbacks that were above the expert-assessed value published by Sherwood et al. (2020). They also noted that the high cloud altitude feedback had the largest number of models falling outside of these best-estimate ranges. Additionally, the Intergovernmental Panel on Climate Change (IPCC) Assessment Report 6 (AR6), which corresponds to CMIP6, labels the sign of the tropical high cloud amount feedback with "low confidence," while the sign of the subtropical marine low cloud feedback is assessed with "high confidence" (Forster et al., 2021), demonstrating substantial improvements from AR5 in the understanding of changes to low clouds without accompanying advancements regarding high clouds. This persistent uncertainty warrants further research into the drivers of variability in tropical high cloud feedbacks in particular.

2.1 High Cloud Feedback Components

Cloud feedbacks are often separated by physical mechanism, typically into amount, altitude, and optical depth feedback components. These cloud feedback components describe the radiative effect of changes to total cloud amount, redistribution of cloud fraction across altitudes, and redistribution of cloud fraction across optical thicknesses under warming, assuming the other components are held constant (Zelinka et al., 2012b). Each feedback component describes a different physical process contributing to unique changes in cloud characteristics that can be

assessed across models and observations. The high cloud altitude feedback has been assessed as robustly positive due to the strength of evidence supporting its underlying physical mechanisms. Observations show that tropical high clouds have risen across the satellite era (Raghuraman et al., 2024; Richardson et al., 2022) and increased in altitude in response to interannual surface warming (Zelinka & Hartmann, 2011; Zhou et al., 2014). To explain this phenomenon, Hartmann and Larson (2002) put forth the Fixed Anvil Temperature (FAT) hypothesis, which argues that tropical anvil clouds remain at a constant emission temperature regardless of surface warming. They assert that convective detrainment preferentially occurs at a fixed temperature that coincides with the temperature at which the efficacy of clear sky radiative cooling by water vapor declines. Given the dependence of humidity on the Clausius-Clapeyron relationship, they contend that the decline in radiative cooling will remain at an isotherm regardless of surface temperature, with anvil tops following suit. This implies that cloud altitude will increase as the tropical troposphere deepens with warming (Ramaswamy et al., 2001) while the emission temperature of cloud tops will remain the same, yielding a positive feedback due to the constant longwave emission to space despite the positive radiative forcing. This hypothesis was modified by Zelinka and Hartmann (2010) with the proposal of the Proportionally Higher Anvil Temperature (PHAT) hypothesis. They assert that increases in upper tropospheric static stability with warming cause a slight increase in cloud top temperature as clouds rise. However, this increase in temperature does not compensate for the radiative forcing causing surface warming, so the net result is still a strong, positive feedback. The PHAT mechanism has found support in both models (Bony et al., 2016; Stauffer & Wing, 2022) and observations (Saint-Lu et al., 2020; Zelinka & Hartmann, 2011), and the IPCC AR6 assesses the high cloud altitude feedback as positive with “high confidence.” However, despite the consensus surrounding the sign and

physical mechanism of the high cloud altitude feedback, its magnitude varies significantly among GCMs (Po-Chedley et al., 2019; Sherwood et al., 2020; Zelinka et al., 2022), indicating that further work is needed to constrain this feedback in models.

There is less certainty surrounding the magnitude and sign of the high cloud amount feedback. Lindzen et al. (2001) proposed an "Iris Feedback" to explain the reduction of high cloud fraction with warming. They contend that under warming, enhanced precipitation efficiency causes a contraction of high clouds in the tropics such that outgoing longwave radiation is enhanced, resulting in a negative feedback. Following this initial hypothesis, Zelinka and Hartmann (2010) and Bony et al. (2016) formed the "Stability Iris" hypothesis, which draws on similar physics underlying the PHAT hypothesis. They argue that enhanced upper tropospheric stability reduces convective outflow and a contraction of clouds at the level where cloud fraction is climatologically greatest. In line with theory, tropical high cloud amount has been shown to reduce in response to interannual warming in observations (Saint-Lu et al., 2020; Saint-Lu et al., 2022; Su et al., 2017; Zelinka & Hartmann, 2011). Additionally, there is observational evidence that changes to upper tropospheric stability (Ito & Masunaga, 2022; Wilson Kemsley et al., 2024), precipitation efficiency (Choi et al., 2017), and convective aggregation (Bony et al., 2020) contribute to changes in tropical anvil extent. In contrast, modelling studies demonstrate mixed results. While some idealized simulations similarly show a reduction of high cloud amount with warming (Cronin & Wing, 2017; Wing et al., 2020), other work suggests that high cloud fraction increases with rising surface temperatures (Ohno et al., 2019; Tsushima et al., 2014). Moreover, while it has been shown that increases to precipitation efficiency (Li et al., 2022; Li et al., 2023) and upper tropospheric stability (Bony et al., 2016) are linked to contraction of tropical high clouds under warming in models, other factors such as

model resolution (Jeevanjee & Zhou, 2022), sensitivity of cloud lifetime to warming (Beydoun et al., 2021; Seeley et al., 2019), and intermodel variability in changes to ascent area (Schiro et al., 2019; Su et al., 2017) are also linked to the response of high cloud extent under warming in GCMs. Additionally, the resulting sign of the high cloud amount feedback is uncertain, with recent studies suggesting a neutral feedback (Chao et al., 2024; McKim et al., 2024; Raghuraman et al., 2024) in contrast to the original hypothesis that a reduction of high cloud amount acts to mitigate warming.

The redistribution of cloud fraction across optical thicknesses separate from an overall loss in coverage in response to surface warming further complicates the interpretation of anvil feedbacks. Tropical anvils, which consist of a diverse array of clouds ranging from deep convective cores to thinner anvil cirrus, have been shown to have an approximately neutral cloud radiative effect (Hartmann & Berry, 2017). However, small changes in the relative proportion of clouds across optical thicknesses could impose a large optical depth feedback owing to the cancellation between large positive longwave and negative shortwave effects that produces a near-neutral effect in the mean state (Hartmann et al., 2018). Unlike the high cloud amount and altitude feedbacks, the high cloud optical depth feedback lacks theoretical support aside from suggestions that changes to precipitation efficiency with warming could cause changes to anvil optical thickness (Li et al., 2019). In observations, there is evidence that cirrus fraction reduces in the tropical Western Pacific in response to interannual warming (Choi et al., 2017), resulting in an overall "thickening" of high clouds and a corresponding negative high cloud optical depth feedback. Similarly, other recent studies find that tropical anvil albedo is positively sensitive to warming on interannual timescales (Chao et al., 2024; McKim et al., 2024). However, there are also contradictory findings that high clouds are thinning over the tropical Western Pacific (Kubar

& Jiang, 2019) and in the tropical-mean (Raghuraman et al., 2024) in response to warming. Idealized models also yield mixed results, with some demonstrating a thinning of high clouds with warming (Li et al., 2019; Sokol et al., 2024) and others showing a thickening (Gasparini et al., 2021). Regardless, changes to high cloud optical depth have not been extensively studied in fully-coupled GCMs separate from changes to high cloud amount (Ceppi et al., 2017), and diagnosing mechanisms underlying changes to anvil optical depth has been highlighted in the literature as a topic that requires further work (Gasparini et al., 2023).

2.2 Emergent Constraints

One method for relating the variation in cloud feedbacks to the spread of climate sensitivity across GCMs is to perform analysis within an emergent constraint framework. Emergent constraints describe correlations between present-day climate variability or mean state climate variables and ECS across a model ensemble in conjunction with a physical mechanism to explain the relationship (Klein & Hall, 2015). By establishing a plausible linkage between variability in an observable parameter and variability in climate sensitivity across models, emergent constraints provide an opportunity to narrow the spread of ECS using observations of the current climate predictor as a constraint. Tropical clouds have been the subject of several proposed emergent constraints. For example, Volodin (2008) finds that models with less cloud coverage in the tropics relative to the midlatitudes have higher climate sensitivity, and Siler et al. (2017) suggest that models with higher sensitivity have lower mean-state tropical cloud albedo than models with lower sensitivity. While boundary layer cloud feedbacks and characteristics have been a particular area of interest for establishing emergent constraints (Brient et al., 2016; Brient & Schneider, 2016; Zhai et al., 2015), tropical high cloud feedbacks have not been widely represented in the emergent constraint literature. Though they do not discuss the relationship

between high cloud feedbacks and climate sensitivity, Po-Chedley et al. (2019) find that a model's climatology of tropical high clouds can explain changes in tropical upper tropospheric cloud fraction by assuming that cloud fields track with isotherms and that warming in the tropics follows a dilute moist adiabat. This result implies that changes to tropical high clouds are related to mean state high cloud fraction through the high cloud altitude feedback, which could be used as a constraint on climate sensitivity if the tropical high cloud altitude feedback were found to be correlated to ECS. Thus, although relatively unexplored, high cloud feedbacks represent an area that could help to relate variability in mean state high cloud characteristics to variability in climate sensitivity and expand on the existing emergent constraint literature.

2.3 Convective Sensitivity to Moisture

The amount of tropical high clouds produced by GCMs varies, with some suggestions that tropical upper tropospheric cloud fraction is greater in high ECS models than low ECS models (Su et al., 2014). One approach for analyzing why mean state high cloud coverage varies across models is to analyze the extent to which the diversity of parameterizations of processes governing cloud formation is related to variability in climatological high cloud fraction. This question has most commonly been approached using a perturbed parameter ensemble (PPE) technique, which involves varying parameters that characterize deep convective activity or microphysical processes within a single model and comparing the resulting output across different model configurations. The literature suggests that parameter choices that characterize the sub-grid scale processes that represent cloud formation have a large impact on the mean state high cloud fields that a model produces. For example, Schiro et al. (2019) conclude that perturbing convective parameters across a PPE results in highly varied high cloud climatologies by influencing climatological tropical circulation. Other PPE studies have highlighted

entrainment of environmental air into a convective plume (Tsushima et al., 2020), representation of ice autoconversion (Proske et al., 2022), and the threshold of relative humidity for high cloud formation (Zhang et al., 2012) as key parameters influencing climatological high cloud amount. While the representation of deep convective processes has a direct impact on the formation of thick high clouds, thinner cirrus clouds are also intrinsically linked to convection as about half of tropical cirrus are formed from convective detrainment (Luo & Rossow, 2004). Although improvement of small-scale microphysics processes has been highlighted as key for improving the model representation of the amount and radiative effect of tropical cirrus (Atlas et al., 2024; Gasparini et al., 2023; Turbeville et al., 2022), results have also shown that deep convective processes are equally influential for modelling anvil cirrus (Muhlbauer et al., 2014). Thus, characterizing deep convective processes is an important step in understanding variability in tropical high cloud amount across different cloud types in GCMs.

While PPEs have been a useful tool for highlighting specific parameters that have a strong impact on the amount of high clouds present in a model, they are limited in their generalizability given that they only apply to a single model. Ahmed and Neelin (2021) present a method for characterizing a model's convective sensitivity to atmospheric moisture that can be applied to an ensemble of GCMs and thus characterize variability in convective parameterizations without directly perturbing parameters. This method builds on the tendency of convection to exhibit a "precipitation pickup," which describes a phase transition from weak to strong convection beyond a critical value of column water vapor that is also marked by a sharp increase in precipitation (Peters & Neelin, 2006). This phase transition has been related to the effects of entrainment on plume buoyancy, with suggestions that entraining plumes have enhanced buoyancy in environments with higher column water vapor (Holloway & Neelin,

2009). Ahmed and Neelin (2018) present a precipitation-buoyancy framework in which a metric of lower free tropospheric buoyancy accurately captures the sharp pickup of precipitation with increasing column water vapor that has been noted in other papers (Neelin et al., 2009; Schiro et al., 2016). They conclude that using a profile of deep inflow (Schiro et al., 2018) into an entraining plume, environmental buoyancy integrated from the top of the boundary layer to the freezing level captures the onset of precipitation in the tropics, providing evidence that tropospheric moisture is key for explaining the behavior of precipitation pickup in the tropics through its contributions to entrained buoyancy into a rising plume. Ahmed and Neelin (2021) expand on these results by applying the same framework to an ensemble of CMIP6 models, finding that the sensitivity of precipitation to lower-tropospheric subsaturation varies across models. This finding suggests that intermodel variability in convective activity is related to variability in convective sensitivity to entrainment of tropospheric air such that models that are more sensitive to entrainment will experience convection only under relatively moist conditions whereas models with lower sensitivities will see convection across a broader range of environmental conditions. While these results shed light onto this systematic difference in the way that GCMs represent convective processes and the resulting behavior of precipitation, the relationship between variability in convective sensitivity to moisture and variability in climatological high cloud fraction remains unexplored.

2.4 Precipitation Efficiency

Precipitation efficiency, defined as the ratio of surface precipitation rate to the rate at which cloud particles condense (Lutsko et al., 2023), has been highlighted in the literature as a potential modulator of tropical high cloud feedbacks across different scales. A distinction is often made between microphysical precipitation efficiency, which considers condensation as the net

result of microphysical processes such as vapor deposition across a single cloud type, and bulk precipitation efficiency, which characterizes the average efficiency across many different cloud types and multiple convective systems (Lutsko et al., 2023). Both have been explored with respect to the response of high clouds to warming. The relationship between changes to microphysical precipitation efficiency and high cloud feedbacks were first highlighted by Lindzen et al. (2001), who postulated that an increase in the conversion efficiency of clouds results in a contraction of anvil cloud fraction with increasing surface temperature, yielding a negative high cloud amount feedback. Idealized modelling studies suggest that microphysical precipitation efficiency should increase with increasing surface temperatures as condensation efficiency increases due to an increase in cloud density (Lutsko & Cronin, 2018). Moreover, inclusion of this behavior in GCMs causes a reduction in climate sensitivity (Mauritsen & Stevens, 2015), providing some evidence that increasing precipitation efficiency with warming has a stabilizing effect on the climate. However, Li et al. (2019) find that an increase in microphysical efficiency increases climate sensitivity due to increased thinning of anvil clouds, which results in a more positive optical depth feedback. Thus, the net result of increasing microphysical precipitation efficiency with warming from high cloud reduction and thinning remains uncertain.

While bulk precipitation efficiency has also been found to increase in a single model across different parameter schemes in response to surface warming (Zhao, 2014), the responses of CMIP6 models are varied (Li et al., 2022; Li et al., 2023). Zhao (2014) finds that model runs with greater increases in bulk precipitation efficiency under warming experience a greater loss of low and middle cloud fraction relative to high cloud fraction and a more positive shortwave cloud feedback, attributing this behavior to preference towards deeper convection. Li et al.

(2023) similarly suggest that an increase in bulk precipitation efficiency under warming results in an increase in climate sensitivity via more positive cloud feedbacks, finding that among 36 CMIP6 models, the 24 models that increase in efficiency generally see more positive high cloud feedbacks in the West Pacific and more positive low cloud feedbacks in the East Pacific than models that decrease in precipitation efficiency. They suggest that this is related to the slowdown of the Walker Circulation wherein an increase in precipitation efficiency implies a weakening of the Walker Circulation, which they connect to a contraction and thinning of high clouds in the West Pacific and suppression of stratocumulus decks in the East Pacific. However, assessment of the relationship between the explicitly decomposed high cloud feedback components and changes to precipitation efficiency across GCMs has not been performed thus far, necessitating further analysis to verify these suggestions in the literature.

2.5 Convective Organization

Convective aggregation, or convective clustering, is a phenomenon in which convection spatially organizes in groups. Convective organization has been investigated primarily in idealized radiative-convective equilibrium (RCE) experiments, which represent an approximation of the tropical atmosphere that follows an energy balance between radiative cooling and convective heating (Wing et al., 2020). RCE experiments demonstrate clustering that occurs spontaneously even under homogenous initial and boundary conditions, referred to as convective self-aggregation (Wing et al., 2017). Clustering is maintained through positive longwave feedbacks from clouds in moist regions (Wing & Emmanuel, 2014), though this has been found to decrease as aggregation progresses and cloud amount decreases (Pope et al., 2021). High cloud amount tends to decrease with clustering in RCE experiments (Wing & Cronin, 2016; Wing et al., 2020) as well as observations (Bony et al., 2020; Stein et al., 2017;

Tobin et al., 2012), presenting a potential mechanism to explain changes to tropical high cloud extent under different conditions. However, RCE experiments do not exhibit a clear relationship between warming and aggregation (Wing et al., 2020), so the relationship between aggregation and the high cloud amount feedback in idealized models is unclear.

Limited work has been done to assess the relationship between intermodel variability in convective organization and tropical high cloud feedbacks across fully-coupled GCMs. At the mesoscale, a majority of CMIP6 models demonstrate an increase in aggregation under warming, but the intermodel spread is substantial (Bläckberg & Singh, 2022) and has not evaluated with respect to high cloud feedbacks. At the planetary scale, changes in the width of the Intertropical Convergence Zone (ITCZ), the near-equatorial zone of large-scale ascent where the surface trade winds converge, can be thought of as the largest scale of convective organization. Observations indicate that the ITCZ has narrowed in response to surface warming (Wodzicki & Rapp, 2016), and this behavior is present across a majority of CMIP5 models (Byrne & Schneider, 2016). This has been linked to a decrease in tropical high cloud fraction (Schiro et al., 2019), which relates to intermodel variability in changes to tropical outgoing longwave radiation (OLR) such that a greater tightening of tropical ascent results in a greater loss of tropical high clouds and enhanced OLR (Su et al., 2017). Moreover, both models (Su et al., 2019) and observations (Su et al., 2020) suggest that tightening tropical ascent is also associated with an increase in ascent strength, which has been further linked to changes in high cloud amount (Schiro et al., 2019). Unlike CMIP5 models, the CMIP6 ensemble demonstrates variable changes to tropics-wide ascent area in response to warming with models that decrease in area demonstrating a greater loss of tropical high and low cloud fraction, resulting in a more positive tropical net cloud feedback (Schiro et al., 2022). As noted in Bony et al. (2015), the role of convective aggregation in climate remains a

key question, particularly as a potential mechanistic explanation for the relationship between changes to precipitation efficiency and high cloud amount (Lutsko et al., 2023). However, changes to convective organization across different scales have not been explicitly linked to high cloud feedback components across fully-coupled GCMs, representing a key avenue for continued work.

In summary, tropical high cloud feedbacks account for a non-negligible portion of uncertainty in ECS. The high cloud altitude feedback has strong physical support for being positive, but its magnitude varies across models. The high cloud amount feedback is likely small in magnitude owing to the neutral radiative effect of tropical anvil clouds, and it shares similar physics to the high cloud altitude feedback. On the other hand, the sign, magnitude, and physical basis of the high cloud optical depth feedback are uncertain in models and observations. Analysis of drivers of variability of tropical high cloud feedbacks across models, such as differences in changes to precipitation efficiency and convective organization under warming, could help to reduce the spread of feedbacks across models. Additionally, analysis of systematic differences in the ways that GCMs represent convective sensitivity to moisture is an approach for understanding intermodel variability of climatological tropical high cloud amount. More broadly speaking, pursuing these research questions with an emergent constraint framework presents an opportunity to constrain intermodel variability in climate sensitivity, which has the potential to make a large impact on the state of climate science.

3. Research Questions

Q1: To what extent does the intermodel variability in tropical high cloud feedbacks contribute to the intermodel variability in equilibrium climate sensitivity across fully coupled GCMs?

The first objective of this study is to assess the extent to which the tropical net high cloud feedback and its decomposed parts are driving the variability of ECS across the most recent generations of fully-coupled GCMs. Although literature has highlighted the variability of the tropical high cloud feedback across models, a quantification of its direct contribution to the variability in estimates of climate sensitivity has not been performed. Doing so would contextualize the importance of tropical high cloud feedbacks for driving climate sensitivity relative to more commonly studied feedbacks, such as the subtropical marine low cloud feedback.

Q2: How do climatological tropical high cloud characteristics vary with equilibrium climate sensitivity and tropical high cloud feedbacks across GCMs?

In line with recent emergent constraint literature, the second objective of this study is to analyze whether mean cloud characteristics, including high cloud fraction and thickness, vary with climate sensitivity across a model ensemble. In addition, relationships between mean cloud characteristics and high cloud feedbacks are analyzed to provide a mechanistic explanation for relationships found between mean state cloud characteristics and ECS. Convective sensitivity to moisture is investigated as a potential mechanism driving intermodel variability in climatological tropical high cloud fraction. In conjunction with conclusions surrounding the contribution of variability in high cloud feedbacks to variability in ECS, this analysis helps identify any relationships that could be used to form new emergent constraints based on tropical high cloud climatologies.

Q3: Can model representation of changes to precipitation efficiency and convective organization under warming explain intermodel differences in tropical high cloud feedbacks?

Recent focus in the tropical high cloud feedback literature, particularly surrounding the high cloud amount and optical depth feedbacks, has been placed on changes to precipitation efficiency and convective aggregation in response to surface warming as potential physical explanations for changes to tropical high cloud amount and opacity. While these topics have been investigated in idealized experiments, limited work has been done to analyze how they influence intermodel variability in tropical high cloud feedbacks in fully-coupled GCMs. Thus, the third objective of this study is to analyze the extent to which variability in large scale measures of precipitation efficiency and convective organization can explain variability in the tropical high cloud amount and optical depth feedbacks in GCMs.

4. Data

4.1. High Cloud Feedback Relationship to ECS

To assess the relationship between tropical high cloud feedbacks and climate sensitivity, output is used from 22 models that participated in CMIP5 (8 models) and CMIP6 (14 models) (Taylor et al., 2012; Eyring et al., 2016; see Table 1 for a list of models). High cloud feedbacks are computed by comparing monthly output from years 1-10 and years 131-140 of the abrupt-4xCO2 run, an experiment wherein CO_2 is quadrupled relative to preindustrial levels and then held fixed (Eyring et al., 2016). Computing cloud feedbacks relative to an early period of the abrupt-4xCO2 run rather than a period from a control experiment where CO_2 is held at preindustrial levels removes the effect of rapid adjustments of clouds to CO_2, which are traditionally defined separately from long-term cloud feedbacks (Zelinka et al., 2013).

Cloud fraction is characterized using the cloud fraction variable *clisccp* produced by the International Satellite Cloud Climatology Project (ISCCP) simulator run inline with model experiments (Klein & Jacob, 1999). The ISCCP simulator mimics the method of measuring

cloud fraction that is employed by a collection of satellites contributing to ISCCP observational datasets, allowing for direct comparisons to be made between modelled and observed output. The simulator divides each model grid cell into a set of subgrid columns in which each altitude level is either read as completely cloudy or clear, remaining consistent with a model's cloud overlap parameterization. A single value of cloud top pressure (CTP) is found by applying a radiative transfer model to each subgrid column to determine a brightness temperature that is then converted to a cloud temperature, which is collocated with a pressure level using the vertical temperature profile of the column. A column integrated optical depth (τ) is computed as the sum of reported τ from cloudy layers. The subgrid values of cloud fraction organized by CTP and τ are then averaged and expressed in a joint histogram of 49 different cloud types across seven discretized CTP categories and seven τ groups (Klein et al., 2013). Output from the ISCCP simulator is advantageous for computing cloud feedbacks as it considers only radiatively relevant cloud coverage in terms of top-of-atmosphere fluxes (Zelinka et al., 2012a) and allows for decomposition of cloud feedbacks into contributions by specific cloud types rather than reporting a bulk quantity.

To compute cloud feedbacks using the method of Zelinka et al. (2013), monthly near-surface temperature (*tas*) is downloaded for the early and late periods of the abrupt-4xCO2 experiment. Additionally, monthly downwelling (*rsdscs*) and upwelling (*rsuscs*) clear-sky shortwave radiation from the early period of the abrupt-4xCO2 experiment are downloaded to assign grid boxes into surface albedo categories. To consider feedbacks constrained to ascent and descent regions, monthly vertical pressure velocity (ω) from the early period of the abrupt-4xCO2 experiment is utilized. ECS values are taken from Zelinka et al. (2020) for the models that are available. For models that do not have published ECS values, climate sensitivity is

computed using years 1-150 of monthly output from the abrupt-4xCO2 experiment and piControl experiment of top-of-atmosphere (TOA) outgoing longwave (*rlut*) and shortwave (*rsut*) radiation, TOA incoming shortwave radiation (*rsdt*), and surface termperature (*ts*).

Table 1

List of the models used to investigate tropical high cloud feedbacks.

Model	CMIP Generation	Variant	Control Experiment	ECS
MIROC6	CMIP6	r1i1p1f1	piControl	2.60
MRI-CGCM3	CMIP5	r1i1p1	piControl	2.61
MIROC-ES2L	CMIP6	r1i1p1f2	piControl	2.66
MIROC5	CMIP5	r1i1p1	piControl	2.71
MRI-ESM2-0	CMIP6	r1i1p1f1	piControl	3.13
MPI-ESM-LR	CMIP5	r1i1p1	piControl	3.63
CanESM2	CMIP5	r1i1p1	piControl	3.70
GFDL-CM4	CMIP6	r1i1p1f1	piControl	3.89
E3SM-2-0-NARRM	CMIP6	r1i1p1f1	piControl	3.93
E3SM-2-0	CMIP6	r1i1p1f1	piControl	3.97
IPSL-CM5A-MR	CMIP5	r1i1p1	piControl	4.11
IPSL-CM5A-LR	CMIP5	r1i1p1	piControl	4.13
IPSL-CM6A-LR-INCA	CMIP6	r1i1p1f1	piClim-control	4.13
HadGEM2-ES	CMIP5	r1i1p1	piControl	4.60
MIROC-ESM	CMIP5	r1i1p1	piControl	4.65
IPSL-CM6A-LR	CMIP6	r1i1p1f1	piControl	4.70

Model	CMIP Generation	Variant	Control Experiment	ECS
CNRM-ESM2-1	CMIP6	r1i1p1f2	piClim-control	4.79
CNRM-CM6-1	CMIP6	r1i1p1f2	piClim-control	4.90
E3SM-1-0	CMIP6	r1i1p1f1	piControl	5.31
UKESM1-0-LL	CMIP6	r1i1p1f2	piControl	5.36
HadGEM3-GC31-LL	CMIP6	r1i1p1f3	piClim-control	5.55
CanESM5	CMIP6	r1i1p2f1	piClim-control	5.57

4.2 Mean State High Cloud Relationships to ECS and High Cloud Feedbacks

To characterize the climatological cloud fields of the 22 models that are utilized in the feedback analysis, monthly output is taking from either the piControl experiment, which holds CO_2 concentrations at pre-industrial levels, or the piClim-control experiment, a 30-year experiment in which pre-industrial conditions are applied to the model but sea surface temperatures and sea ice concentrations are held constant (Pincus et al., 2016), as done in Zelinka et al. (2022). piClim-control is utilized to represent the mean state high cloud fields of 5 models that do not have available output for the piControl experiment. Years 21-30 are used for the piClim-control experiments, and years 121-130 or the closest available 10-year period are used for the piControl experiments. Cloud fraction is represented using both ISCCP simulator output (*clisccp*) and 2-dimensional cloud area fraction (*cl*), which outputs the percentage of a gridbox covered by clouds at each model pressure level. To characterize the dynamical regimes of mean state clouds, monthly vertical pressure velocity (ω) and monthly vertical pressure velocity at 500 hPa (ω_{500}) are taken from the corresponding control experiment and time period.

To analyze the relationship between convective sensitivity to moisture and mean high cloud fraction, 19 CMIP6 models are considered from the models used by Ahmed and Neelin (2021) (see Table 2 for a list of models). Data are taken from the historical experiment from January 2012 to December 2014. 6-hourly instantaneous specific humidity (*hus*) and temperature (*ta*) and 3-hourly mean precipitation rate (*pr*) are utilized. In conjunction, mean cloud fraction is characterized using monthly 2-dimensional cloud area fraction (*cl)* from the same period. IPSL-CM5A2-INCA is excluded due to a lack of availability of *cl* output. Additionally, monthly vertical pressure velocity (ω) is utilized to characterize the dynamic regime of clouds across the ensemble.

Table 2

List of the CMIP6 models used in the characterization of convective sensitivity to moisture.

Model	Variant
BCC-CSM2-MR	r1i1p1f1
IPSL-CM6A-LR	r1i1p1f1
NESM3	r1i1p1f1
IPSL-CM5A2-INCA	r1i1p1f1
CanESM5	r1i1p1f1
MRI-ESM2-0	r1i1p1f1
MPI-ESM1-2-LR	r1i1p1f1
TaiESM1	r1i1p1f1
CNRM-CM6-1-HR	r1i1p1f2
AWI-ESM-1-1-LR	r1i1p1f1

Model	Variant
ACCESS-ESM1-5	r1i1p1f1
MPI-ESM1-2-HR	r1i1p1f1
GFDL-CM4	r1i1p1f1
CMCC-ESM2	r1i1p1f1
MIROC-ES2L	r1i1p1f2
CNRM-CM6-1	r1i1p1f2
GISS-E2-1-G	r1i1p1f1
MIROC6	r1i1p1f1
FGOALS-g3	r1i1p1f1

4.3 Precipitation Efficiency and Convective Organization Relationship to High Cloud Feedbacks

To assess the relationship between changes to precipitation efficiency, convective organization, and high cloud feedbacks, output is considered for 21 of the 22 models used to compute the cloud feedbacks (HadGEM2-ES is excluded due to lack of data availability). To calculate bulk precipitation efficiency, monthly data is downloaded for years 1-10 and 131-140 of the abrupt-4xCO2 experiment. Surface precipitation rate (*pr*) and vertically-integrated cloud water path that includes ice and liquid water (*clwvi*) are used to calculate the change in precipitation efficiency as is done in Li et al. (2022). To calculate changes to mesoscale organization, daily *pr* is utilized from years 1-10 and 131-140 of the abrupt-4xCO2 experiment. To compute planetary scale changes to organization, monthly vertical pressure velocity at 500 hPa (ω_{500}) are taken from the same time periods.

5. Methods

5.1 High Cloud Feedback Relationship to ECS

5.1.1 Cloud Radiative Kernels

One commonly used method for quantifying feedbacks in climate models and observations is the application of radiative kernels. Radiative kernels represent the radiative flux at TOA that accompanies an incremental change in a climate variable (Shell et al., 2008). While several different versions of cloud radiative kernels have been developed, the most detailed version is published by Zelinka et al. (2012a). These kernels utilize cloud fraction from the ISCCP simulator output such that changes in radiative fluxes resulting from changes to cloud fraction are detailed across different CTP-τ groups. Zelinka et al. (2012a) compute each kernel for a given CTP-τ bin by differencing the radiative flux associated with a single cloud of that CTP-τ group from the radiative flux under clear skies at every latitude, month, and at three surface albedo values of 0, 0.5, and 1. Figure 1 depicts the global mean longwave, shortwave, and net cloud radiative kernels of Zelinka et al. (2012a).

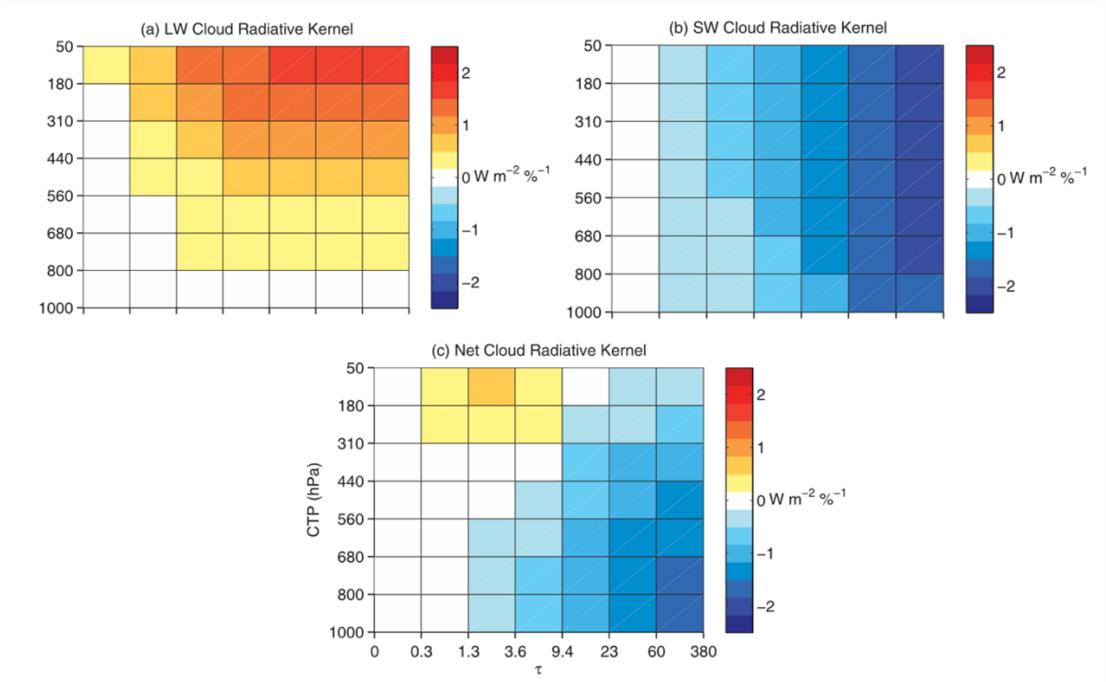

Fig. 1. The longwave (top left), shortwave (top right), and net (bottom middle) ISCCP cloud radiative kernels. From Zelinka et al. (2012a).

To apply the cloud radiative kernels, normalized cloud fraction anomaly matrices are first produced by subtracting the early period abrupt-4xCO2 run *clisccp* matrix from the late period abrupt-4xCO2 run *clisccp* matrix (subtracting a percentage cloud fraction from a percentage cloud fraction) and normalizing by the global average change in surface temperature (dT_s) following interpolation to a common 2° x 2.5° grid. The longwave and shortwave cloud feedbacks are computed by multiplying the normalized cloud fraction anomaly matrices by the cloud radiative kernels, assigning the kernels to the correct latitude, surface albedo, and month. The total net cloud feedback is calculated as the summation of the longwave and shortwave cloud feedbacks. Each bin of the radiative kernel represents the change in radiative flux in W m^{-2} $\%^{-1}$ that results from a 1% increase in cloud fraction for that cloud type; therefore, multiplying the radiative kernel by the change in cloud fraction normalized by the change in global mean

surface temperature yields the feedback associated with the change in that cloud type in units of W m^{-2} K^{-1}.

The net cloud feedback is then decomposed into the amount, altitude, and optical depth feedbacks using the methods of Zelinka et al. (2013). Each of these components represents the effect of changes to the cloud field across the corresponding category assuming that the distribution of clouds across the other two categories remains constant relative to the control period. This feedback decomposition is performed by dividing the cloud fraction anomaly histogram ($\Delta C_{p\tau}$) into two components:

$$\Delta C_{p\tau} = \left(\frac{C_{p\tau}}{C_{tot}}\right) \Delta C_{tot} + \Delta C^{*}_{p\tau} \quad (1)$$

Here, C_{tot} is the total cloud fraction summing across the entire histogram, $C_{\rho\tau}$.The first term represents the change in total cloud fraction holding the distribution of the cloud field constant across CTP-τ groups. The second term represents changes to cloud cover associated with the redistribution of clouds across CTP-τ groups assuming that total cloud cover remains constant. The cloud radiative kernel ($K_{\rho\tau}$) is also decomposed into 2 terms:

$$K_{\rho\tau} = K_0 + K'_{p\tau} \quad (2)$$

The first term is the average of the radiative kernel across each CTP-τ group weighted by the proportion of total cloud cover represented in each category:

$$K_0 = \sum_{p=1}^{P} \sum_{\tau=1}^{T} \left(\frac{C_{p\tau}}{C_{tot}}\right) K_{\rho\tau} \quad (3)$$

Multiplying this first kernel term by the total change in cloud cover represents the amount feedback. The second term of the decomposed radiative kernel can further be divided into altitude (K'_p), optical depth (K'_τ), and residual components (K'_R):

$$K'_{p\tau} = K'_p + K'_\tau + K'_R \quad (4)$$

The altitude kernel component, for example, represents an effective kernel summed across all τ groups and weighted by the proportion of cloud cover in each τ group, accounting for systematic variations in τ with CTP:

$$K'_p = \sum_{\tau=1}^{T}(K'_{p\tau} \sum_{p=1}^{P} \frac{C_{p\tau}}{C_{tot}}) \quad (5)$$

Finally, the altitude and optical depth effective kernels are multiplied by the portion of the anomaly histogram decomposition that accounts for changes to cloud fraction across CTP-τ groups, summing over the other category. The final cloud induced radiative anomalies (ΔR_C) are expressed as follows:

$$\Delta R_C = K_0 \Delta C_{tot} + \sum_{p=1}^{P}(K'_p \sum_{\tau=1}^{T} \Delta C^*_{p\tau}) + \sum_{\tau=1}^{T}(K'_\tau \sum_{p=1}^{P} \Delta C^*_{p\tau}) + \sum_{p=1}^{P}\sum_{\tau=1}^{T} K'_R \Delta C^*_{p\tau} \quad (6)$$

Here, the first term represents the amount feedback, the second the altitude feedback, the third the optical depth feedback, and the final is the residual. The altitude feedback portion is composed of the effective altitude kernel (K'_p) being multiplied by the anomaly histogram component summed across optical depths ($\sum_{\tau=1}^{T} \Delta C^*_{p\tau}$), representing the total change in cloud fraction at each CTP bin. The final result is an altitude feedback computed by multiplying an effective radiative kernel that varies with CTP with the total change in cloud fraction at each CTP. This method, in comparison to the decomposition method first proposed by Zelinka et al. (2012b), minimizes the residual term and is therefore a better representation of the individual feedback components.

To avoid an unrealistic influence of changes to boundary layer clouds on free tropospheric clouds, this decomposition is applied separately for the bottom two rows of the ISCCP histogram, representing pressures of 1000 hPa < CTP < 680 hPa, and the top five rows, representing pressures of 680 hPa < CTP < 50 hPa, as done in Zelinka et al. (2016). Additionally, due to the anomalous assignment of partly cloudy pixels to low optical depth bins by the ISCCP

algorithm (Pincus et al., 2012), the feedbacks are computed only using cloud fraction from $.3 < \tau < 380$ (the right six columns of the ISCCP histogram). High cloud feedbacks are therefore defined as the radiative anomalies imposed by the changes to cloud fields summed from 680 hPa < CTP < 50 hPa and $.3 < \tau < 380$.

5.1.2 Gregory Method

For 3 models (E3SM-2-0, E3SM-2-0-NARRM, and CanESM5) that do not have ECS values published by Zelinka et al. (2020), ECS is estimated using the methods of Gregory et al. (2004). While true climate sensitivity is most accurately represented by running millennia-length experiments (Rugenstein et al., 2019), this is computationally expensive and CMIP protocol requires experiments to be run for several hundred years (Eyring et al., 2016). Thus, climate sensitivity is often estimated using 150 years of model output, characterizing a transient "effective climate sensitivity" (Murphy, 1995) that is used as an approximation of the true equilibrium value.

Climate sensitivity is estimated using the following equation from Gregory et al. (2004):

$$N = F + \lambda T \tag{7}$$

Here, N is the net top-of-atmosphere (TOA) radiation (W m^{-2}), F is the effective radiative forcing (W m^{-2}), λ is the net feedback parameter (W m^{-2} K^{-1}), and T is the change in global mean surface temperature (K). Gregory et al. (2004) apply data from the first 20 years of the abrupt-4xCO2 experiment to Equation 7, quantifying a radiative forcing for a doubling of CO_2 as half of the y-intercept and the feedback parameter as the slope. ECS is then computed as the x-intercept of the linear regression using the estimated forcing and feedback terms. Here, ECS values are computed using a similar method. First, data from the piControl and abrupt-4xCO2 experiments are interpolated to a common 2° x 2.5° degree grid. Global monthly means of *rlut*, *rsut*, *rsdt*, and

ts are found and the future and control TOA imbalance are calculated following *rsdt* - *rsut* - *rlut* (downwelling minus upwelling radiation). For the piControl run, a 21-year centered moving monthly mean is calculated for the net TOA imbalance and *ts*. Finally, annual means are taken of the piControl and abrupt-4xCO2 net TOA imbalance and *ts* and subtracted from each other to yield 150 values of dN and dT_s, representing the evolution of TOA radiative imbalance and corresponding surface temperature change following a radiative forcing associated with a quadrupling of CO_2 relative to preindustrial levels. A linear regression is computed between dN and dT_s, and a final ECS value is obtained by solving for T in Equation 7 using the slope (net feedback parameter) and half of the y-intercept (radiative forcing associated with a doubling of CO_2) computed from the regression. An example Gregory regression is shown in Figure 2.

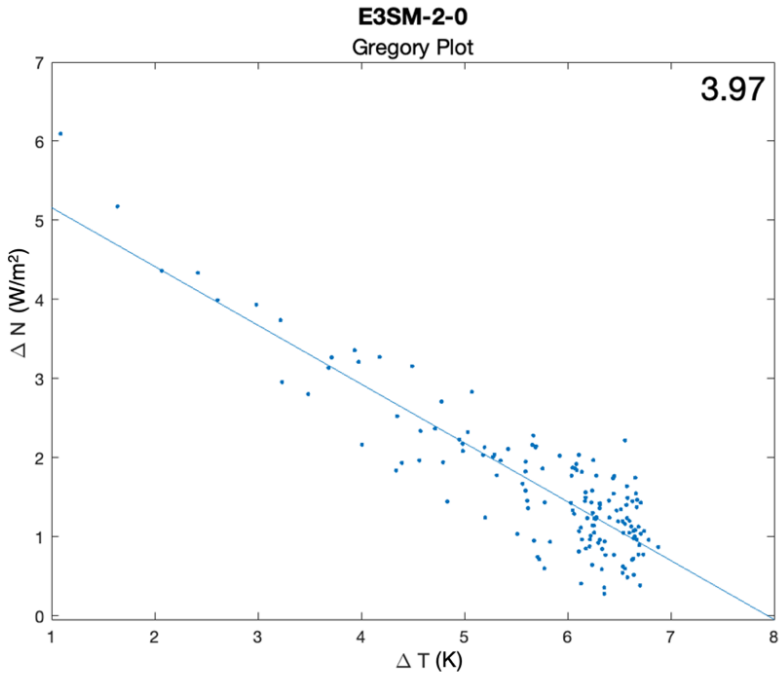

Fig. 2. Gregory regression for E3SM-2-0. The y-axis is the global mean net radiative imbalance following a quadrupling of CO_2, and the x-axis is the change in surface temperature relative to the piControl experiment. Each point represents the change in radiative imbalance and temperature for one year in the 150 year abrupt-4xCO2 experiment relative to the piControl experiment, and the blue line represents the line of best fit. The equilibrium climate sensitivity is shown in the top right corner.

5.1.3 Feedback Relationships to ECS

To analyze the contribution of intermodel variability in tropical high cloud feedbacks to intermodel variability in climate sensitivity, Pearson correlation coefficients are computed between the tropical mean (30°S - 30°N) cloud feedback components and ECS. The net feedback, which in part determines the magnitude of climate sensitivity, is traditionally decomposed into additive components including Planck, water vapor, lapse rate, albedo, and cloud feedback terms (Caldwell et al., 2016). Thus, while all cloud feedback components

contribute to the net feedback as portions of a sum, individual cloud feedback components may be correlated or anticorrelated with ECS. Due to the causal relationship between the cloud feedback magnitude and ECS arising from the contribution of the cloud feedback to λ in Equation 7, positive correlations between a cloud feedback component and ECS are interpreted as an indication that the intermodel spread in the cloud feedback is driving intermodel variability in ECS; an anticorrelation between a cloud feedback component and ECS suggests that, while serving as a portion of net feedback, the variability in the cloud feedback component among models is not strongly influencing the intermodel spread in ECS. This isolates particular cloud feedback components as the most important for determining the magnitude of ECS and highlights opportunities for constraint. Additionally, ascent and descent region cloud feedbacks are computed as an area-weighted average constrained to grid boxes where the mean ω_{500} over years 1-10 of the abrupt-4xCO2 experiment is < 0 hPa day^{-1} for ascent regions and > 0 hPa day^{-1} for descent regions.

Pearson correlation coefficients are also computed between the local cloud feedback components and ECS and visualized over space. This highlights regions where the intermodel spread of the high cloud feedbacks is more likely to contribute to the intermodel spread of ECS. However, relative to the tropics-wide, ascent, or descent correlations, these are less clearly indicative of causation given that the magnitude of the feedbacks vary significantly across space. A significant correlation between the high cloud feedback at a given grid point and ECS could be relatively unimportant for the tropics-wide relationship if the range of the feedback magnitudes across the ensemble is relatively small at that location. To account for this, the high cloud feedback components are composited across different ECS groups. The high ECS group is defined as 7 models with ECS values ≥ 4.7 K and the low ECS group as 7 models with ECS

values ≤ 3.7 K, representing the highest and lowest thirds of the ensemble with respect to ECS. Differencing the high and low composites highlights regions where the feedbacks differ the most between the groups and can be compared to the regions where significant correlations between local feedback values and ECS appear across the entire ensemble. This verifies that significant local correlations are important for driving the tropical mean spread in the feedback.

5.2 Mean State High Cloud Relationship to ECS and High Cloud Feedbacks

5.2.1 High Cloud Characterization

Several characterizations of climatological high cloud fraction are considered. Using the ISCCP simulator output for the piControl/piClim-control experiments, tropical mean (30°S - 30°N) time mean histograms are first computed. Total high cloud fraction is defined as the sum of cloud fraction across 680 hPa < CTP < 50 hPa and .3 < τ < 380. Thin high cloud fraction is defined as the sum of cloud fraction across 680 hPa < CTP < 50 hPa and .3 < τ < 9.4, and thick high cloud fraction is defined as the sum of cloud fraction across 680 hPa < CTP < 50 hPa and 9.4 < τ < 380. Additionally, mean high cloud opacity is characterized by taking the ratio of thick to thin high cloud fraction, where values > 1 (unitless) are indicative of relatively more thick high clouds than thin high clouds and values < 1 represent relatively more thin high clouds than thick high clouds. Additionally, ascent and descent region climatological cloud fraction are computed as area weighted averages constrained by monthly ω_{500} values across the piControl/piClim-control experiments, where ascent regions are characterized by ω_{500} < 0 hPa day^{-1} and descent regions > 0 hPa day^{-1}. For analysis over space in relationship to climate sensitivity and cloud feedbacks, high cloud definitions are computed as time means at each tropical grid box.For analysis of 2-dimensional cloud area fraction (*cl*) utilized in the characterization of high and low ECS model composites, cloud fraction is interpolated to

common standard pressure levels, constrained to the tropical region, and binned by monthly ω values.

5.2.2 Convective Sensitivity to Moisture

Convective sensitivity to moisture is characterized using the methods of Kuo et al. (2018). They find that precipitation rates increase dramatically beyond a threshold value of column water vapor (CWV). This threshold is found first by conditionally averaging precipitation rate on column water vapor across different saturation specific humidity groups (Figure 3a). The threshold increases with saturation specific humidity, displaying a dependence of the relationship on the temperature of the column. To account for this, the pickup curves are collapsed (Figure 3b). To collapse the curves, a common reference precipitation rate is first defined, marking the transition between non-precipitating and precipitating states. For each of the precipitation curves, the threshold CWV corresponding to the reference precipitation rate is found and the curves are shifted by this CWV value such that the x-axis becomes CWV minus the reference CWV and all curves transition to a precipitating state at a normalized CWV value of 0. This allows for the curves to collapse, eliminating the temperature dependence. Finally, a critical CWV is defined as the x-intercept of a best-fit line through a range of precipitation rates greater than the one chosen as the threshold rate. Values of lower critical CWV and less steep linear regression slopes are representative of convection that is less sensitive to entrainment of tropospheric air whereas convection that is more sensitive to entrainment of tropospheric air is associated with higher critical CWV values and a steeper slope of the pickup.

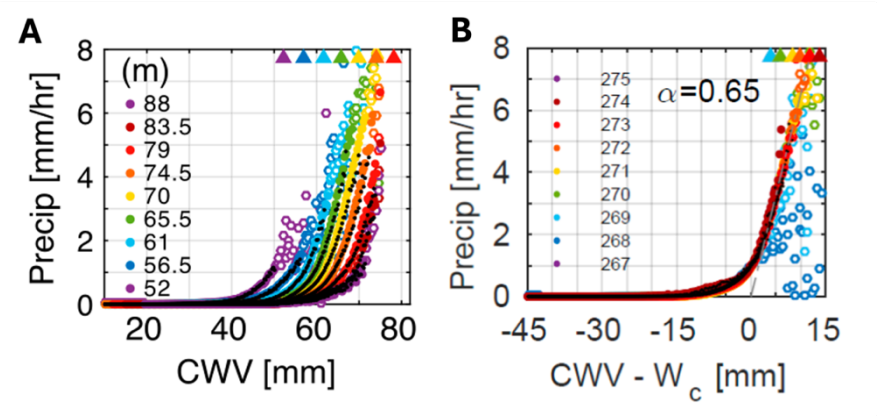

Fig. 3. a) Precipitation rate averaged across CWV bins and separated by column-integrated saturation specific humidity in mm. b) Collapsed precipitation rate averaged across CWV bins and separated by column-integrated temperature in K. The grey line indicates the line of best fit for the computation of the critical value. From Kuo et al. (2018).

In discussing the moisture-precipitation relationship across the CMIP ensemble, a steeper slope is also indicative of higher rates of entrainment in a given model. This is clearly illustrated by the modeling results of Kuo et al. (2017) (Figure 4), whereby a reduction of the entrainment rate below default values reduces the slope of the pickup considerably. This is indicative of deep convection onset at lower CWV and generally across a broader range of CWV values (see also probability and PDFs in Figure 4) and, therefore, a reduced sensitivity of convective precipitation to CWV, as one would expect.

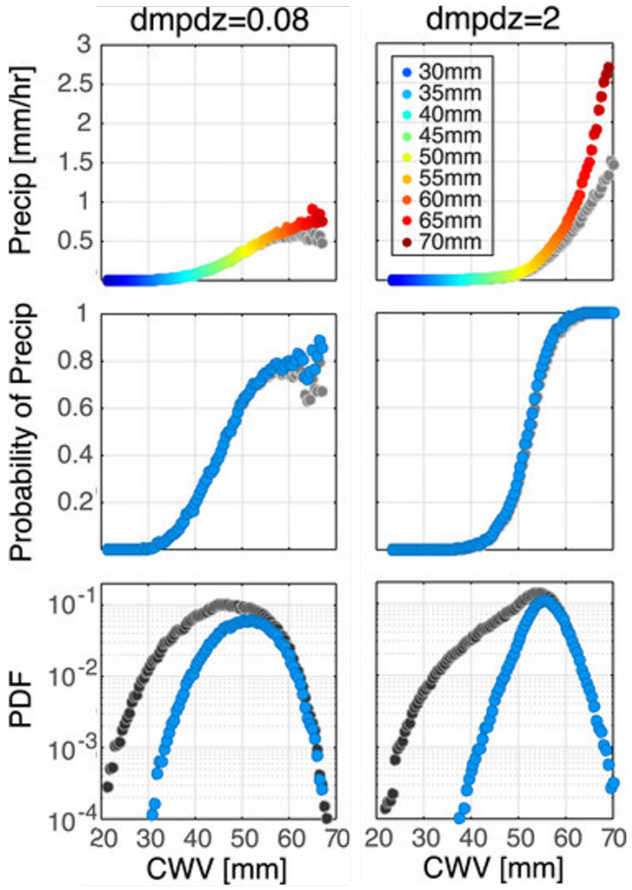

Fig. 4. The CESM-simulated convective transition statistics at a site in the tropical western Pacific (Manus Island, at location of DOE ARM site) for various entrainment (dmpdz) cases: (left) 0.08 km^{-1} (low entrainment) and (right) 2.0 km^{-1} (high entrainment). Note that the CESM default in this model version is 1 km^{-1}. (top) The average total (color) and convective (gray) precipitation rate conditionally averaged by column water vapor (CWV). (middle) The probability of total (blue; $P >$ 0.1 mm h^{-1}) and convective (gray; $P_c >$ 0.1 mm h^{-1}) precipitation. (bottom) The PDF of CWV for all (dark gray) and precipitating (blue; $P >$ 0.1 mm h^{-1}) events. Adapted from Kuo et al. (2017).

To apply this method, first, at every grid box and timestep, vertical profiles of specific humidity are integrated into column-integrated mass-weighted specific humidity. Additionally, vertical profiles of temperature are converted to saturation specific humidity and integrated over the column. 6-hourly column relative humidity (CRH) is then calculated as the ratio of specific

humidity to saturation specific humidity. Then, instantaneous temperature and CRH are collocated with precipitation rates for the following 3-hourly period. Considering values from 20°N-20°S, precipitation curves are conditionally averaged on CRH for each column average temperature from 267 to 274 K. This is adjusted to the four most common temperatures following the finding that the middle quartiles of data for each model fall across varying temperature ranges. To collapse the precipitation curves, the threshold for precipitation is defined as .15 mm/hr and each curve is shifted by the CRH value corresponding to that precipitation rate such that the transition to precipitating regimes across all curves is placed at 0 on the x-axis. The critical CRH value is computed as the x-intercept of the linear regression of points falling between .2 and .4 mm/hr. Because this analysis is focused on the increase of precipitation with increasing environmental moisture and there are fewer data points at the higher precipitation rates which may cause a fluctuation of precipitation rates at the highest CRH values, points are only included in the regression that increase monotonically.

Finally, for analysis of the relationship between convective sensitivity to moisture and high cloud fraction using 2-dimensional cloud area fraction (*cl*), model output is first interpolated to common standard pressure levels, and tropical mean (30°S - 30°N) time mean *cl* vertical profiles are computed. High cloud fraction is defined as the maximum of cloud fraction between 400 and 150 hPa to characterize the coverage of anvil clouds, which typically exist at the level of maximum detrainment at around 200 hPa (Hartmann & Larson, 2002).

5.3 Precipitation Efficiency and Convective Organization Relationship to High Cloud Feedbacks

5.3.1 Precipitation Efficiency

Precipitation efficiency is calculated using the large-scale definition published by Li et al. (2022). Efficiency is defined following:

$$\varepsilon = \frac{P_S}{CWP} \quad (8)$$

Here, ε is precipitation efficiency, P_s is surface precipitation rate, and CWP is vertically integrated condensed water and ice in the column. To compute the tropical mean change in precipitation efficiency, a ratio is taken as *pr*/*clwvi* at every monthly timestep and gridbox in both the early and late abrupt-4xCO2 periods. Li et al. (2022) note that particularly in arid regions such as the Arabian Peninsula, local precipitation efficiency can be large and is therefore not a suitable metric. This is observed at some grid points and timesteps in which precipitation efficiency is computed as infinite or very large ($> 10^6$ s^{-1}). To account for these outliers, a filter is applied before taking a tropical and time mean such that any precipitation efficiency values > 1 s^{-1} are removed from the data. This threshold is chosen because the inverse of precipitation efficiency represents the residence time for condensed water in the atmosphere (Li et al., 2022), so a timescale of 1 second represents a conservative lower bound. After applying this filter, tropical mean (30°S - 30°N) and time mean averages are taken across the early and late abrupt-4xCO2 periods, differenced, and divided by the global mean change in surface temperature. Ascent and descent region precipitation efficiency are computed as area weighted averages constrained by monthly ω_{500} values across the early abrupt-4xCO2 experiments, where ascent regions are characterized by $\omega_{500} < 0$ hPa day^{-1} and descent regions > 0 hPa day^{-1}.

5.3.2 Convective Organization

Mesoscale convective organization is defined using the methods employed by Bläckberg and Singh (2022). First, in both the early and late abrupt-4xCO2 experiments, tropical (30°S - 30°N) grid boxes are filtered at every timestep to include only *pr* values that are greater than or equal to the 97th percentile of tropical precipitation rate computed across all grid points at that timestep and within a given model. This guarantees that the total area fraction representing

convection remains the same, ensuring an apples-to-apples comparison between models (Tobin et al., 2012). Convective objects are then defined using 8-connectivity, meaning that contiguous boxes including those that are situated diagonally, are considered a single "cluster."

Following definition of convective objects, Radar Organization Metric (ROME) is utilized to characterize the organization of convection (Retsch et al., 2020). ROME is a measure of organization that considers both the distance between convective objects and their size. Between two convective objects, ROME assigns a measure of organization defined as follows:

$$ROME = A_a + \min\left(1, \frac{A_b}{A_d}\right) A_b \quad (9)$$

Here, A_a is the area of the larger object in km^2, A_b is the area of the smaller object in km^2, and A_d is the square of the shortest distance between the two objects (Figure 5). This yields a metric composed of the summation of the larger object's area with the smaller object's area weighted by the distance between the two objects. As a result, objects that are larger and closer together are considered more organized and yield higher values of ROME. At every timestep, this calculation is applied to each unique pair of the 8 largest convective objects across a scene, and an average is taken across all pairs. The change in organization is computed as a difference of the time mean value of ROME across the late abrupt-4xCO2 period and the early abrupt-4xCO2 period normalized by the global mean change in surface temperature. The fractional change in organization is defined as the late period ROME minus the early period ROME, normalized by the early period ROME and the global mean change in surface temperature.

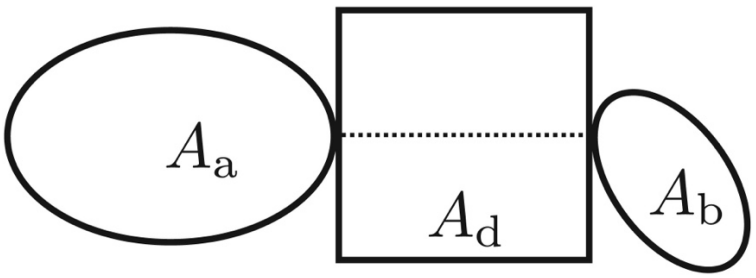

Fig. 5. Schematic depicting two convective objects and the dimensions used to calculate ROME. From Retsch et al. (2020).

6. Results

6.1 High Cloud Feedback Relationships to ECS

6.1.1 Net High Cloud Feedback

To quantify the relationship between intermodel variability of the tropical net high cloud feedback and intermodel variability of climate sensitivity, the tropical mean net high cloud feedback (Figure 6a) and the local net high cloud feedback at each grid box (Figure 6b) are correlated with ECS. The tropical mean net high cloud feedback is significantly correlated to ECS ($r = 0.66$; $p < 0.001$). Building on literature highlighting uncertainty in tropical cloud feedbacks (Vial et al., 2013), this relationship signifies that intermodel variability in tropical high clouds is driving a non-negligible portion of intermodel variability in ECS, thus motivating further analysis of the sources of spread in tropical high cloud feedbacks. The strongest positive local correlations between the net high cloud feedback and ECS (red shading) are found in climatological descent regions, particularly in the eastern equatorial Pacific. In contrast, deep convective zones, where high clouds are climatologically most abundant, display weak correlations or anticorrelations (blue shading) between the local net high cloud feedback and

ECS, indicating that variability in high cloud feedbacks in the areas of strongest ascent are not strongly driving the spread in ECS.

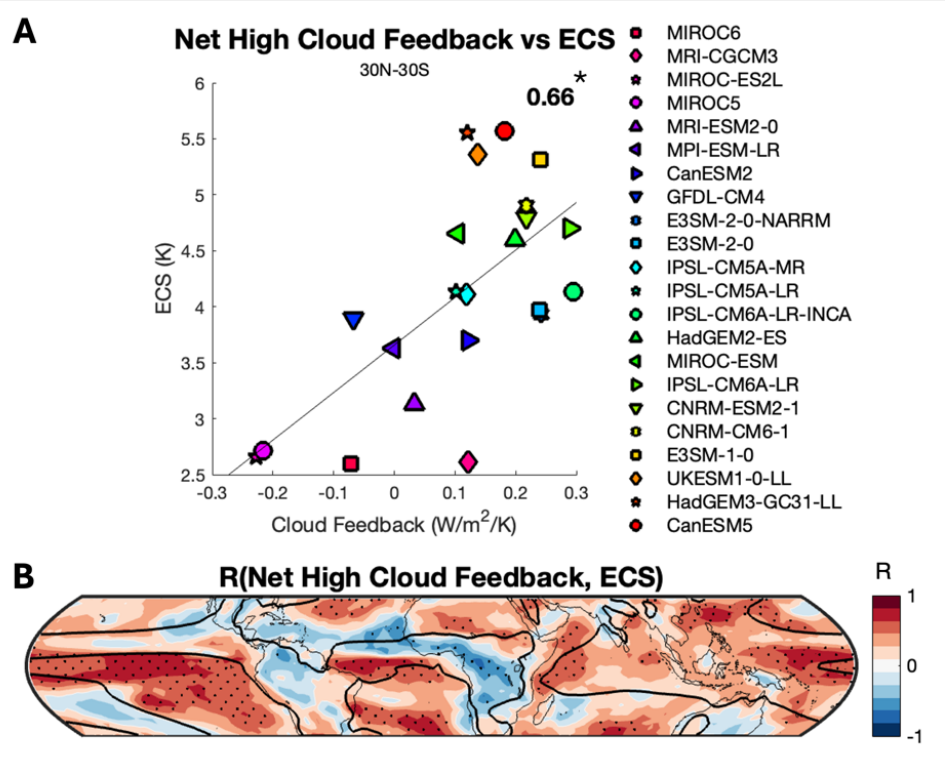

Fig. 6. a) Tropical mean relationship between the net high cloud feedback and ECS. The Pearson correlation coefficient is in bold and statistical significance at $\alpha = .05$ is indicated by an asterisk. Models are listed in order of increasing ECS. b) Spatial correlation of the local net high cloud feedback and ECS. The multi-model mean early period abrupt-4xCO2 experiment $\omega_{500} = 0$ contour is depicted by the thick black line. Significance at $\alpha = .05$ is indicated by stippling.

To compare differences in the spatial arrangement of the net high cloud feedback across the tropics, the high cloud feedback is visualized across a high ECS (Figure 7a) and low ECS (Figure 7b) group. Both show strong, positive feedbacks in narrow bands along the Pacific ITCZ and weaker positive feedbacks across equatorial land regions. Notably, the low ECS composite

displays strong negative feedbacks along the equatorial Pacific and Atlantic regions in addition to subtropical ocean basins, which are absent from the high ECS map. Figure 7c confirms that this near-equatorial band is the region where the feedbacks diverge the most between the two groups. Additionally, this provides supporting evidence that the strongest local correlations shown in Figure 6b are relevant for the tropics-wide relationship between the net high cloud feedback and ECS. Reflecting the spatial pattern of the local correlations between the net high cloud feedback and ECS, the descent region relationship is stronger ($r = 0.71$; $p < 0.001$) than the ascent region relationship ($r = 0.53$; $p = 0.012$). In sum, these results suggest that variability in high cloud feedbacks on convective margins and in regions of climatological descent are more strongly related to the spread in ECS than high cloud feedbacks in tropical deep convective zones.

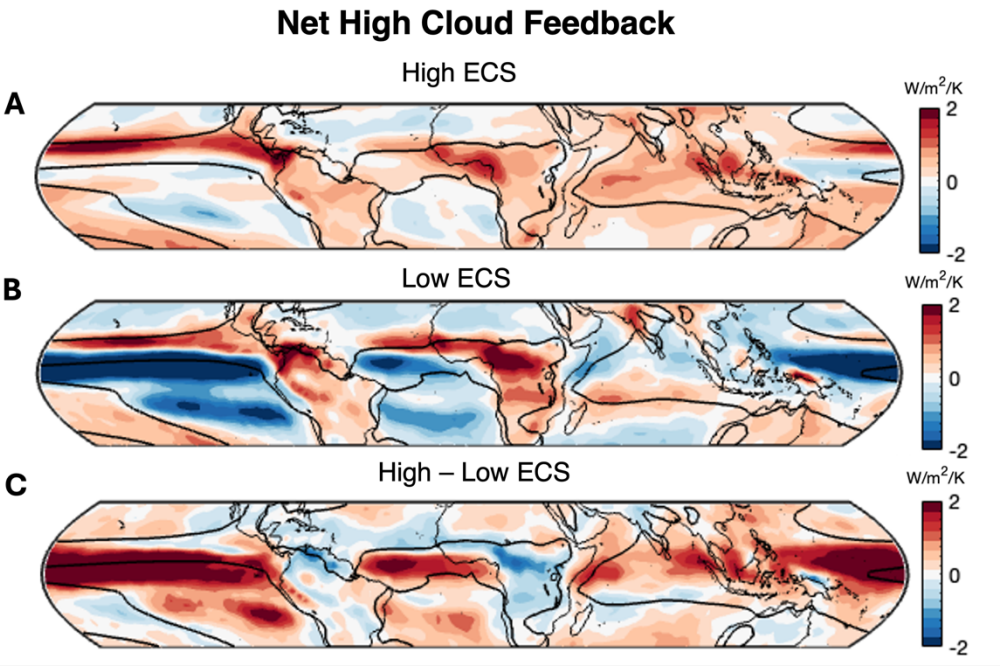

Fig. 7. Net high cloud feedback for the a) high ECS group, (b) low ECS (≤ 3.7 K) group, and c) difference between the high and low ECS groups.

6.1.2 High Cloud Altitude Feedback

Next, the relationship between the tropical high cloud altitude feedback and ECS is analyzed. The tropical mean high cloud altitude feedback is significantly correlated with ECS ($r = 0.55$; $p = 0.007$; Figure 8a). This relationship suggests that the intermodel variability of the high cloud altitude feedback is a non-trivial driver in the intermodel variability in ECS. The tropical mean high cloud altitude feedback is positive in 20 models and near-zero in the remaining two models, mimicking the results found by Zelinka et al. (2022) in an ensemble of 19 GCMs. This is expected given that the high cloud altitude feedback has support for being positive from theory (Hartmann & Larson, 2002; Zelinka & Hartmann, 2010), observations (Xu et al. 2007; Zelinka & Hartmann, 2011), and GCMs (Bony et al., 2016; Zelinka & Hartmann, 2010). Visualizing the correlations between the local high cloud altitude feedback and ECS over space mimics the pattern displayed by the net high cloud feedback (Figure 8b). Both patterns show the strongest correlations to ECS in the equatorial Pacific and east Pacific subtropical ocean and anticorrelations in ascent regions across the Amazon and Congo. The high cloud altitude feedback displays positive correlations that extend further into the Maritime Continent and Warm Pool than demonstrated by the net high cloud feedback.

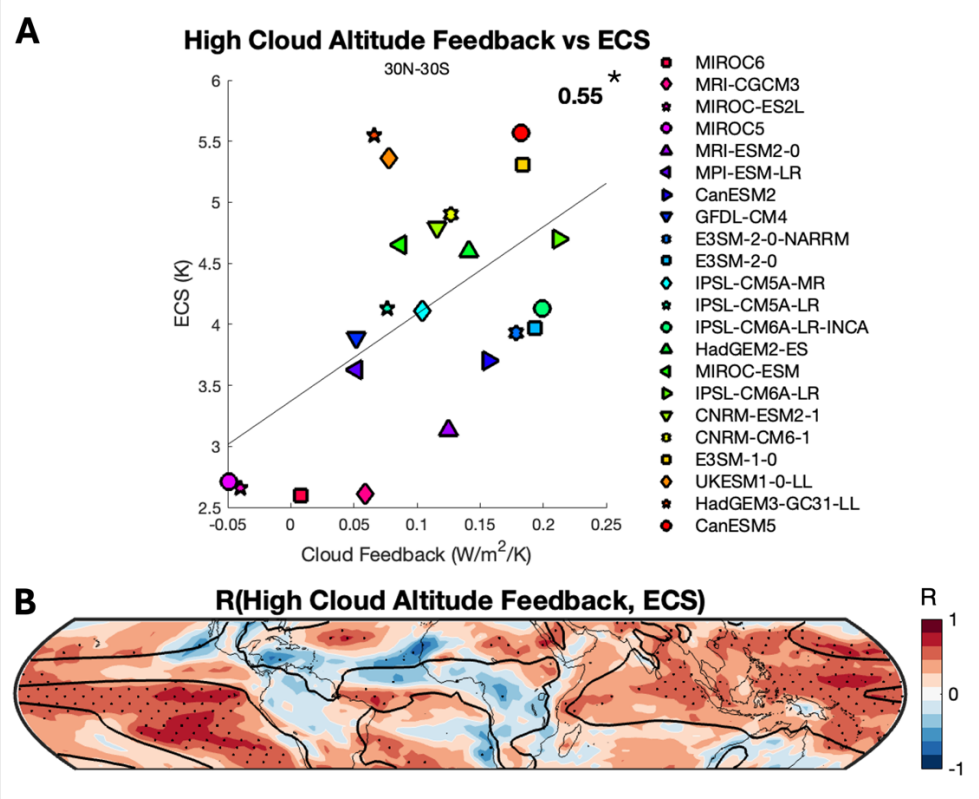

Fig. 8. As in Figure 6, but for the high cloud altitude feedback.

The composited high and low ECS high cloud altitude feedback maps and the difference between them are shown in Figure 9. The high cloud altitude feedback composited for the 7 highest ECS models (Figure 9a) demonstrates positive values across most of the tropics with the largest magnitude in Pacific ITCZ and Congo regions. This is indicative of a rising of high clouds across most of the tropics. In contrast, the high cloud altitude feedback composited for the 7 lowest ECS models (Figure 9b) shows strong, positive values that are limited to the deep convective regions of the ITCZ and Congo and smaller positive magnitudes or even negative high cloud altitude feedbacks across the Pacific basin. The largest difference in the two groups comes from the equatorial central Pacific and east Pacific subsidence regions (Figure 9c), affirming that the significant correlations shown in Figure 8b are relevant for the tropical-mean correlation. This difference is also qualitatively similar to that displayed by the net high cloud

feedback in Figure 7c, albeit with a smaller relative difference along the Pacific equatorial zone. As with the net high cloud feedback relationship to ECS, the correlation between the high cloud altitude feedback constrained to descent regions ($r = 0.63$; $p = 0.017$) and ECS is stronger than the relationship between the ascent region high cloud altitude feedback and ECS ($r = 0.50$; $p = 0.018$). In sum, these results suggest that intermodel variability in the tropical high cloud altitude feedback, particularly across convective margins along the Pacific ITCZ, are contributing to intermodel variability in climate sensitivity and are qualitatively similar to the relationships found between the net high cloud feedback and ECS.

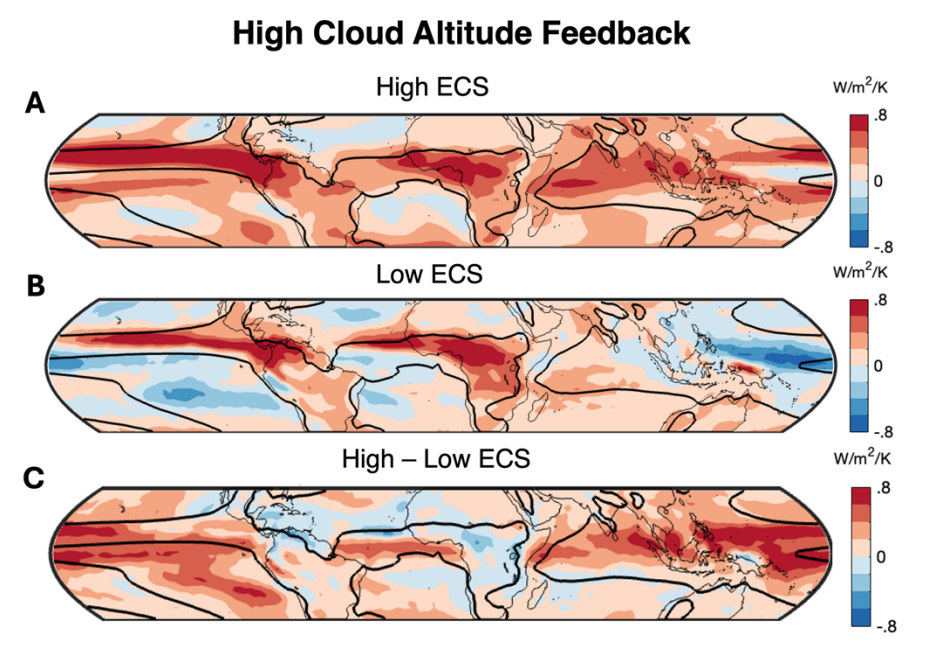

Fig. 9. As in Figure 7, but for the high cloud altitude feedback.

6.1.3 High Cloud Optical Depth Feedback

The correlation between the tropical mean high cloud optical depth feedback and ECS is shown in Figure 10a ($r = 0.54$; $p = 0.01$). As with the high cloud altitude feedback, this significant relationship suggests that variability in the high cloud optical depth feedback is driving variability in climate sensitivity. 10 out of 22 models exhibit a positive high cloud optical

depth feedback, which corresponds to a net thinning of high clouds with warming. The disagreement in the ensemble around the sign of the high cloud optical depth feedback reflects the uncertainty of the net radiative impact of changes to cloud opacity in GCMs that has only been noted in recent intermodel comparisons (Sokol et al., 2024; Zelinka et al., 2022). Visualizing this relationship over space demonstrates that significant positive correlations are limited to convective margins such as the eastern equatorial Pacific, equatorial Atlantic, and North Africa (Figure 10b). While deep convective cores are found in observations primarily across tropical ascent regions (Houze et al., 2015), thinner high clouds are spread more ubiquitously across the tropics (Sassen et al., 2009). Thus, the pattern demonstrated by Figure 10b could indicate that changes to anvils extending away from areas of deep convection are primarily responsible for the overall correlation between the tropical high cloud optical depth feedback and climate sensitivity.

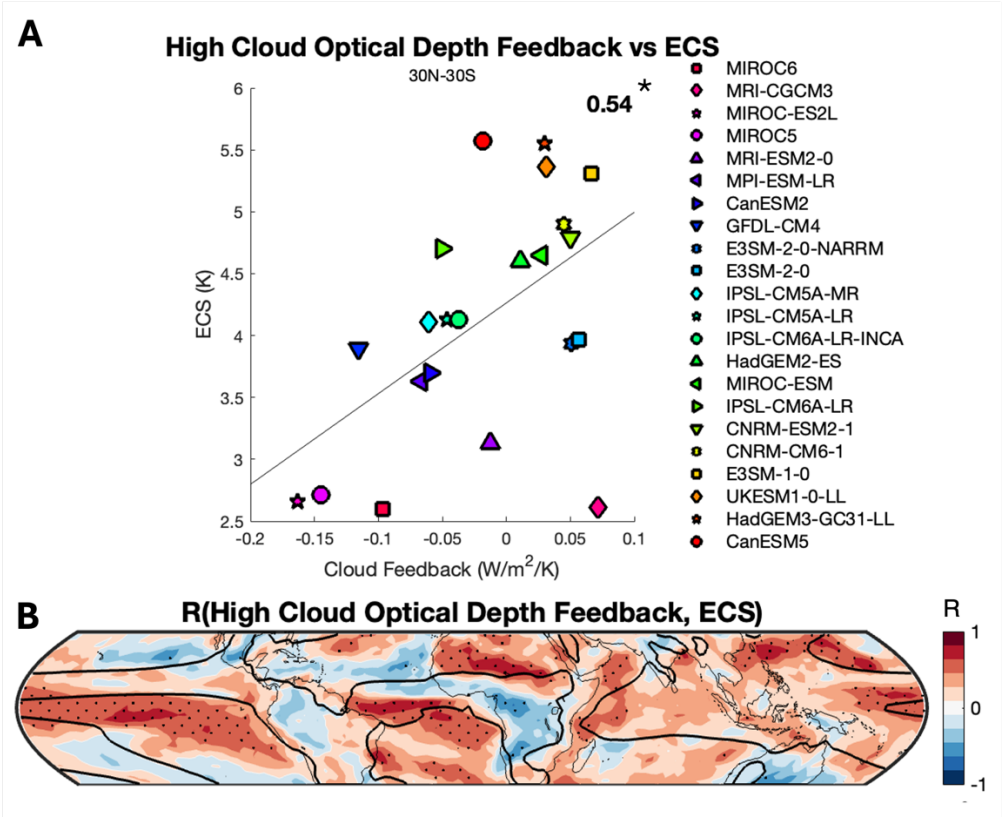

Fig. 10. As in Figure 6, but for the high cloud optical depth feedback.

The high and low ECS composited maps of the high cloud optical depth feedback are shown in Figure 11. Both groups demonstrate a band of positive feedbacks within the east Pacific ITCZ, corresponding to a thinning of high clouds. This is accompanied by negative optical depth feedbacks immediately to the south, representing a thickening of the high cloud population. However, the low ECS composite shows a much more negative magnitude and greater spatial extent of the negative feedbacks, indicating enhanced thickening. This pattern could be representative of a southward and eastward shift of convection across the Pacific under long-term warming that has previously been identified in CMIP models (Mamalakis et al., 2021; Vecchi & Soden, 2007). Visualizing the difference between the high and low ECS groups

confirms that the greatest difference in the changes to high cloud optical depth among models is in the Pacific and Atlantic ITCZ regions (Figure 11c).

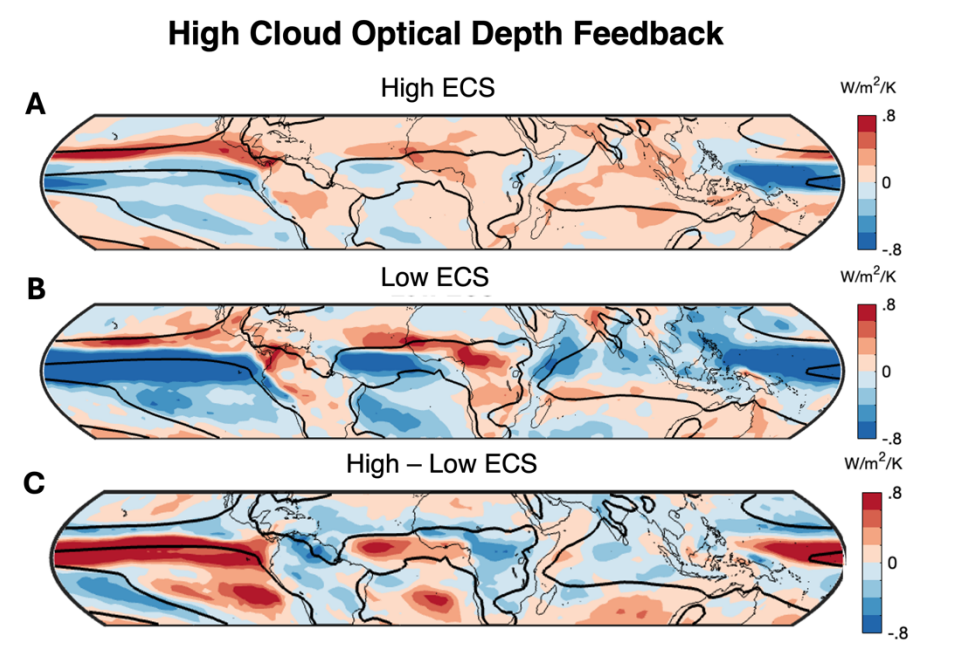

Fig. 11. As in Figure 7, but for the high cloud optical depth feedback.

As with the high cloud altitude feedback, the correlation between the high cloud optical depth feedback constrained to descent regions ($r = 0.64$; $p = 0.001$) and ECS is stronger than the relationship between the ascent region high cloud optical depth feedback and ECS ($r = 0.44$; $p = 0.039$). Considering analysis of both the high cloud altitude and optical depth feedback, these results suggest that variability in the effects of changes to high cloud altitude and optical depth, particularly along convective margins adjacent to the Pacific ITCZ, are contributing to intermodel variability in climate sensitivity such that high ECS models experience a more positive altitude feedback and less negative optical depth feedback in this region, which is driving the tropical-mean spread in the feedbacks.

6.1.4 High Cloud Amount Feedback

Finally, the relationship between the high cloud amount feedback and climate sensitivity is assessed. The high cloud amount feedback is uncorrelated with ECS in the tropical mean ($r = 0.16$; $p = 0.53$; Figure 12a). The weakness of this relationship suggests that the tropical mean high cloud amount feedback is not a primary driver of intermodel variability in climate sensitivity. Moreover, the range of the amount feedback across models is smaller than the range of values produced by the high cloud altitude and optical depth feedbacks, with many models clustering around 0 W m^{-2} K^{-1}. This is not surprising given that anvils have an approximately neutral radiative effect resulting from the cancellation between the large positive longwave and negative shortwave radiative effects of thin and thick clouds (Hartmann & Berry, 2017). The spatial arrangement of local correlations between the high cloud amount feedback and ECS (Figure 12b) does not yield extensive regions of significant correlations between the amount feedback and ECS as the high cloud altitude and optical depth feedbacks did. However, descent regions generally show correlations and ascent regions display anticorrelations, qualitatively matching the pattern exhibited by the net high cloud feedback.

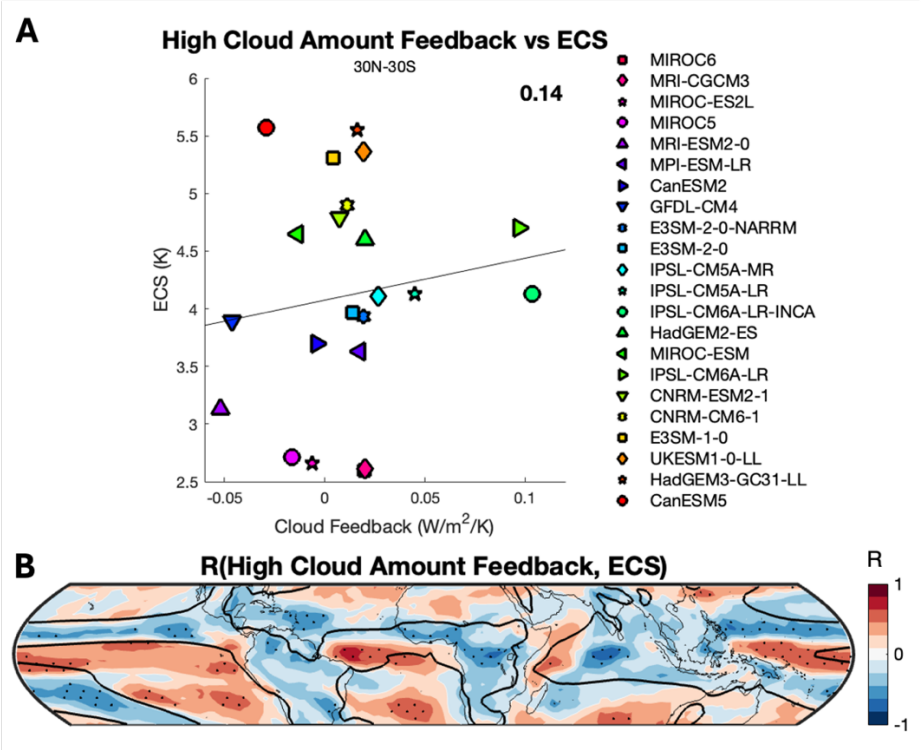

Fig. 12. As in Figure 6, but for the high cloud amount feedback.

The high and low ECS composited maps of the high cloud amount feedback generally demonstrate negative values across descent regions and convective margins and positive values in the regions of strongest ascent (Figure 13a-b). Both the positive and negative high cloud amount feedback magnitudes are stronger in the low ECS composite than the high ECS composite. Because the amount feedback characterizes the radiative effect of a change in high cloud amount separate from changes to cloud opacity or altitude, a loss of high clouds could yield a positive or negative amount feedback depending on the climatological high cloud opacity. Figure 14 shows the local net change in high clouds across the high and low ECS composites. Both groups demonstrate a net loss of high clouds in the deep tropics with warming, corresponding to a positive high cloud amount feedback, and a net increase in high cloud amount in descent regions, corresponding to a negative high cloud amount feedback. Given this

additional context, low ECS models generally see a greater decrease of high clouds in ascent regions and a greater increase in high cloud amount in descent regions, resulting in more positive and negative high cloud amount feedbacks, respectively.

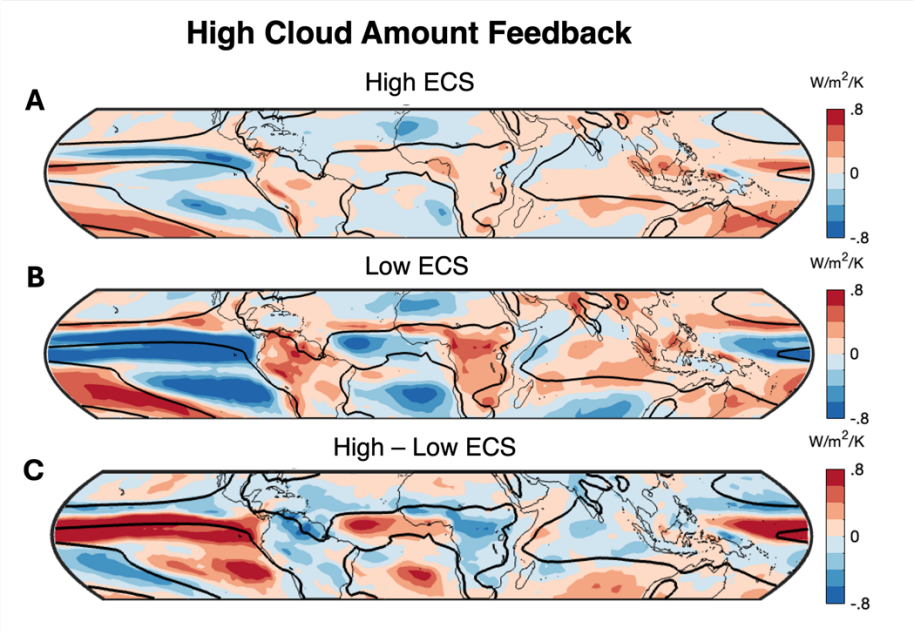

Fig. 13. As in Figure 7, but for the high cloud amount feedback.

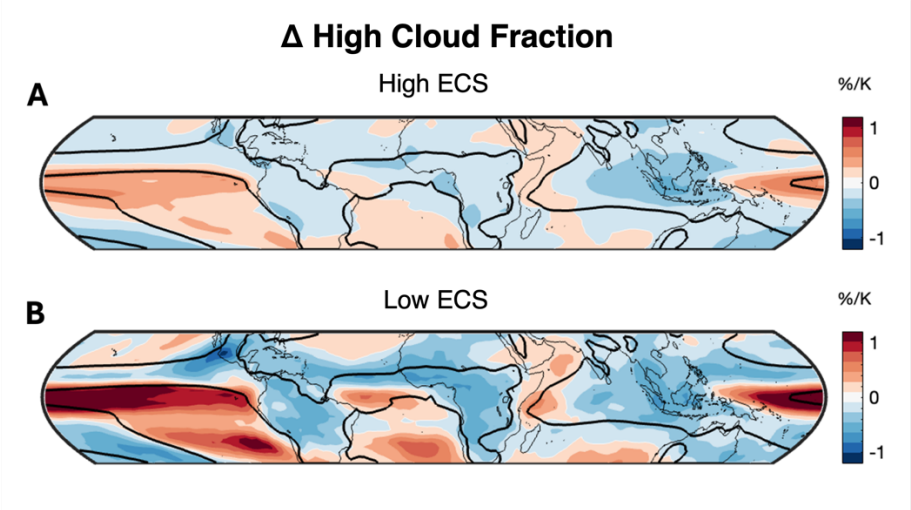

Fig. 14. Normalized change in high cloud fraction (680-50 hPa) for the a) high ECS and b) low ECS group between the early and late abrupt-4xCO2 periods.

These conclusions are limited in their robustness by weak correlations of the ascent ($r = -0.24$; $p = 0.29$) and descent region ($r = 0.44$; $p = 0.04$) high cloud amount feedback with ECS. Overall, these results suggest that variability in the high cloud amount feedback is a relatively weak driver of the intermodel variability of climate sensitivity in comparison to the high cloud altitude and optical depth feedbacks.

In summary, the tropical mean net high cloud feedback is strongly correlated with climate sensitivity, arising from significant tropical mean correlations between the high cloud altitude feedback and high cloud optical depth feedback and ECS. The high cloud amount feedback is a relatively weaker driver of the spread in ECS in comparison. Additionally, the net high cloud feedback, high cloud altitude feedback, and high cloud optical depth feedback relationships to ECS are strongest outside of the deep tropics, highlighting convective margins and descent regions as areas driving the tropics-wide spread in each component.

6.2 Mean State High Cloud Relationships to ECS and High Cloud Feedbacks

6.2.1 High Cloud Relationships to ECS

Following the robust correlations found between high cloud feedbacks and ECS, the relationships between the intermodel spread in mean state high cloud characteristics and intermodel spread in high cloud feedbacks are explored as potential opportunities for emergent constraints. Figure 15 shows the high ECS composite, low ECS composite, and difference in climatological high cloud fraction between the high and low ECS groups averaged from 30°N to 30°S and conditionally sampled on vertical velocity at 500 hPa (ω_{500}) and pressure using output from the *cl* variable. Both groups see a maximum of high cloud fraction in strong ascent conditions around 200 hPa (Figure 15a-b), which corresponds to the level of maximum detrainment where anvil extent is greatest (Hartmann & Larson, 2002; Zelinka & Hartmann,

2011). High ECS models show greater high cloud fraction in the upper troposphere in ascent regions (at vertical velocities < 0 hPa day^{-1}), particularly between 400 hPa and 100 hPa (Figure 15c). This aligns with the findings of Su et al. (2014). Figure 16 displays the high ECS composite, low ECS composite, and difference in climatological cloud fraction between the two groups using ISCCP output organized in CTP-τ space. High ECS models have, in sum, more thin high clouds than low ECS models in the 680-150 hPa bins, whereas low ECS models have more thick high clouds than high ECS models.

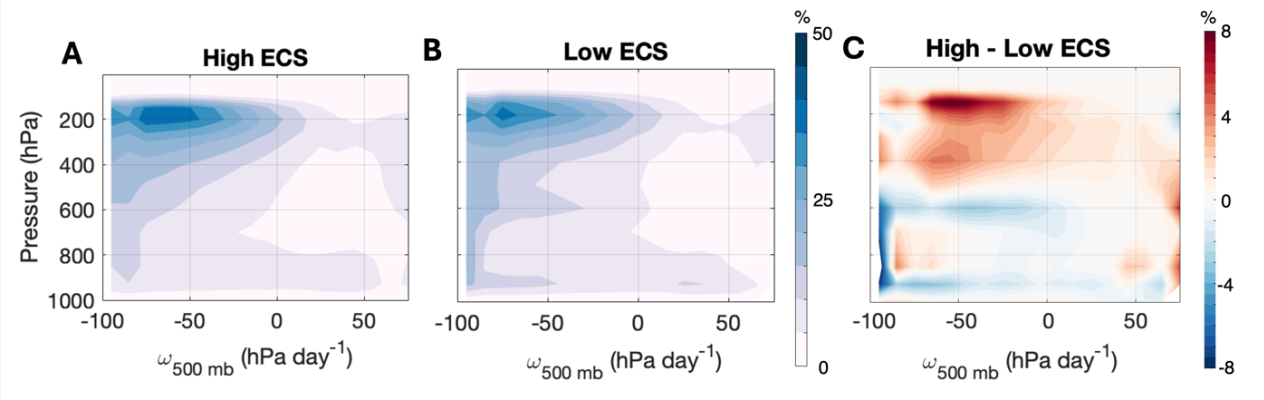

Fig. 15. Composited piControl/piClim-control experiment tropical mean (30°N - 30°S) cloud fraction conditionally averaged on pressure and ω_{500} between the a) high ECS (≥ 4.7 K) group, b) low ECS (≤ 3.7 K) group, and c) difference of high and low ECS groups from the *cl* output.

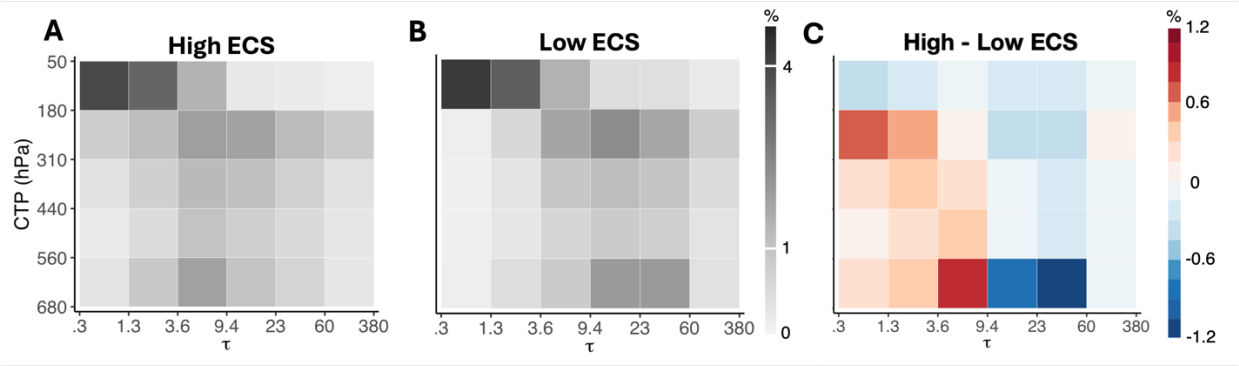

Fig. 16. As in Figure 15, but using ISSCP simulator output from the *clisccp* variable. Only the free tropospheric portion of the histogram is shown.

To further understand how the relationships between mean state high cloud fraction and ECS arrange over space, the local correlations between different measures of high cloud fraction, defined as ISCCP output summed between 680 hPa < CTP < 50 hPa, and ECS at each grid box are mapped. Thin high cloud fraction ($.3 < \tau < 9.4$) is significantly correlated to ECS in regions of climatological ascent, particularly equatorial land regions (Figure 17a). This is reflected in a significant correlation between thin high cloud fraction constrained across each model's ascent region and ECS ($r = 0.50$; $p = 0.018$; Figure 17c). In contrast, thin high cloud fraction is unrelated to ECS across descent regions ($r = 0.20$, $p = 0.38$; Figure 17d).

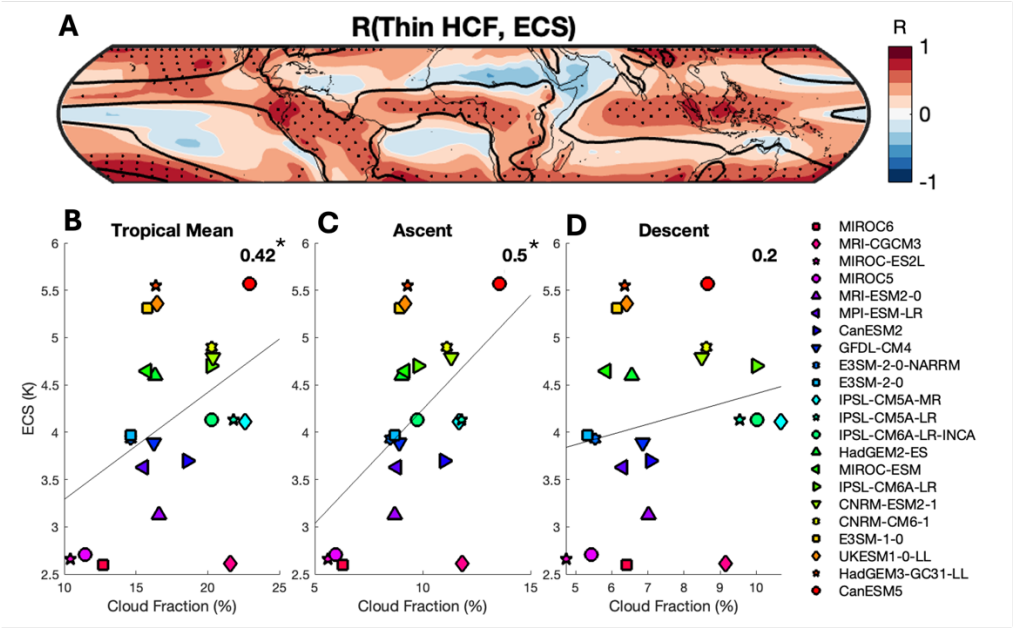

Fig. 17. a) As in Figure 6b but for piControl/piClim-control thin high cloud fraction. b-d) The correlation of piControl/piClim-control thin high cloud fraction and ECS across b) the tropics, c) ascent regions, and d) descent regions.

Next, the relationship between thick high cloud fraction and ECS is examined over space. Thick high cloud fraction ($9.4 < \tau < 380$) is anticorrelated with climate sensitivity across the entire tropical domain, with the strongest relationships coming from convective margins along the South Pacific convergence zone, Warm Pool, and Atlantic subtropical basins (Figure 18a). This relationship computed over the entire tropics ($r = -0.60$; $p = 0.003$; Figure 18b), within ascent regions ($r = -0.58$; $p = 0.005$; Figure 18c), and within descent regions ($r = -0.61$; $p = 0.003$; Figure 18d) varies little, indicating that models with higher ECS values tend to have climatologically fewer thick high clouds distributed across the tropics than models with lower climate sensitivities.

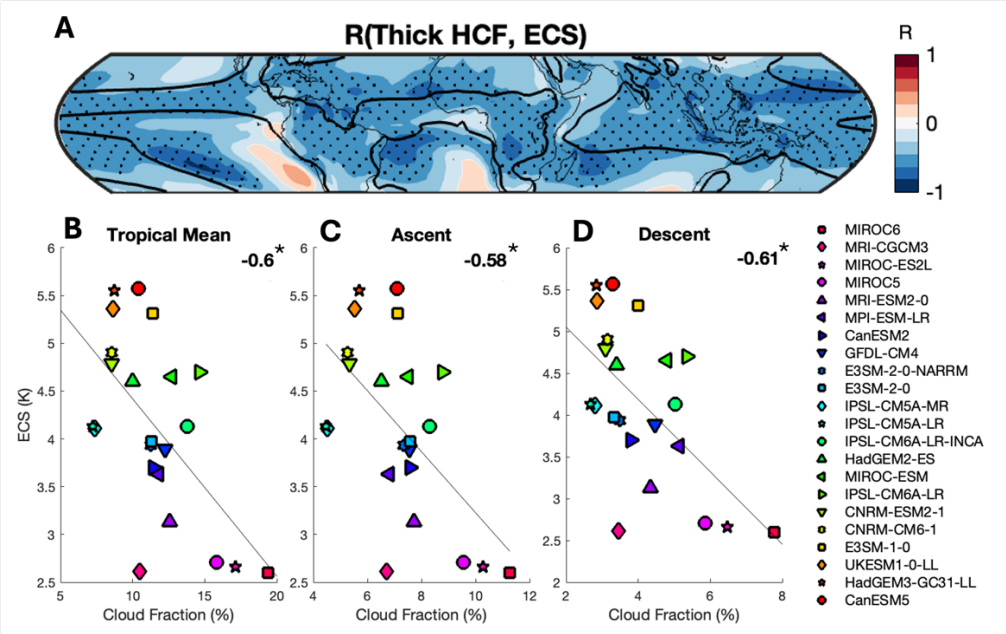

Fig. 18. As in Figure 17, but for thick high cloud fraction.

Finally, to consider mean high cloud opacity separate from high cloud amount, thick and thin high cloud fraction are combined into a single metric by taking the ratio of thick to thin high cloud fraction. Here, a higher ratio signifies a thicker high cloud population. Mean high cloud opacity is significantly anticorrelated to climate sensitivity across most of the tropics (Figure 19a) with ascent regions displaying the strongest relationships. Like the relationship between thick high cloud fraction and ECS, the anticorrelation between the ratio of thick to thin high cloud fraction and ECS is significant when considering the entire tropics ($r = -0.63$; $p = 0.002$; Figure 19b), ascent regions ($r = -0.62$; $p = 0.002$; Figure 19c) and descent regions ($r = -0.62$; $p = 0.002$; Figure 19d). These results suggest that models with higher ECS values tend to have relatively thinner high clouds across the tropics in comparison to models with lower climate sensitivities.

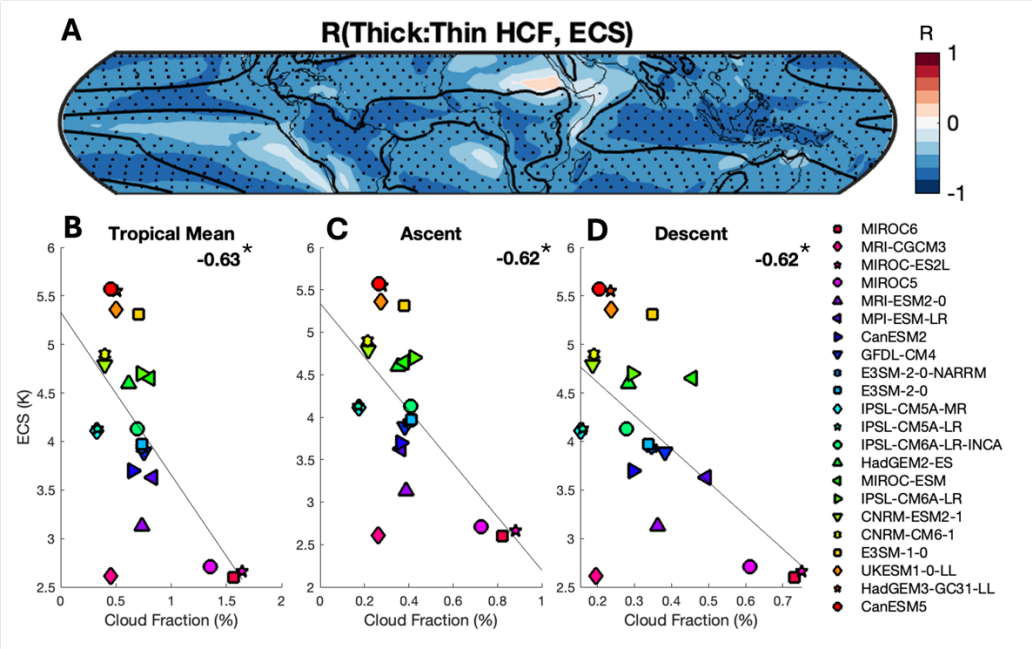

Fig. 19. As in Figure 17, but for the ratio of thick to thin high cloud fraction.

6.2.2 High Cloud Relationships to High Cloud Feedbacks

Next, relationships between mean state high cloud characteristics and high cloud feedbacks are explored to provide mechanistic explanations for the high cloud relationships to climate sensitivity - a necessity for forming emergent constraints (Klein & Hall, 2015). The high cloud altitude feedback is considered first. In their review of cloud feedbacks, Ceppi et al. (2017) suggest that the magnitude of the high cloud altitude feedback in GCMs is related to the change in high cloud top altitude, the associated decrease in longwave radiation emitted per unit increase in altitude, and climatological high cloud fraction. Here, the relationship between climatological high cloud fraction and the high cloud altitude feedback is considered to test the hypothesis that greater mean state high cloud fraction yields a more positive altitude feedback.

Figure 20 shows the correlation between high cloud fraction between 680 and 180 hPa and the high cloud altitude feedback at each grid box. High cloud fraction is summed across the troposphere excluding the highest altitude bin (180-50 hPa). This choice is made because of

discretization of ISCCP output into altitude categories such that mean state high cloud fraction in the 180-50 hPa bin cannot rise to a lower pressure and therefore is not contributing to the magnitude of the high cloud altitude feedback. Significant positive correlations are present across ascent regions characterized by deep convection, including the Amazon, equatorial Africa, and the Maritime Continent. This suggests that models that tend to simulate greater climatological high cloud fraction, particularly across ascending regions of the tropics, see more positive local high cloud altitude feedbacks. This relationship provides a plausible mechanistic linkage between mean high cloud amount and climate sensitivity through the altitude feedback.

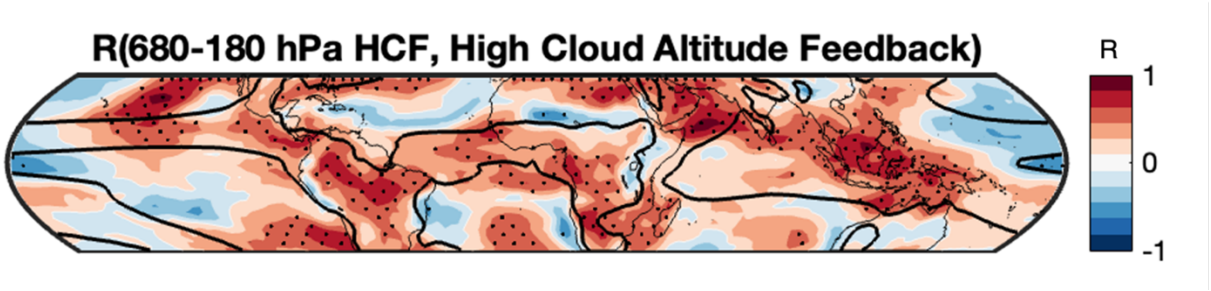

Fig. 20. Spatial correlation of 680-180 hPa cloud fraction and the high cloud altitude feedback. The multimodel mean control experiment $\omega_{500} = 0$ contour is depicted by the thick black line. Significance at $\alpha = .05$ is indicated by stippling.

In addition to the high cloud altitude feedback, correlations between mean state quantities and the high cloud amount and optical depth feedbacks are considered. Hartmann et al. (2001) hypothesize that clear and cloudy areas of the tropics maintain a similar radiative balance through a feedback process between convective intensity, high cloud albedo, and sea surface temperature (SST) gradients. Wall and Hartmann (2018) argue that this feedback could be represented in GCMs such that regions with a positive radiative imbalance will adjust through enhanced convective intensity and an increase in cloud opacity, resulting in a compensatory

decrease in the net radiative balance and a negative feedback. Thus, it is plausible that models with thinner high clouds in tropical ascent regions see an increase in high cloud amount and opacity in response to greenhouse gas forcing relative to models with more thick high clouds.

To test this hypothesis, the ratio of thick to thin high cloud fraction is correlated to the high cloud amount and optical depth feedback at each grid box across the tropics. Mean high cloud opacity is strongly correlated to the high cloud amount feedback broadly across tropical ascent regions (Figure 21). This indicates that models with thicker high clouds in deep convective regions see a more positive high cloud amount feedback, which corresponds to an enhanced loss of high clouds under warming (Figure 14). This result aligns with the logic of the purported "cloud shading feedback" (Wall et al., 2019) such that models with relatively thicker clouds, which have a strong negative shortwave effect, induce a negative radiative effect under warming that causes muted SST increases and moisture convergence alongside increases in stability, thus reducing convective activity relative to models with a thinner cloud population. The relationship flips in descent regions, displaying strong anticorrelations in the equatorial east Pacific and subtropical ocean basins. The cloud shading feedback does not explain why models with thinner clouds on convective margins experience more positive amount feedbacks associated with a muted increase in high cloud fraction. Because the amount feedback considers the effect of changes to cloud amount separate from changes across optical depths and altitudes, it is related to both the change in high cloud fraction and the radiative effect of mean state high clouds. To assess the contribution of changing high cloud amount to the amount feedback, the local correlations between the change in high cloud fraction and the high cloud amount feedback are mapped (Figure 22). In descent regions, models that see a less negative high cloud amount feedback generally have a muted increase in high cloud fraction. Thus, it likely is a combination

of both effects – models with thinner mean high cloud population and a muted increase in high clouds – that results in weaker stabilizing amount feedbacks in descent regions.

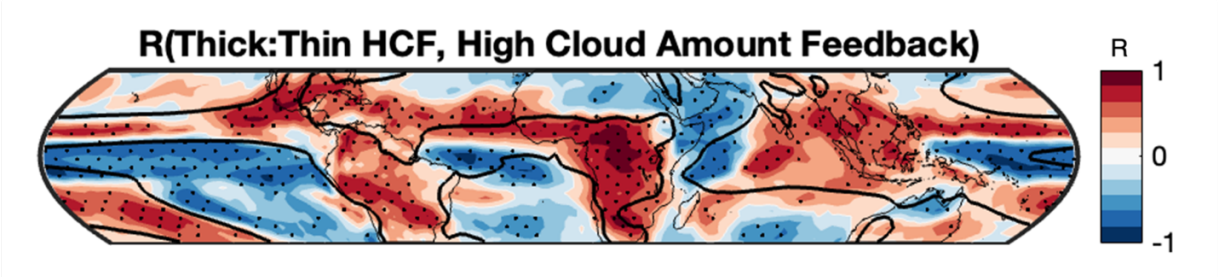

Fig. 21. As in Figure 20, but with the ratio of thick to thin high cloud fraction and the high cloud amount feedback.

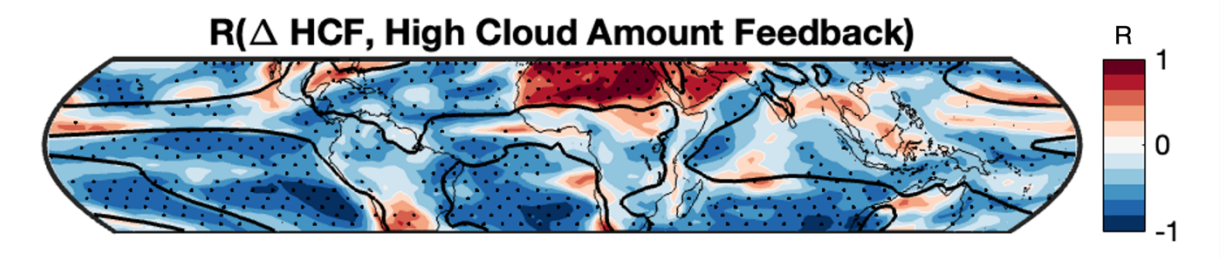

Fig. 22. As in Figure 21, but with the change in high cloud fraction and the high cloud amount feedback.

To test the hypothesis that the cloud shading feedback causes enhanced thickening in models with thinner mean state high clouds, the relationship between mean high cloud opacity and the high cloud optical depth feedback are visualized over space (Figure 23). The relationships are much weaker than those identified for the high cloud amount feedback. Convective margins, including the equatorial Central Pacific and Atlantic, display significant anticorrelations, suggesting that models with thinner high clouds in these regions experience

enhanced thinning. This result highlights behavior that is counter to the expected stabilizing effect of the cloud shading feedback.

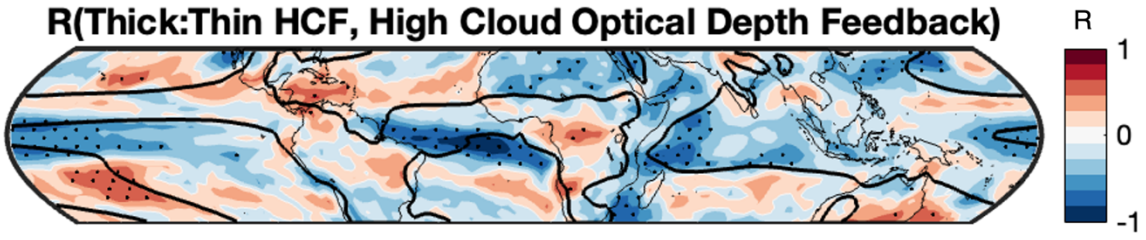

Fig. 23. As in Figure 21, but with the high cloud optical depth feedback.

Finally, to consider tropics-wide relationships between mean high cloud characteristics and high cloud feedbacks, Table 3 summarizes the tropical mean high cloud altitude, optical depth, and amount feedback correlations with mean state total high cloud fraction, thick high cloud fraction, thin high cloud fraction, and the ratio of thick to thin high cloud fraction. Generally, if a model has more thin high clouds or a greater proportion of thin high clouds in the mean state, it will have more positive altitude and optical depth feedbacks than a model with fewer thin high clouds. This helps to explain the result shown in Figure 16. The altitude feedback and total tropical mean state high cloud fraction (HCF) correlation, as well as the amount feedback and total tropical mean state HCF correlation, are significantly correlated, yet the correlation is driven strongly by the two IPSL-CM6A-LR models and thus are not considered to be robust.

Table 3

Tropical mean correlation coefficients between high cloud feedbacks (rows) and mean state high cloud quantities (columns). Significance at a =.05 is indicated by an asterisk..

	Total HCF	Thin HCF	Thick HCF	Thick:Thin HCF
High Cloud Altitude Feedback	0.53*	0.62*	0	-0.53*
High Cloud Optical Depth Feedback	0.25	0.62*	-0.45	-0.76*
High Cloud Amount Feedback	0.68*	0.59*	0.29	-0.18

In summary, high ECS models tend to have greater upper tropospheric cloud fraction than low ECS models, particularly in regions of strong ascent. This relationship is driven predominantly by a greater coverage of thin high clouds. In contrast, low ECS models have greater thick high cloud coverage broadly across the tropics relative to high ECS models. Accounting for high cloud opacity separate from total high cloud amount by taking a ratio of thick to thin high cloud fraction demonstrates that high ECS models have tropical cloud populations that are relatively thinner than shown in low ECS models. In ascent regions, greater mean state cloudiness amplifies the altitude feedback, and more thick high cloud coverage amplifies the amount feedback through a cloud shading mechanism. Finally, models with greater thin high cloud coverage and relatively thinner high cloud populations demonstrate more positive altitude and optical depth feedbacks at the tropics-wide scale.

6.2.3 Climatological High Cloud Fraction and Convective Sensitivity to Moisture

Given that tropical upper tropospheric high cloud fraction is found to vary systematically with ECS across the ensemble (Figure 15), it is worth exploring whether there are systematic relationships between intermodel differences in convective physics and mean state high cloud

properties. While it is easy to point fingers at intermodel differences in convective and microphysical parameterization, it is very difficult to identify specific parameter choices or aspects of a parameterization that differ among such a large climate model ensemble. Hence, an approach is adopted here that characterizes the sensitivity of deep convection to lower tropospheric moisture across the ensemble – a key mechanism relating the two being the entrainment rate of environmental air into updrafts –without explicitly determining intermodel differences in entrainment parameterization, though variations in the entrainment rate would be expressed through such a relationship. A number of studies have highlighted that the mean climate is highly sensitive to variations in the entrainment parameter (Del Genio & Wu, 2010; Mauritsen et al., 2012; Qian et al., 2015; Tsushima et al., 2020; Zhao, 2014), motivating the choice to explore these relationships across the CMIP ensemble.

To characterize convective sensitivity to moisture across an ensemble of GCMs, precipitation is conditionally sampled on column relative humidity (CRH). Figure 24 shows the collapsed pickup curves for 19 models. All models demonstrate a collapsing of precipitation pickup curves, evidenced by best fit-line correlations above $p = 0.85$ and validating the use of this method for characterizing precipitation pickup. Here, the models are arranged in order of increasing critical value such that models with higher critical values have a more rapid increase in precipitation with increasing column relative humidity, which is also evidenced by a steeper slope of the best-fit line. Models with lower critical values exhibit a more gradual increase of precipitation with increasing CRH, characterizing a weaker precipitation pickup. A steeper slope is indicative of higher rates of entrainment in a given model (Kuo et al., 2017), though entrainment is not the only factor controlling the characteristics of the pickup curve (Ahmed et al., 2020).

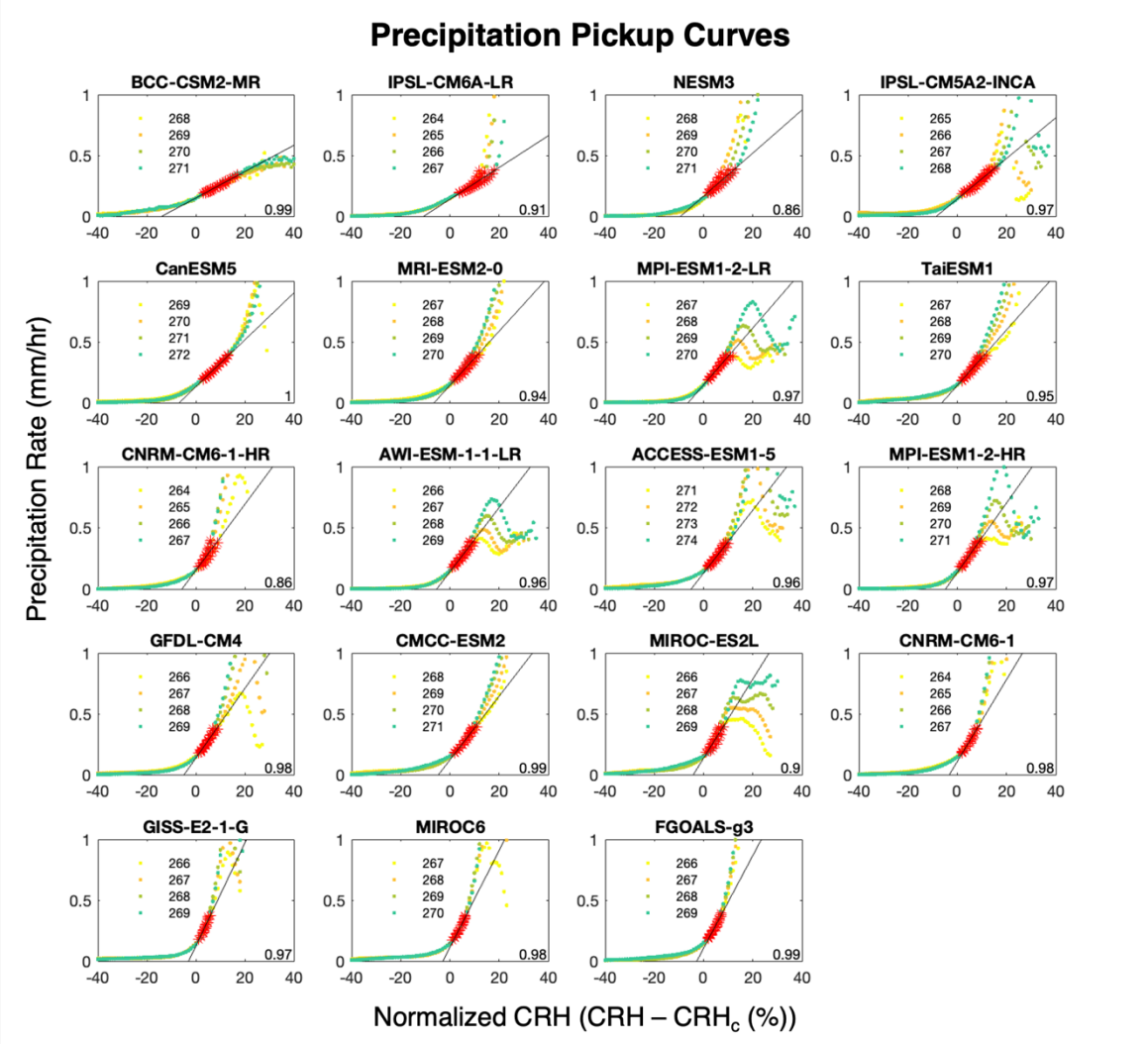

Fig. 24. Collapsed precipitation pickup curves as a function of column relative humidity and column integrated temperature. The red points indicate values that were used in the linear regression that yielded the critical value. The black line represents the best-fit linear regression. The numbers in the bottom corner indicate the correlation of collapsed and precipitation rate for the points used in the regression.

To assess the differences in the climatological cloud fields across models with different sensitivities to entrainment of moisture, cloud fraction is compared across the models with the 7 highest and 7 lowest critical values, averaged from 20°N to 20°S and conditionally sampled on

ω_{500} and pressure using output from the *cl* variable (Fig. 25a-b). The high critical value group has fewer high clouds than the low critical value group, maximizing in strong ascent regions around ω_{500} = -50 hPa day^{-1} and 200 hPa (Fig 25c). This indicates that models that are more sensitive to the entrainment of tropospheric air see fewer high clouds under strong ascent conditions and at the pressure where anvil extent is typically greatest.

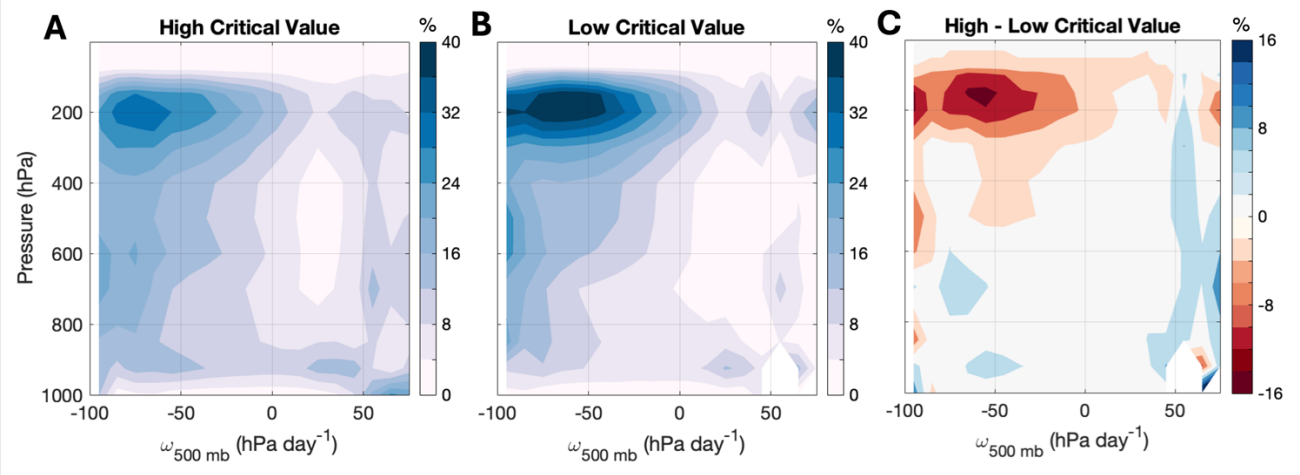

Fig. 25. As in Fig. 15 but for the a) high critical value group, b) low critical value group, and c) difference between the two groups considering output from 20°N to 20°S. The high critical value group is an average of models with the 7 highest critical values, and the low critical value group is an average of models with the 7 lowest critical values.

To identify the regions where the relationship between convective sensitivity to moisture and high cloud fraction is strongest, the local correlations between critical values and the maximum of cloud fraction between 400 and 100 hPa are visualized across the tropics (Figure 26). Significant anticorrelations are present across the Maritime Continent, Warm Pool, and South Pacific Convergence Zone. These anticorrelations highlight strong ascending regions across the Pacific as the dominant driver of the variability in climatological high cloud fraction across the groups shown in Figure 25.

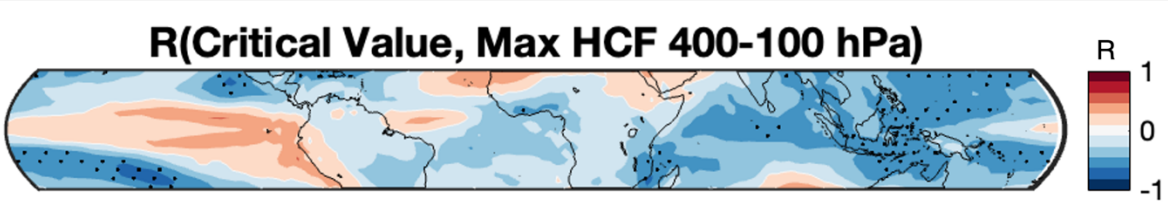

Fig. 26. Spatial correlation of critical values and maximum cloud fraction between 400 and 100 hPa from 20°N to 20°S.

Finally, to confirm that the significant anticorrelations shown in Figure 26 are indicative of regions that contain the largest spread in cloud fraction across the ensemble, composited maps of maximum cloud fraction between 400 and 100 hPa for the high and low groups and the difference between the two groups are plotted in Figure 27. While high cloud fraction is maximized across the Maritime Continent in both groups, the low critical value group demonstrates greater coverage across the Warm Pool. Additionally, the low critical value group also shows greater cloud fraction across the Atlantic ITCZ, Congo, and Amazon regions, highlighting other ascent regions as zones where high cloud fraction varies between the two groups, albeit these areas lack statistically significant correlations to critical values across the entire ensemble.

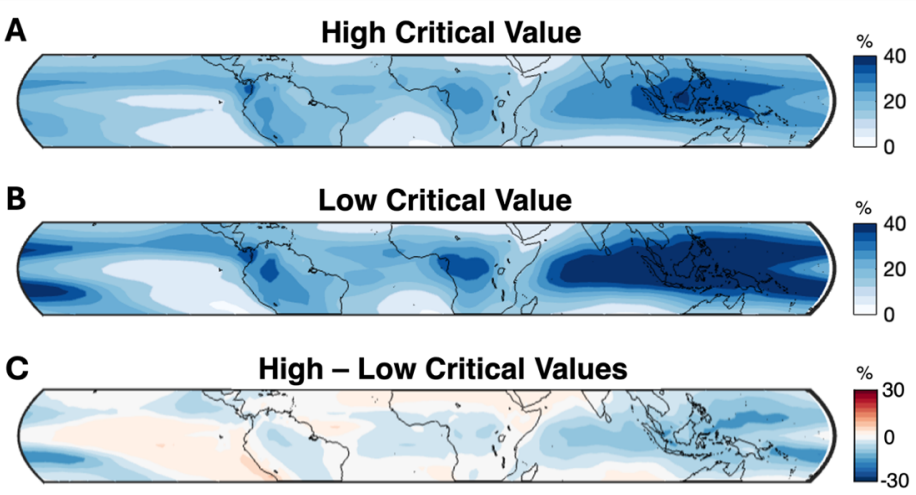

Fig. 27. Composited maximum high cloud fraction between 400 and 100 hPa between 20°N and 20°S for the a) high critical value group, b) low critical value group, and c) difference between the two groups.

In summary, intermodel variability in convective sensitivity to moisture acts as a non-trivial driver of intermodel variability in climatological high cloud fraction. Models that are more sensitive display a sharper precipitation pickup and higher critical value, exhibiting relatively fewer high clouds in strong ascending regimes particularly across the West Pacific and Indian Oceans. Models that are less sensitive experience convection across a broader range of environmental conditions and consequently display greater high cloud coverage in the deep tropics.

6.3 Precipitation Efficiency, Convective Organization, and Tropical High Cloud Feedbacks

6.3.1 Convective Organization

Next, convective organization is considered as a potential mechanism explaining variability in the high cloud amount and optical depth feedbacks across the ensemble. Similar to the results published by Bläckberg and Singh (2022), there is agreement on the sign of the

change in mesoscale organization under warming, with 19 out of the 21 models experiencing an increase in aggregation. To assess the relationship between the change in mesoscale organization under warming and the high cloud net, amount, and optical depth feedbacks, the tropical mean change in ROME is correlated to the local high cloud feedbacks and visualized across the tropics (Figure 28). All three maps demonstrate qualitatively similar patterns of relationships wherein models that see a greater increase in mesoscale organization demonstrate more positive feedbacks over the Maritime Continent, the South Pacific Convergence Zone, and northward of the climatological ascent regions along the Atlantic ITCZ (red shading). Additionally, models with a greater increase in mesoscale organization yield more negative feedbacks along the equatorial central Pacific, North Africa, and within the Atlantic ITCZ (blue shading). While none of the tropical mean correlations between the change in ROME and the net, optical depth, or amount feedbacks are significant ($r = -0.15$, $p = 0.51$; $r = 0.16$, $p = 0.49$; $r = -0.35$, $p = 0.12$, respectively), the dipole-like pattern of relationships across the Pacific, with correlations in strong ascent regions and anticorrelations on convective margins, may be indicative of dynamical shifts related to the weakening and eastward shift of the Pacific Walker circulation, the climatological pattern of ascent in the West Pacific and descent in the East Pacific, with surface warming.

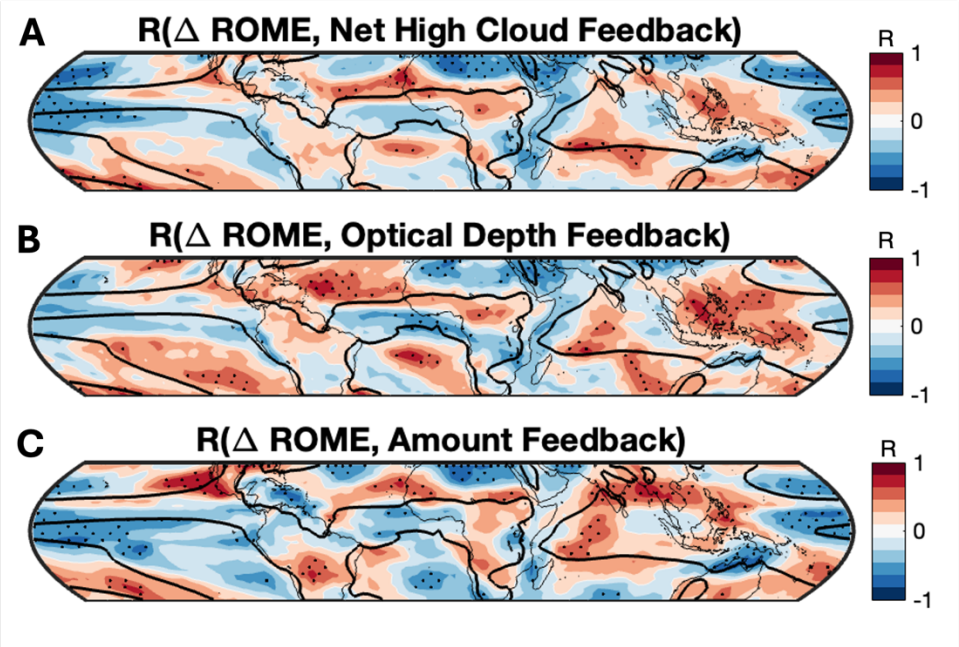

Fig. 28. Correlation of tropical mean fractional change in ROME normalized by change in surface temperature to the local a) net high cloud feedback, b) high cloud optical depth feedback, and c) high cloud amount feedback.

To test the hypothesis that the relationship between the changes in mesoscale organization and high cloud feedbacks are related to changes to the Pacific Walker circulation, the tropical mean change in ROME is correlated with the change in ω_{500} and mapped (Figure 29a). The strong correlation in the West Pacific suggests that models with a greater increase in mesoscale organization tend to see a greater weakening of ascent in this region. Note also that significant anticorrelations along the Atlantic ITCZ indicate that a greater increase in mesoscale organization is associated with a strengthening of ascent, perhaps indicative of changes in the Hadley circulation, encompassing the rising of air near the equator and subsidence in the subtropics, separate from the changes seen in the Pacific Walker circulation. These differences in the change of ascent strength are confirmed by composites of the change in ω_{500} across the groups of models representing a strong increase in ROME, weak increase or decrease in ROME,

and the difference between them (Figure 29b-d). Both sets of models generally experience a weakening of ascent in the deep tropics, a weakening of descent across subsidence regions, and a strengthening of ascent or weakening of descent along convective margins across the equatorial Pacific. The largest difference between the two composites is situated in the West and Central Pacific where models with a greater increase in aggregation demonstrate a more pronounced eastward shift and weakening of the Walker circulation than models with a weaker increase in aggregation.

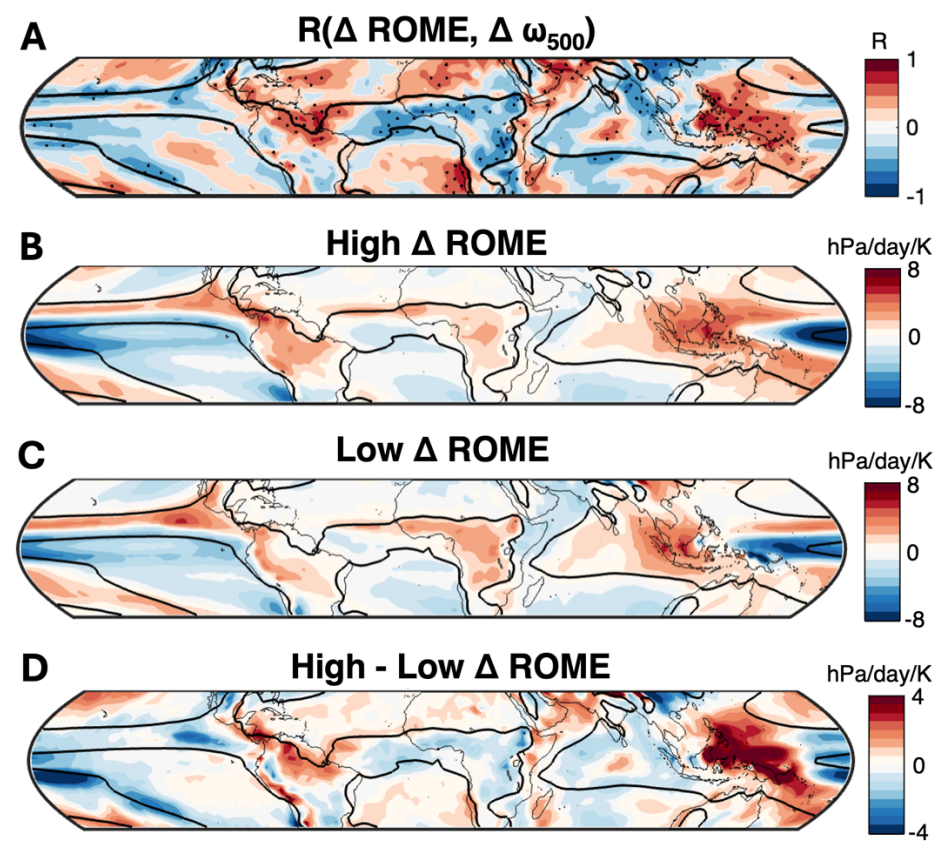

Fig. 29. a) As in Fig. 28a but with the local change in ω_{500}. b-d) Composites of the change in local ω_{500} across the 7 models with the most positive change in ROME, the 7 models with the least positive or negative change in ROME, and the difference between the high and low groups.

To further isolate the effects of changes to the Walker Cell, vertically resolved changes to vertical velocity averaged from 20°N to 20°S across the West and Central Pacific are plotted for the high and low change in ROME groups (Figure 30a-b). Both sets of models demonstrate a weakening of the Walker cell, evidenced by tendency towards descent in climatological ascent regions and tendency towards ascent in climatological descent regions. However, the high composite experiences a stronger trend towards descent over the West Pacific and a stronger trend towards ascent over the Central Pacific than the low composite. These relationships are also statistically significant across the ensemble (Figure 30c), affirming that models that experience a stronger increase in mesoscale organization demonstrate a greater weakening of the circulation. These results confirm that the spatial pattern of correlations in Figure 29a represents a tendency for models that have a stronger increase in mesoscale organization to experience a greater eastward shift and weakening of the Pacific Walker circulation under warming than models with a weaker increase in organization.

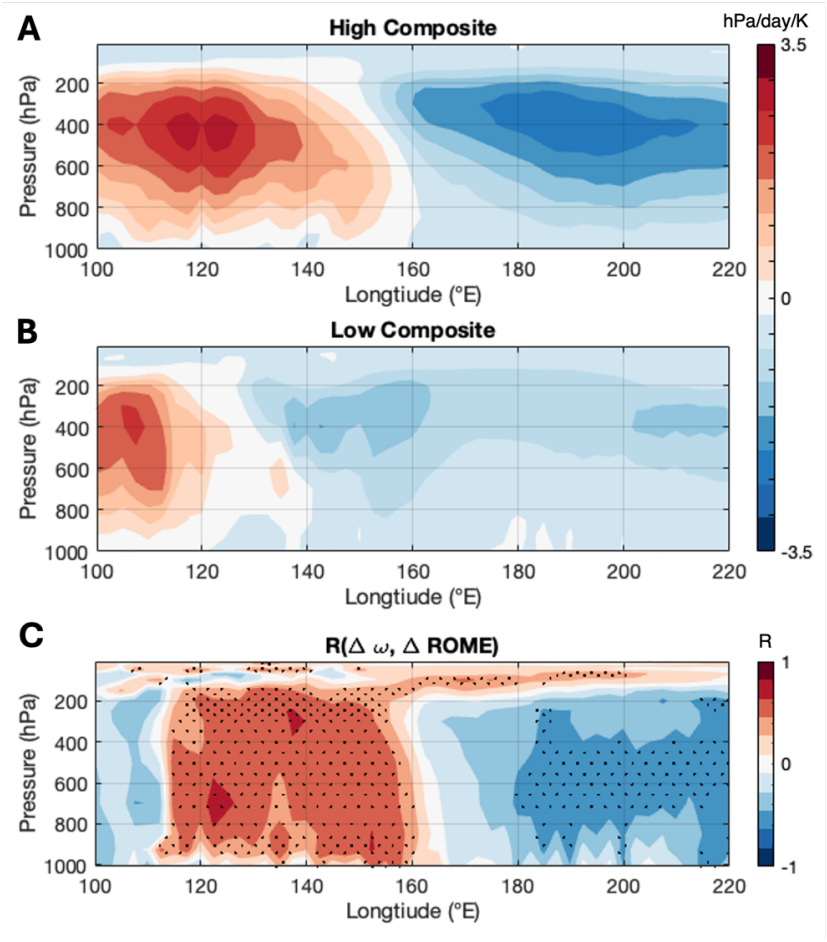

Fig. 30. Change to vertical pressure velocity normalized by global mean change in surface temperature averaged between 20°N and 20°S for the a) high Δ ROME group, b) low Δ ROME group, and c) the correlation of the change in vertical pressure velocity and Δ ROME.

Unlike mesoscale organization, there is disagreement across the ensemble on the change in tropics-wide ascent area under warming with 9 out of 21 models demonstrating a loss of fractional ascent. None of the tropical mean correlations between the change in ascent area and the net, optical depth, or amount feedbacks are significant ($r = -0.29$; $p = 0.19$; $r = -0.31$, $p = 0.17$; $r = -0.35$, $p = 0.12$, respectively), indicating that changes to organization at the scale of the ITCZ are not driving variability in high cloud feedbacks, at least not considering the tropical means. To assess these relationships spatially, correlations between the fractional change in

ascent area and the local high cloud net, optical depth, and amount feedbacks are visualized (Figure 31). Again, the most notable relationships between changes to convective organization (at any scale) and high cloud feedbacks are expected to be with the optical depth and amount feedbacks, hence the choice to analyze these high cloud feedbacks most closely. All three feedbacks show modest significant anticorrelations, illustrating that models that experience a decrease in ascent area under warming tend to have more positive high cloud feedbacks along equatorial convective margins. Interestingly, there are significant positive correlations between each feedback and the change in ascent area along the South Pacific Convergence Zone. At present, an explanation for this behavior is not obvious.

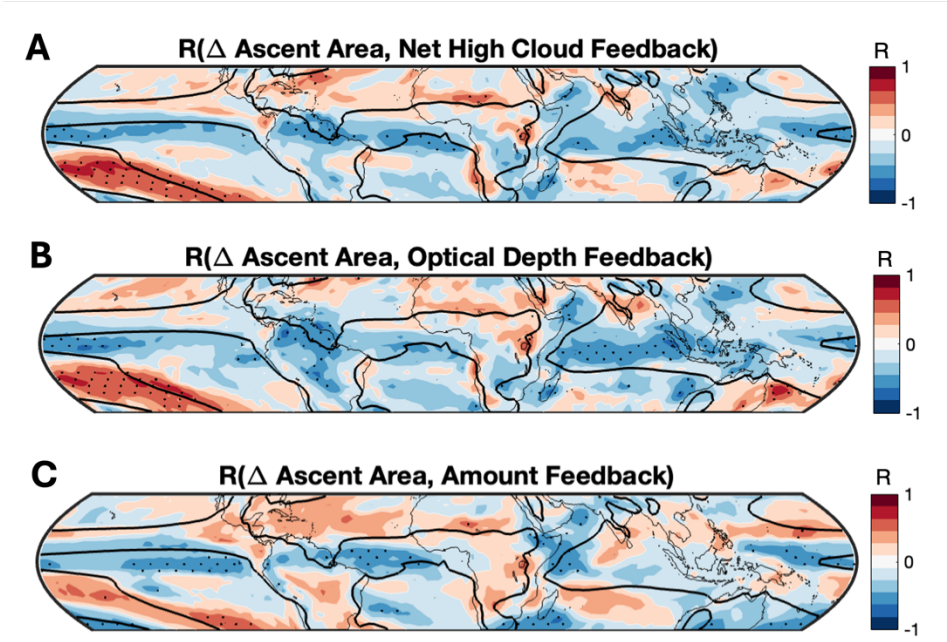

Fig. 31. Correlation between the tropics-wide (30°N - 30°S) fractional change in ascent area normalized by change in global mean surface temperature and local a) net high cloud feedback, b) high cloud optical depth feedback, and c) high cloud amount feedback.

The constraint of this relationship to convective margins along the ITCZ suggests that changes to the local dynamic environment associated with the shifting of tropical ascending

regions is important for high cloud feedbacks along convective margins. However, ascent area fraction is only one metric capturing changes to the large-scale circulation and does not explicitly account for changes in circulation occurring in descent regimes. Therefore, to expand this analysis, the local change in vertical velocity at 500 hPa is correlated with the local high cloud feedbacks (Figure 32). Across the net, optical depth, and amount feedbacks, there are strong, significant correlations between the local changes in ω_{500} and the local high cloud feedbacks covering the equatorial Pacific and Atlantic, South Pacific Convergence Zone, parts of the Warm Pool, the eastern Amazon, and the subtropical North Atlantic basin. In areas of climatological descent, a positive correlation indicates that models that see a lesser weakening of descent experience more positive (or less negative) high cloud feedbacks, whereas in regions of climatological ascent, a correlation represents an association between enhanced weakening of ascent and more positive high cloud feedbacks. In other words, positive correlations in this map are interpreted to mean that a reduction of ascent and/or strengthening of descent along convective margins relates to more positive high cloud feedbacks.

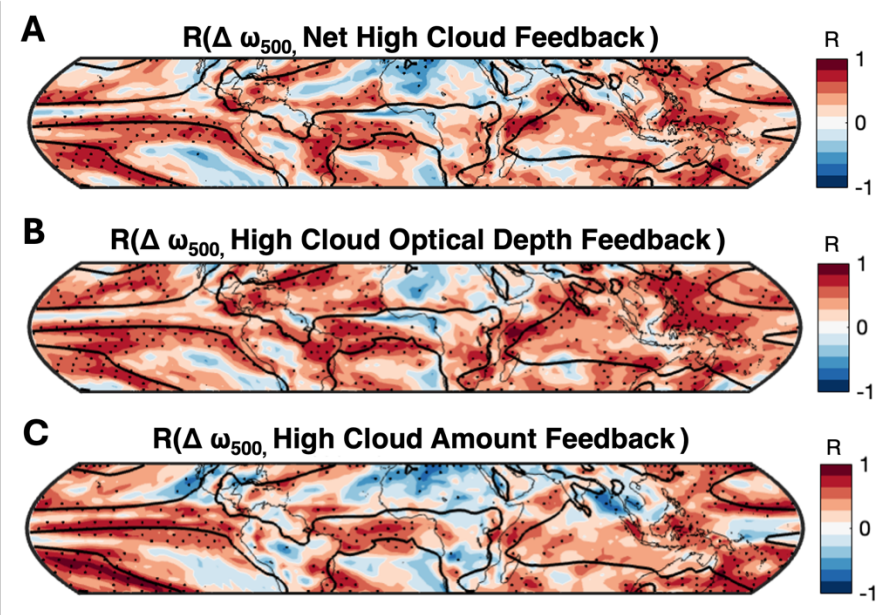

Fig. 32. Correlation between the local change in ω_{500} normalized by change in global mean surface temperature and local a) net high cloud feedback, b) high cloud optical depth feedback, and c) high cloud amount feedback.

Finally, to isolate the climatological conditions in which the relationships between local dynamic shifts and high cloud feedbacks are the strongest, correlations between the change in ω_{500} and high cloud feedbacks are computed across climatological ω_{500} regimes binned in 10 hPa increments (Figure 33). The net high cloud feedback, as well as the optical depth and amount feedbacks, yield significant correlations to the change in ω_{500} in the weak ascent and weak subsidence regimes of $-10 < \text{hPa} < 10$, reflective of the convective margin shifts highlighted in Figure 32. This confirms that models that experience enhanced weakening of ascent or greater increase in descent strength adjacent to climatological ascent regions tend to experience an enhanced thinning and decrease in high cloud amount under warming on those margins.

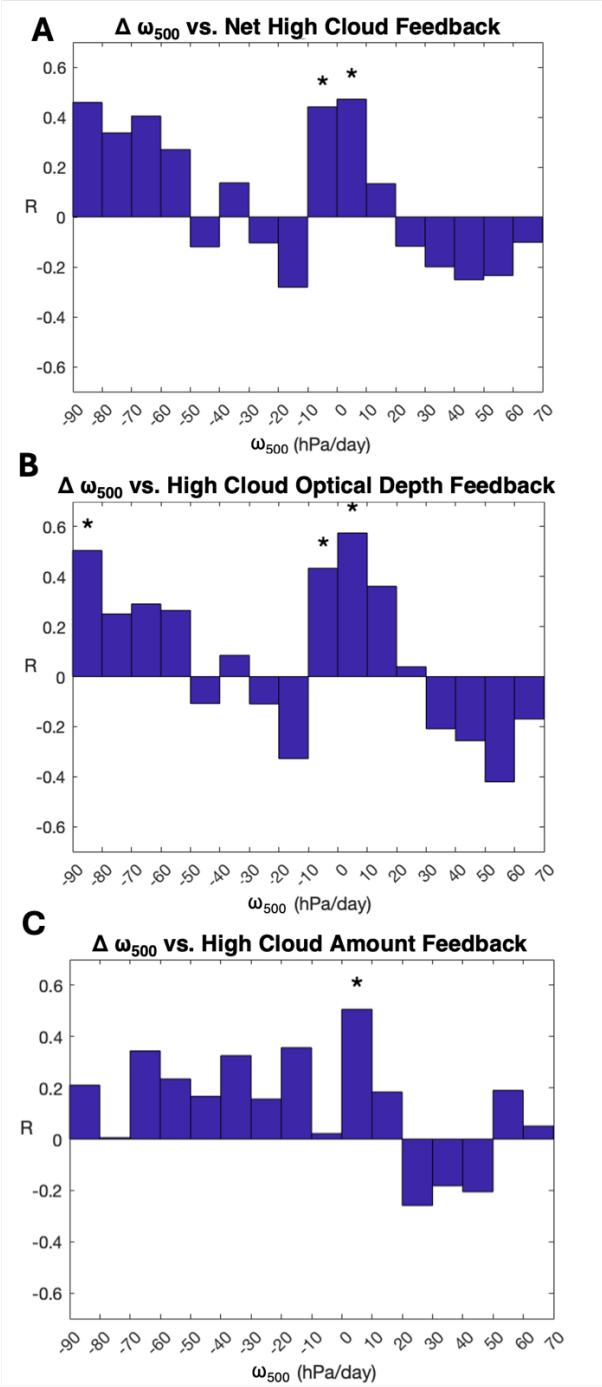

Fig. 33. Correlation between the local change in ω_{500} normalized by change in global mean surface temperature and local a) net high cloud feedback, b) high cloud optical depth feedback, and c) high cloud amount feedback across climatological ω_{500} groups. Significance at α =.05 is indicated by an asterisk

In summary, enhanced mesoscale aggregation is associated with a pronounced weakening of the Walker Circulation, which results in an enhanced loss and thinning of high clouds in the West Pacific and co-occurring thickening and increase of high clouds in the Central Pacific, contributing to more negative high cloud feedbacks particularly across the equatorial Pacific. Elsewhere, an increase in mesoscale organization is associated with more positive high cloud feedbacks along convective margins. A reduction of tropics-wide ascent area – or enhanced planetary-scale convective organization – is also moderately associated with more positive high cloud feedbacks along convective margins. However, a stronger relationship exists between changes in local dynamic environments and high cloud feedbacks such that greater decreases in high cloud amount and albedo in climatological weak descent regimes are related to a general tendency for these regimes to be more strongly subsiding in the future.

6.3.2 Precipitation Efficiency

To assess the extent to which intermodel variability in changes to precipitation efficiency are driving intermodel variability in high cloud feedbacks, the high cloud net, altitude, optical depth, and amount feedbacks are correlated with the tropical mean change in efficiency (Figure 34). None of the relationships are statistically significant, but this is in part driven by two outlier models with large decreases in efficiency, IPSL-CM5A-MR and IPSL-CM5A-LR. Similar to Li et al. (2023), the ensemble varies on the sign of the change in tropics-wide precipitation efficiency. Following their division of models into those with positive and negative sensitivities of precipitation efficiency to warming, the 15 models that increase in tropics-wide efficiency are correlated to each of the high cloud feedback components (Figure 35). None of correlations are statistically significant at the $\alpha = .05$ level, though the correlation to the high cloud optical depth feedback has a p-value of 0.07. These results suggest that the intermodel variability in changes to

precipitation efficiency are not strongly related to variability in high cloud feedbacks tropics-wide.

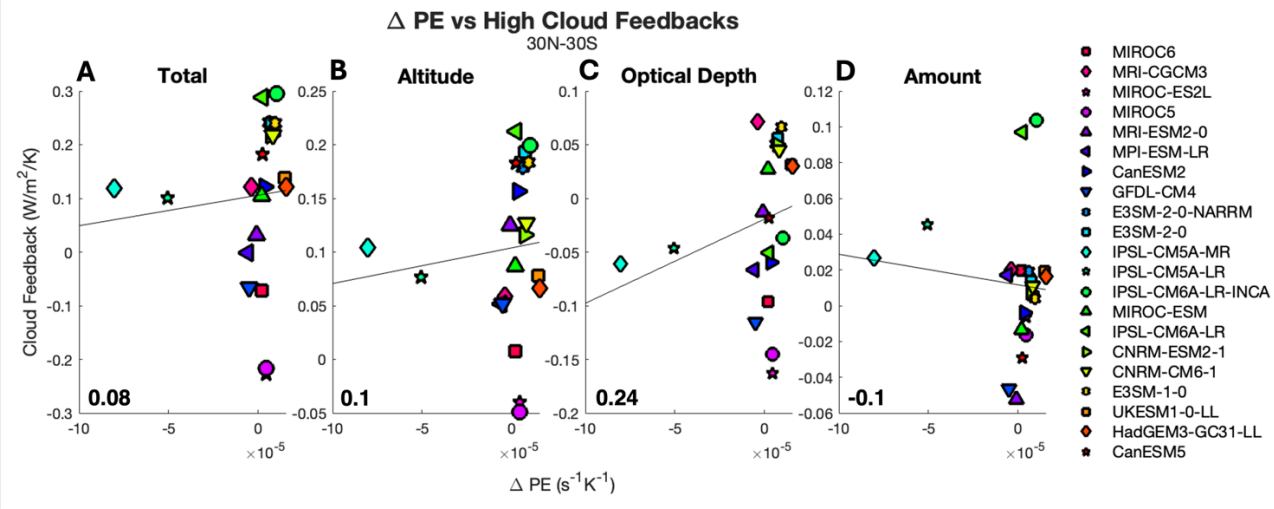

Fig. 34. Correlation between the tropical mean (30°N - 30°S) change in precipitation efficiency normalized by the global mean change in surface temperature and the high cloud a) net feedback, b) altitude feedback, c) optical depth feedback, and d) amount feedback. The Pearson correlation coefficient is in bold and statistical significance at $\alpha = .05$ is indicated by an asterisk.

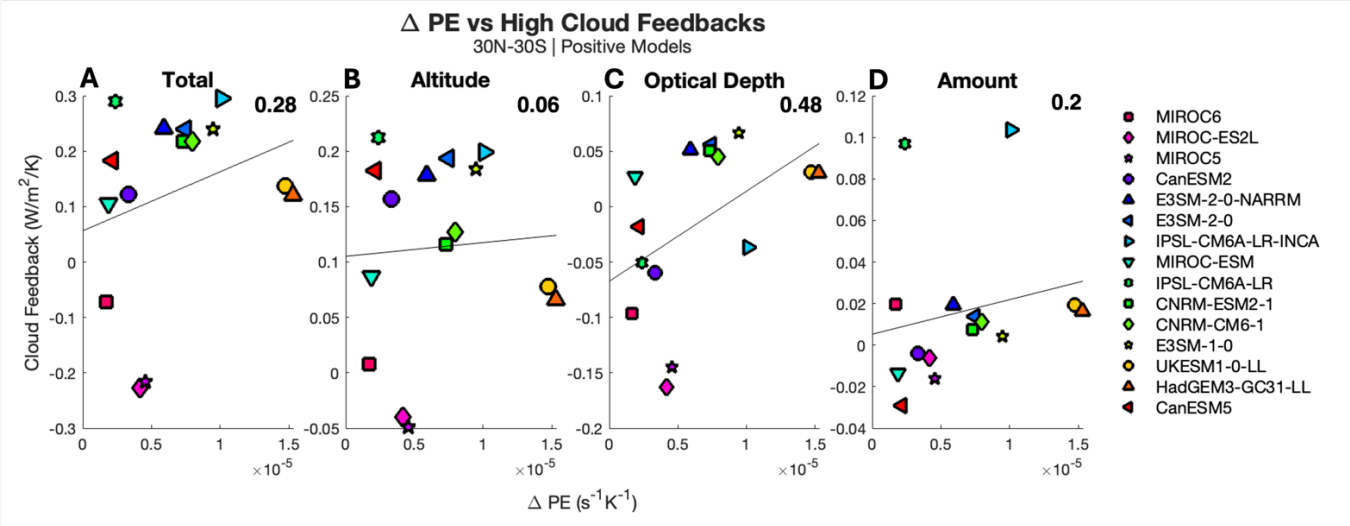

Fig. 35. As in Figure 34, but for the 15 models that increase in tropical mean precipitation efficiency.

To further test the hypothesis that a greater increase in precipitation efficiency is associated with enhanced thinning of high clouds as described by Li et al. (2019), the local net high cloud optical depth feedback is correlated with the change in efficiency across models that increase in efficiency (Fig 36a). The high cloud optical depth feedback is significantly correlated to the tropics-wide change in efficiency in the subtropical south Pacific and Atlantic basins and along the equatorial Pacific, indicating that models with a greater increase in precipitation efficiency under warming experience more positive high cloud optical depth feedbacks in these regions of climatological descent. This yields a statistically significant correlation across descent regions ($r = 0.55$; $p = 0.03$). Dividing the ensemble into the 7 models with the greatest increase in precipitation efficiency (Fig 36b) and the 7 models with the smallest increase in efficiency (Fig 36c) affirms that the most pronounced difference between the groups comes from the equatorial Pacific region adjacent to the ITCZ wherein models with stronger increases in precipitation efficiency experience muted increases in high cloud albedo, leading to less negative high cloud optical depth feedbacks in this region relative to models with a weaker increase in efficiency.

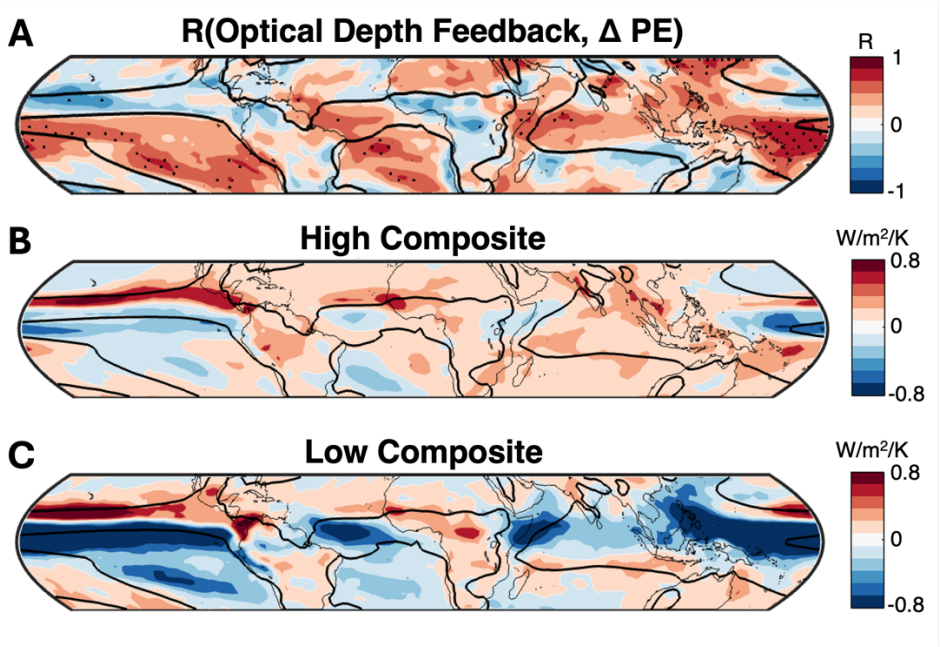

Fig. 36. a) Spatial correlation of the local high cloud optical depth feedback and tropical mean change in precipitation efficiency normalized by the global mean change in surface temperature. Significance at α =.05 is indicated by stippling. High cloud optical depth feedback composited for the b) 7 models with the strongest increase and c) 7 models with the weakest increase in tropical-mean precipitation efficiency.

Additionally, the spatial arrangement of the relationship between the high cloud amount feedback and precipitation efficiency in models that increase in precipitation efficiency under warming is considered (Figure 37a). The pattern is qualitatively similar to that displayed by the high cloud optical depth feedback, wherein the Central and East Pacific basins and subtropical Atlantic demonstrate significant correlations while broad ascent regions across the Amazon and equatorial Africa present anticorrelations. Comparing the high and low composites (Figure 37b-c) demonstrates much stronger positive feedbacks across ascent regions and stronger negative feedbacks across descent regions in the models that experience a weaker increase in efficiency. The correlation is statistically significant across descent regions ($r = 0.52$; $p = 0.05$), suggesting

that models that demonstrate a weaker increase in efficiency see a greater increase in high cloud amount along convective margins and descent regions, particularly across the Pacific.

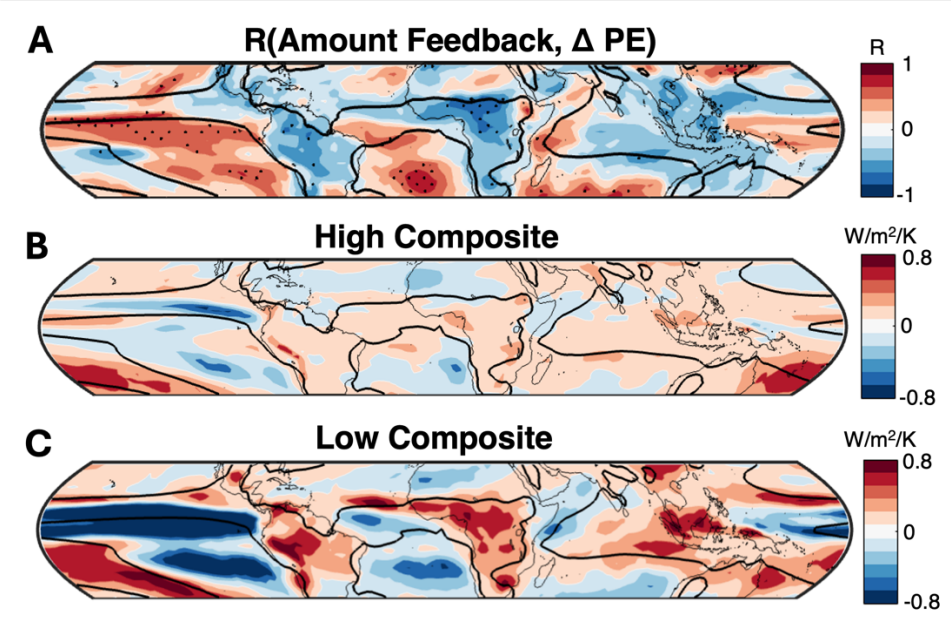

Fig. 37. As in Figure 36, but with the high cloud amount feedback.

Similar to the spatial pattern displayed by the relationships between the change in tropics-wide mesoscale organization and high cloud feedbacks (Figure 28), the dipole-like pattern of correlations between high cloud feedbacks and changes to precipitation efficiency across the equatorial Central Pacific and anticorrelations in the West Pacific suggests that changes to the tropical circulation may account for the connection between changes to precipitation efficiency and high cloud feedbacks. While Li et al. (2023) conclude that broadly speaking, models that increase in efficiency see an enhanced slowdown of the Walker circulation relative to models that decrease in efficiency, they do not assess the extent to which intermodel variability in changes to the strength of the Walker circulation drive variability in the magnitude of the increase in precipitation efficiency under warming. To analyze this question, vertically resolved

changes to vertical velocity averaged from 20°N to 20°S across the West and Central Pacific are plotted for the 7 models with the strongest increase in efficiency and the 7 models with the weakest increase in efficiency (Figure 38a-b), and changes to vertical pressure velocity are correlated with the tropical mean change in precipitation efficiency across all 15 models (Figure 38c). The changes to the Walker circulation are not significantly related to the tropics-wide change in precipitation efficiency. Moreover, the composited maps suggest that the models with a weaker increase in efficiency experience a stronger weakening of the circulation, contrary to the hypothesis based on the results of Li et al. (2023) that models displaying a stronger increase in efficiency experience a greater weakening of the circulation.

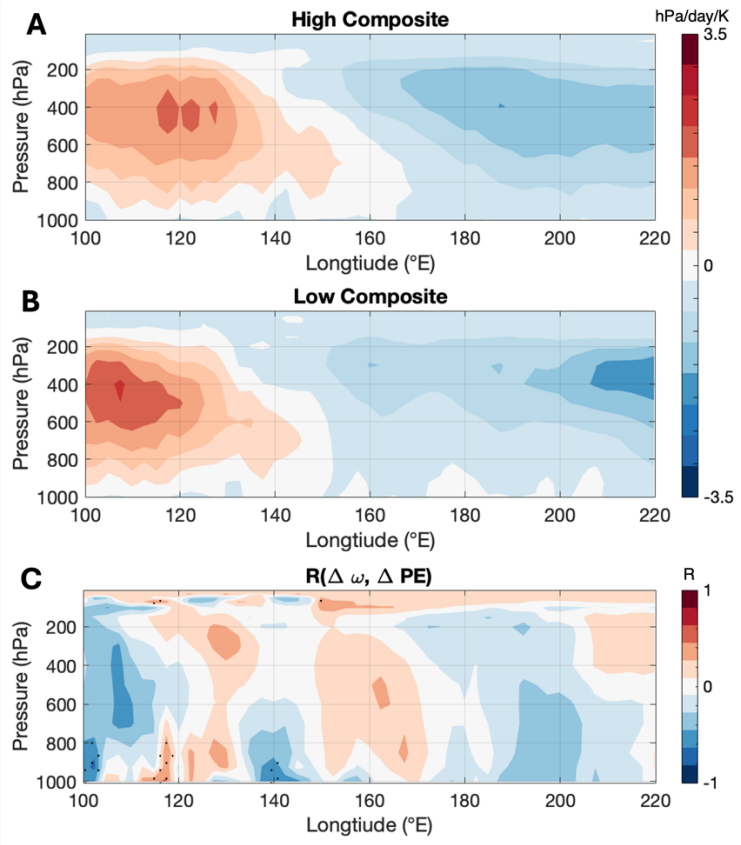

Fig. 38. As in Figure 30, but for changes to precipitation efficiency across models that increase in tropical-mean efficiency.

In summary, the relationships between changes to precipitation efficiency under warming and high cloud feedbacks are weak in the tropical-mean. While there is some evidence that models that see a greater increase in efficiency under warming experience more positive high cloud optical depth and amount feedbacks in descent regions, particularly in the Central and Eastern Pacific, these relationships are modest and are not explained by changes to the strength of the Walker circulation as highlighted previously in the literature.

7. Discussion and Future Work

This study highlights that the intermodel variability of the tropical high cloud altitude and optical depth feedbacks is related to the spread of equilibrium climate sensitivity. While the uncertainty of the high cloud altitude and anvil feedbacks has been noted in recent assessments of cloud feedbacks across GCMs (Zelinka et al., 2022; Sherwood et al., 2020), a quantification of the contribution of this variability to uncertainty in ECS has not been performed. Although the disparate responses of subtropical marine low clouds to warming are also highly uncertain across models (Sherwood et al., 2020; Zelinka et al., 2020; Bony & Dufresne, 2005), the results shown here underscore the importance of constraining changes to tropical high cloud altitude and opacity for reducing the uncertainty of climate sensitivity across future generations of climate models.

Assessment of the spatial arrangement of correlations between the tropical net high cloud feedback and ECS illustrates that the strongest relationships exist outside of regions of deepest climatological ascent. This is likely reflective of uncertainty in the response of anvils and thinner cirrus extending away from deep convective zones, which have been highlighted as difficult for coarse models to represent (Gasparini et al., 2023) and could be related to variability of both convective and microphysical processes. Convection may influence the frequency of occurrence

of thin high clouds through mechanisms such as convective aggregation (Wing & Cronin, 2016), convective detrainment (Bony et al., 2016), and entrainment of air into a convective plume (Tsushima et al., 2020). Moreover, recent work has highlighted microphysical parameters and processes such as ice autoconversion size threshold (Duffy et al., 2024), cloud lifetime and decay (Seeley et al., 2019), and ice fall speed and density (Schiro et al., 2019; Tsushima et al., 2020; Wang et al., 2020) as factors impacting anvil cloud fraction. Additionally, comparisons of global storm resolving models – which explicitly simulate convection but parameterize cloud microphysics – find significantly variable cloud radiative effects of tropical cirrus across microphysics schemes (Atlas et al., 2024; Turbeville et al., 2022). However, missing from this discussion, aside from recent work by Sokol et al. (2024) analyzing idealized convection permitting simulations, is the somewhat unsurprising finding that intermodel variability in tropical high cloud feedbacks is most strongly related to intermodel variability in climate sensitivity in regions dominated by thinner high clouds. Because disentangling the particular mechanisms underlying the variability in thin high cloud responses across an ensemble of fully-coupled models is not feasible and results of PPE studies are limited in their applicability to broader conclusions across models, the attribution of intermodel variability in tropical high cloud feedbacks to differences in parameterizations is somewhat speculative. However, in alignment with the conclusions of Sokol et al. (2024), given that regions dominated by thinner high clouds drive the most variability in ECS and that a multitude of parameters contribute to the representation of thin high clouds within GCMs, it is likely that a non-negligible portion of intermodel variability in tropical high cloud feedbacks highlighted in this study is related to the radiative, dynamic, and microphysical processes that impact the representation of thin high clouds across models.

In line with an emergent constraint framework, this study also provides support for a relationship between mean state high cloud fraction and the altitude feedback in areas of ascent where climatological tropical high cloud fraction is largest, aligning with the logic noted by Ceppi et al. (2017). Limited evidence of the relationship between climatological high cloud amount and the high cloud altitude feedback has been suggested in the literature aside from the results of Po-Chedley et al. (2019) that demonstrate that the rise of high clouds in GCMs can be predicted from a model's climatology and Zelinka et al. (2022), who find that weather regimes dominated by high clouds see a more pronounced increase in cloud altitude under warming in comparison to regimes dominated by other cloud types. While this constraint applies to climatological ascent regimes over continental regions (Figure 20), the relationship between local high cloud amount and the high cloud altitude feedback is not ubiquitous across the tropics. Moreover, significant correlations are absent across the equatorial Pacific region where the high cloud altitude feedback displays the strongest correlation to climate sensitivity and varies the most between high and low ECS models (Figure 9). Thus, while climatological high cloud amount may provide a suitable constraint on the high cloud altitude feedback in the deep tropics, it does not provide a sufficient explanation for the variability of the high cloud altitude feedback along convective margins. Moreover, the relationship between climatological high cloud amount and the altitude feedback does not help to explain why models with more thin high clouds tend to see a more positive high cloud altitude feedback in the tropical mean (Table 3). On the contrary, as noted in Ceppi et al. (2017), all else being equal, one might expect that models with thicker high clouds would produce more positive altitude feedbacks given that clouds with higher optical depths induce a more positive longwave radiative effect than thinner clouds (Figure 1). These results suggest that other factors may be influencing the magnitude of the high cloud altitude

feedback. Tropical upper tropospheric warming has been shown to vary significantly across models (Keil et al., 2021; Mitchell et al., 2020), so some of the unexplained variability may be related to differences in the degree of upward shifting of high clouds and changes to stability of the upper tropospheric environment in which they exist. Additionally, different representations of cloud microphysics may be playing a role, but analysis of this contribution is beyond the scope of this work.

This study also highlights a robust relationship between mean high cloud opacity and the high cloud amount feedback with opposing signs across ascent and descent regions. While significant correlations between high cloud opacity and the high cloud amount feedback in ascent regions could be due to a cloud shading feedback that acts to dampen radiative forcings through changes to convective intensity (Hartmann et al., 2001; Wall & Hartmann, 2018), a mechanistic explanation for the relationship between mean opacity and the high cloud amount feedback away from deep convective zones is less clear. Regardless, the opportunity to utilize this relationship as a constraint on climate sensitivity is limited by the weak correlation of the high cloud amount feedback to ECS. Unlike the high cloud amount feedback, relating mean high cloud opacity to responses of high cloud optical depth through the cloud shading feedback mechanism could reasonably be used as the basis for an emergent constraint given the significant correlation between the high cloud optical depth feedback and ECS (Figure 10a). However, the lack of coherent correlations between opacity and the optical depth feedback across ascent regions in conjunction with anticorrelations along convective margins (Figure 23) suggest that the cloud shading feedback mechanism does not explain optical depth changes across the ensemble. On the contrary, significant anticorrelations between mean high cloud opacity and the high cloud optical depth feedback in the tropical mean (Table 3) suggest that changes to cloud

albedo act to enhance the radiative effects of the mean state cloud population rather than dampen them. In other words, models that tend to exhibit a thinner high cloud climatology experience relative thinning in the tropical mean. The reason that a model simulating a climatology of clouds with lower opacity in the mean state would tend to simulate an enhanced thinning of those clouds under warming remains unclear.

The variability in climatological high cloud fraction in the tropics, particularly in regions of strong ascent, is found to systematically relate to variability in the sensitivity of convection to the entrainment of tropospheric air. The importance of deep convective parameterizations for influencing climatological high cloud amount have been highlighted in PPE studies (Schiro et al., 2019; Tsushima et al., 2020; Zhang et al., 2012), suggesting that alongside microphysical parameters, the variable representation of deep convection across models drives spread in tropical high cloud fraction. The precipitation pickup behavior has been related to three factors: entrainment rate (Kuo et al., 2017), undilute buoyancy characterizing environmental instability separate from the effects of entrainment, and dilution of buoyancy by dry air from the lower free-troposphere (Ahmed & Neelin, 2021). Thus, the tropical vertical stability profile, degree of subsaturation of the lower free-troposphere, and entrainment rate prescribed in a model can all affect the phase transition from non-precipitating to precipitating states. Because CMIP6 models display a wide range of sensitivities to environmental stability and free tropospheric moisture (Ahmed & Neelin, 2021), and entrainment, typically understood through entraining plume models (Zhang & McFarlane, 1995), may vary across different parameterization schemes, this analysis cannot isolate the individual effects of each of these components on high cloud amount. However, given that an increase in entrainment and increasing sensitivities to both instability and moisture result in a stronger pickup (Ahmed & Neelin, 2021), it can be inferred that GCMs with

fewer high clouds in ascent areas exhibit some combination of these characteristics and provide a mechanistic explanation for the intermodel variability of tropical high cloud amount. Future research could test whether the strength of precipitation pickup systematically varies with ECS and analyze whether it mechanistically relates to climate sensitivity through its impact on climatological high cloud-high cloud feedback relationships such as the mean high cloud fraction relationship to the altitude feedback highlighted previously.

The importance of dynamical regime shifts, their correlation to convective organization across scales, and their relationship to the variability of high cloud feedbacks are also highlighted in this study. Increases in organization – a greater decrease in ascent area and a greater increase in ROME – are associated with more positive high cloud feedbacks across different regions but broadly characterize the same behavior. For example, change to ascent area is anticorrelated to each of the cloud feedback components within weak ascent regimes (Figure 31), exhibiting a greater thinning and loss of cloud amount at the edges of the ITCZ as ascent area reduces. In conjunction, changes to mesoscale organization at daily timescales are correlated to high cloud feedbacks in weak subsidence regimes (Figure 28), signaling high cloud thinning and loss as convection becomes more organized. Whereas ascent area drives changes to high cloud feedbacks within weak ascent regimes, ROME displays strong relationships to feedbacks along weak subsidence regions that are not captured by tropics-wide ascent changes. Thus, both metrics capture different aspects of the same tendency for models that increase in large scale organization under warming to exhibit more positive high cloud feedbacks on convective margins.

The arrangement of ascent area relationships to feedbacks along the equator suggest that changes to tropical deep convective organization predominantly characterize the effects of ITCZ

narrowing or expansion. A majority of CMIP5 models predict a reduction of ITCZ width under warming and this change is associated with a shift of the southern edge to the north (Byrne & Schneider, 2016), reflecting the patterns shown in Figure 30. In contrast, studies of cloud resolving models (CRMs) run in RCE demonstrate an increase in ascent fraction under warming (Mackie & Byrne, 2023). A loss of ascent area has previously been characterized by an increase in ascent strength and convective activity in the core of the ITCZ and a reduction of ascent strength along its edges across GCMs (Byrne & Schneider, 2018; Su et al., 2014) and in observations (Wodzicki & Rapp, 2022), termed the "deep tropics squeeze" (Lau & Kim, 2015). This yields dynamic cloud feedbacks that are the most positive in the heart of the ITCZ in the multimodel mean stemming from a positive longwave component (Byrne & Schneider, 2018). While positive high cloud feedbacks are produced along a narrow band of the Pacific ITCZ across the ensemble (Figure 7a-b), this region is not characterized by a strong relationship between changes to ascent strength and the magnitude of the high cloud feedbacks. Rather, the equatorial Pacific demonstrates the strongest relationship between changes in ω_{500}, ascent area, and high cloud feedbacks (Figures 31-32). Given that changes to tropics-wide ascent area are more strongly related to changes in ascent strength than descent strength (Su et al., 2019), it is unsurprising that feedbacks along convective margins under weakly ascending and descending conditions see a stronger relationship to local changes in ω_{500} than changes to tropical mean ascent area. Thus, while acknowledging that dynamic and thermodynamic cloud feedback components are not explicitly separated in this study, these results underscore that regime shifts along convective margins rather than changes to ascent in the climatological deep tropics relate most strongly to variability in tropical high cloud feedbacks, providing an alternative perspective

to the current body of literature focused on intermodel variability of changes to ascent width and strength (Byrne et al., 2018; Byrne & Schneider, 2018; Su et al., 2019).

In addition to capturing the effects of changes to tropical ascent within convective margins, the response of mesoscale convection to warming strongly relates to intermodel variability of high cloud feedbacks through variability in changes to the strength of the Pacific Walker cell. This is demonstrated through the prominent dipole-like feature in the Pacific basin shown in Figure 29d, wherein models with a strong increase in ROME experience a greater weakening of the Walker circulation than models with weaker increases in organization, resulting in more positive high cloud feedbacks in the West Pacific and more negative high cloud feedbacks along convective margins in the Central Pacific as convection moves eastward. Related to the coupling of clouds and circulation, studies have assessed how differential SST warming patterns, commonly referred to as the "Pattern Effect" (Stevens et al., 2016), impact the strength of the Pacific Walker circulation. The literature has focused primarily on how changes to the overturning circulation impact low cloud feedbacks in the East Pacific (Andrews, 2015; Zhou et al., 2017), wherein more El Niño-like warming patterns reduce the east-west SST gradient across the Pacific basin, weaken the Walker circulation, and result in a reduction of stratocumulus decks in subsidence regions. However, the significant relationship between Pacific high cloud feedbacks and Walker circulation changes shown here hints at a potential relationship between the Pattern Effect and variability of high cloud feedbacks, presenting an avenue for future work to expand on the existing Pattern Effect literature.

The relationship between intermodel variability in changes to the Pacific Walker circulation and convective organization under warming have not been highlighted in the literature. Most studies that consider the relationships between circulation changes and

organization utilize idealized RCE scenarios that represent a simplification of the tropical atmosphere. While there is a general consensus that large-scale circulation weakens in RCE simulations in response to increasing SSTs (Silvers et al., 2023), and that large-scale aggregation is present in large-domain RCE simulations (Stauffer & Wing, 2022; Wing et al., 2020), there is disagreement in the response of aggregation to warming (Wing et al., 2020). "Mock-Walker" experiments represent a novel approach for investigating the effects of SST gradients and the induced large-scale circulation in RCE setups (Wing et al., 2024), but a comprehensive intermodel comparison has only recently been proposed in the second iteration of the RCE intermodel comparison project, RCEMIP-II. While an individual mock-Walker study suggests that longwave cloud radiative effects act to enhance aggregation and circulation strength below 500 hPa, it does not identify significant effects of aggregation on the mean circulation strength (Silvers & Robinson, 2021). Moreover, CRMs and GCMs run in standard RCE setups see similar levels of organization across different levels of convective intensity, though this could be reflective of self-aggregation rather than aggregation induced by circulation changes (Silvers et al., 2023). Thus, confirmation that intermodel variability in decreased circulation strength systematically relates to increases in mesoscale organization with warming requires further work and should be pursued in RCEMIP-II.

Changes to the Pacific Walker circulation have been most directly connected to high cloud feedbacks through a framework of precipitation efficiency (Li et al., 2022; Li et al., 2023), wherein GCMs that exhibit an increase in precipitation efficiency experience an enhanced slowdown of the Walker cell, demonstrating a loss of anvil coverage in climatological ascent regions of the West Pacific and stratocumulus extent in the East Pacific (a positive feedback).

Counter to these findings, the relationship between changes to Walker cell strength and the magnitude of precipitation efficiency increase under warming is not significant here (Figure 38c). Moreover, the tropics-wide change in mesoscale organization is not significantly correlated with the change in precipitation efficiency among models that increase in efficiency ($r = -0.42$; $p = 0.11$), undermining increased organization as a potential mechanism explaining enhanced efficiency under warming highlighted by Lutsko et al. (2023), at least in the CMIP ensemble. Lending some support to the conclusions of Li et al. (2023), models that experience a greater increase in efficiency demonstrate modest positive high cloud optical depth feedbacks over the Indian Ocean and Maritime Continent in contrast to the negative optical depth feedback displayed in models with a weak increase in efficiency (Figure 36b-c). However, the regions accounting for the greatest difference between the groups and containing statistically significant relationships across the ensemble are the equatorial Central Pacific and subsidence zones of the East Pacific (Figure 36a). Correlations here suggest that models that demonstrate an enhanced increase in efficiency experience a less pronounced increase in high cloud albedo - a more muted negative high cloud feedback - along climatological margins. While this result generally aligns with the PPE results from Li et al. (2019), it does not support the linkage between changes to precipitation efficiency and changes to the Pacific Walker cell strength. Given that a weakening of the Walker circulation is associated with the movement of convection eastward under El Niño-like conditions when warming is enhanced in the East Pacific (Bayr et al., 2014; Plesca et al., 2018), one would reasonably expect that an enhancement of Walker weakening would produce more negative high cloud feedbacks in the central Pacific as convection shifts eastward in conjunction with warm SSTs, in contrast to the results shown here. Considering the small size of the ensemble and methodological limitations related to precipitation efficiency outliers in arid

regions, analysis of the relationship between the high cloud optical depth feedback, changes to precipitation efficiency, and changes to the strength of the Walker circulation require further examination across a more comprehensive ensemble of GCMs.

8. Conclusions

This work demonstrates that intermodel variability of the tropical high cloud altitude and optical depth feedbacks is related to the spread of equilibrium climate sensitivity. The strongest relationships between high cloud feedbacks and climate sensitivity exist outside of regions of deepest climatological ascent, highlighting the uncertainty with which thinner anvils and cirrus respond to warming. Analysis of the relationship between mean state high cloud characteristics and climate sensitivity shows that high ECS models have greater mean state high cloud fraction and thinner high clouds than low ECS models, evidenced by greater thin high cloud coverage across tropical ascent regions and fewer thick high clouds broadly across the tropics. Given the significant, positive correlations between the tropical high cloud altitude and optical depth feedbacks and ECS, in addition to significant relationships between climatological high cloud characteristics and ECS, these results motivate analysis of relationships between cloud fraction and high cloud feedbacks within an emergent constraint framework.

To test the applicability of the cloud shading feedback to the ensemble, the relationship between mean high cloud opacity and the amount and optical depth feedbacks are analyzed. While ascent regions suggest that high cloud opacity modulates the high cloud amount feedback under this mechanism, descent regions do not support this argument and suggest that models with thinner high clouds experience enhanced thinning of high clouds and a muted increase of high cloud fraction. Additionally, the relationship between high cloud amount and the altitude feedback is tested, demonstrating correlations across ascent areas and in the tropical-mean but

not ubiquitously across the tropics nor along convective margins where the high cloud altitude feedback varies the most. Moreover, models with thinner high clouds tend to see enhanced optical depth and altitude feedbacks in the tropical-mean, but these relationships lack a physical mechanism. Thus, while this analysis highlights relationships between mean state high cloud characteristics, high cloud feedbacks, and ECS, none are coherent enough to propose a new emergent constraint. Disentangling the underlying drivers of these correlations, whether that be differences in cloud microphysics schemes and deep convective parameterizations, additional mean state parameters, or variability in the response of other components of the modeled atmosphere to warming, remains an important task.

To better explain the intermodel variability of tropical high cloud fraction, this study analyzes the systematic relationship between convective sensitivity to the entrainment of environmental air into deep convective updrafts and climatological high cloud amount across models. Models that are more sensitive to tropospheric moisture and display a stronger precipitation pickup exhibit lesser high cloud coverage in strong ascent regions than models that experience convection across a variety of environmental conditions, characterized by a weaker precipitation pickup. Although not explicitly perturbing deep convective parameters, this result emphasizes the influence that the representation of convection has on a model's high cloud climatology and underscores the diversity of model representation of sub-grid scale processes as a driver of the variability in not only mean high cloud characteristics but also, as evidenced through the relationship between high cloud amount and the altitude feedback, changes to high clouds with warming.

Additionally, this work emphasizes the strong relationship between changes to the local dynamic environment and the responses of high clouds under warming within weak ascent and

weak subsidence regimes. Decreases in tropics-wide ascent area result in more positive high cloud feedbacks along the southern edges of the ITCZ, while increases in mesoscale organization yield more positive high cloud feedbacks along convective margins in weak subsidence regimes. Additionally, increases in mesoscale organization are associated with more positive feedbacks in the West Pacific and more negative feedbacks in the equatorial Central Pacific through an enhanced weakening and eastward shift of the Walker circulation. Moreover, along convective margins where descent weakens less (or ascent weakens more), high cloud feedbacks are found to be more positive through enhanced cloud thinning and loss. These results suggest that processes that affect the shift of convective margins play a key role in driving variability of high cloud feedbacks in these regions. Given that variability in tropical high cloud feedbacks along convective margins systematically relates to variability in ECS, the strong relationship between local dynamics and cloud feedbacks shown here could be used to constrain climate sensitivity in future work.

In sum, this study outlines the extent to which tropical high cloud feedbacks drive intermodel variability in climate sensitivity, considers variables that could drive spread in the high cloud feedbacks, and explores relationships between modeled high cloud climatology, high cloud feedbacks, and ECS. While factors including intermodel variability in responses of precipitation efficiency, the overturning circulation, and convective organization are analyzed, other processes such as low cloud feedbacks, changes to tropospheric stability, and the pattern of warming are not considered. Thus, there is non-zero likelihood that certain correlations with ECS presented here are influenced non-trivially by high cloud feedback relationships to other cloud changes or atmospheric processes that drive substantial spread in ECS. Nevertheless, this work demonstrates the need to strongly consider tropical high cloud contributions, particularly the

high cloud altitude and optical depth feedbacks, to the intermodel spread in ECS in efforts to constrain future warming.

References

Ahmed, F., Adames, Á. F., & Neelin, J. D. (2020). Deep Convective Adjustment of Temperature and Moisture. *Journal of the Atmospheric Sciences, 77*(6), 2163-2186. https://doi.org/10.1175/JAS-D-19-0227.1

Ahmed, F., & Neelin, J. D. (2018). Reverse Engineering the Tropical Precipitation-Buoyancy Relationship. *Journal of the Atmospheric Sciences, 75*(5), 1587-1608. https://doi.org/10.1175/JAS-D-17-0333.1

Ahmed, F., & Neelin, J. D. (2021). A Process-Oriented Diagnostic to Assess Precipitation-Thermodynamic Relations and Application to CMIP6 Models. *Geophysical Research Letters, 48*(14). https://doi.org/10.1029/2021GL094108

Andrews, T., Gregory, J. M., Webb, M. J., & Taylor, K. E. (2012). Forcing, feedbacks, and climate sensitivity in CMIP5 coupled atmosphere-ocean climate models. *Geophysical Research Letters, 39*(9). https://doi.org/10.1029/2012GL051607

Atlas, R. L., Bretherton, C. S., Sokol, A. B., Blossey, P. N., & Khairoutdinov, M. F. (2024). Tropical cirrus are highly sensitive to ice microphysics within a nudged global storm-resolving model. *Geophysical Research Letters, 51*, e2023GL105868. https://doi.org/10.1029/2023GL105868

Bayr, T., Dommenget, D., Martin, T., & Power, S. B. (2014). The eastward shift of the Walker Circulation in response to global warming and its relationship to ENSO variability. *Climate Dynamics*, *43*, 2747-2763. https://doi.org/10.1007/s00382-014-2091-y

Beydoun, H., Caldwell, P. M., Hannah, W. M., & Donahue, A. S. (2021). Dissecting anvil cloud response to sea surface warming. *Geophysical Research Letters, 48*(15), e2021GL094049. https://doi.org/10.1029/2021GL094049

Blackberg, C. P. O., & Singh, M. S. (2022). Increased Large-Scale Convective Aggregation in CMIP5 Projections: Implications for Tropical Precipitation Extremes. *Geophysical Research Letters, 49*(9). https://doi.org/10.1029/2021GL097295

Bony, S., Colman, R., Kattsov, V. M., Allan, R. P., Bretherton, C. S., Dufresne, J.-L., Hall, A., Hallegatte, S., Holland, M. M., Ingram, W., Randall, D. A., Soden, B. J., Tselioudis, G., & Webb, M. J. (2006). How Well Do We Understand and Evaluate Climate Change Feedback Processes? *Journal of Climate, 19*(15), 3445-3482. https://doi.org/10.1175/JCLI3819.1

Bony, S., & Dufresne, J. L. (2005). Marine boundary layer clouds at the heart of tropical cloud feedback uncertainties in climate models. *Geophysical Research Letters, 32*(20), L20806. https://doi.org/10.1029/2005GL023851

Bony, S., Semie, A., Kramer, R. J., Soden, B., Tompkins, A. M., & Emanuel, K. A. (2020). Observed modulation of the tropical radiation budget by deep convective organization and lower-tropospheric stability. *AGU Advances*, *1*(3), e2019AV000155. https://doi.org/10.1029/2019AV000155

Bony, S., Stevens, B., Coppin, D., Becker, T., Reed, K. A., Voigt, A., & Medeiros, B. (2016). Thermodynamic control of anvil cloud amount. *Proceedings of the National Academy of Sciences, 113*(32), 8927–8932. https://doi.org/10.1073/pnas.1601472113

Bony, S., Stevens, B., Frierson, D. M. W., Jakob, C., Kageyama, M., Pincus, R., Shepherd, T. G., Sherwood, S. C., Siebesma, A. P., Sobel, A. H., Watanabe, M., & Webb, M. J. (2015). Clouds, circulation and climate sensitivity. *Nature Geoscience*, *8*, 261-268. https://doi.org/10.1038/ngeo2398

Brient, F., & Schneider, T. (2016). Constraints on climate sensitivity from space-based measurements of low-cloud reflection. *Journal of Climate, 29*(16), 5821–5835. https://doi.org/10.1175/JCLI-D-15-0897.1

Boucher, O., Reddy, M. S., & Myhre, G. (2013). *Clouds and aerosols*. In T. F. Stocker, D. Qin, G.-K. Plattner, M. Tignor, S. K. Allen, J. Boschung, A. Nauels, Y. Xia, V. Bex, & P. M. Midgley (Eds.), *Climate change 2013: The physical science basis* (pp. 571–657). Cambridge University Press. https://doi.org/10.1017/CBO9781107415324.016

Byrne, M. P., Pendergrass, A. G., Rapp, A. D., & Wodzicki, K. R. (2018). Response of the Intertropical Convergence Zone to Climate Change: Location, Width, and Strength. Current *Climate Change Reports*, *4*, 355-370. https://doi.org/10.1007/s40641-018-0110-5

Byrne, M. P., & Schneider, T. (2016). Narrowing of the ITCZ in a warming climate: Physical mechanisms. *Geophysical Research Letters, 43*(21), 11,350–11,357. https://doi.org/10.1002/2016GL070396

Byrne, M. P., & Schneider, T. (2018). Atmospheric Dynamics Feedback: Concept, Simulations, and Climate Implications. *Journal of Climate*, *31*(8), 3249-3264. https://doi.org/10.1175/JCLI-D-17-0470.1

Brient, F., Schneider, T., Tan, Z., Bony, S., Qu, X., & Hall, A. (2016). Shallowness of tropical low clouds as a predictor of climate models' response to warming. *Climate Dynamics, 47*, 433–449. https://doi.org/10.1007/s00382-021-05675-2

Caldwell, P. M., Zelinka, M. D., Taylor, K. E., & Marvel, K. (2016). Quantifying the sources of intermodel spread in equilibrium climate sensitivity. *Journal of Climate, 29*(2), 513–524. https://doi.org/10.1175/JCLI-D-15-0352.1

Ceppi, P., Brient, F., Zelinka, M. D., & Hartmann, D. L. (2017). Cloud feedback mechanisms and their representation in global climate models. *Wiley Interdisciplinary Reviews: Climate Change, 8*(4), e465. https://doi.org/10.1002/wcc.465

Charney, J. (1979). Carbon Dioxide and Climate: A Scientific Assessment. Washington, DC: The National Academies Press. https://doi.org/10.17226/12181

Chao, L.-W., Zelinka, M. D., & Dessler, A. E. (2024). Evaluating cloud feedback components in observations and their representation in climate models. *Journal of Geophysical Research: Atmospheres, 129*(2), e2023JD039427. https://doi.org/10.1029/2023JD039427

Choi, Y.-S., Kim, W., Yeh, S.-W., Masunaga, H., Kwon, M.-J., Jo, H.-S., & Huang, L. (2017). Revisiting the iris effect of tropical cirrus clouds with TRMM and A-Train satellite data. *Journal of Geophysical Research: Atmospheres, 122*(11), 5917–5931. https://doi.org/10.1002/2016JD025827

Cronin, T. W., & Wing, A. A. (2017). Clouds, circulation, and climate sensitivity in a radiative–convective equilibrium channel model. *Journal of Advances in Modeling Earth Systems, 9*(8), 2883–2905. https://doi.org/10.1002/2017MS001111

Del Genio, A. D., & Wu, J. (2010). The Role of Entrainment in the Diurnal Cycle of Continental Convection. *Journal of Climate, 23*(10), 2722-2738. https://doi.org/10.1175/2009JCLI3340.1

Duffy, M. L., Medeiros, B., Gettelman, A., & Eidhammer, T. (2024). Perturbing parameters to understand cloud contributions to climate change. *Journal of Climate, 37*(1), 213–227. https://doi.org/10.1175/JCLI-D-23-0250.1

Eyring, V., Bony, S., Meehl, G. A., Senior, C. A., Stevens, B., Stouffer, R. J., & Taylor, K. E. (2016). Overview of the Coupled Model Intercomparison Project Phase 6 (CMIP6)

experimental design and organization. *Geoscientific Model Development*, *9*(5), 1937-1958. https://doi.org/10.5194/gmd-9-1937-2016

Forster, P., Storelvmo, T., Armour, K., Collins, W., Dufresne, J., Frame, D., … Zhang, H. (2021) 2021: The Earth's Energy Budget, Climate Feedbacks, and Climate Sensitivity. In Climate Change 2021: The Physical Science Basis. Contribution of Working Group I to the Sixth Assessment Report of the Intergovernmental Panel on Climate Change [Masson-Delmotte, V., P. Zhai, A. Pirani, S.L. Connors, C. Péan, S. Berger, N. Caud, Y. Chen, L. Goldfarb, M.I. Gomis, M. Huang, K. Leitzell, E. Lonnoy, J.B.R. Matthews, T.K. Maycock, T. Waterfield, O. Yelekçi, R. Yu, and B. Zhou (eds.)]. Cambridge University Press, Cambridge, United Kingdom and New York, NY, USA, pp. 923–1054, https://doi.org/10.1017/9781009157896.009.

Gasparini, B., Rasch, P. J., Hartmann, D. L., Wall, C. J., & Dütsch, M. (2021). A Lagrangian perspective on tropical anvil cloud lifecycle in present and future climate. *Journal of Geophysical Research: Atmospheres, 126*(4), e2020JD033487. https://doi.org/10.1029/2020JD033487

Gasparini, B., Sullivan, S. C., Sokol, A. B., Kärcher, B., Jensen, E., & Hartmann, D. L. (2023). Opinion: Tropical cirrus – from micro-scale processes to climate-scale impacts. *Atmospheric Chemistry and Physics, 23*(24), 15413–15444. https://doi.org/10.5194/acp-23-15413-2023

Gregory, J. M., Ingram, W. J., Palmer, M. A., Jones, G. S., Stott, P. A., Thorpe, R. B., Lowe, J. A., Johns, T. C., & Williams, K. D. (2004). A new method for diagnosing radiative forcing and climate sensitivity. *Geophysical Research Letters, 31*(3), L03205. https://doi.org/10.1029/2003GL018747

Hartmann, D. L., & Berry, S. E. (2017). The balanced radiative effect of tropical anvil clouds. *Journal of Geophysical Research: Atmospheres, 122*(9), 5003–5020. https://doi.org/10.1002/2017JD026460

Hartmann, D. L., Gasparini, B., Berry, S. E., & Blossey, P. N. (2018). The life cycle and net radiative effect of tropical anvil clouds. *Journal of Advances in Modeling Earth Systems*, *10*(12), 3012–3029. https://doi.org/10.1029/2018MS001484

Hartmann, D. L., & Larson, K. (2002). An important constraint on tropical cloud-climate feedback. *Geophysical Research Letters, 29*(20), 1926. https://doi.org/10.1029/2002GL015835

Hartmann, D. L., Moy, L. A., & Fu, Q. (2001). Tropical convection and the energy balance at the top of the atmosphere. *Journal of Climate, 14*(24), 4495–4511. https://doi.org/10.1175/1520-0442(2001)014<4495:TCATEB>2.0.CO;2

Hartmann, D. L., M. E. Ockert-Bell, & Michelsen, M. L. (1992). The Effect of Cloud Type on Earth's Energy Balance: Global Analysis. *Journal of Climate*, *5*(11), 1281-1304. https://doi.org/10.1175/1520-0442(1992)005<1281:TEOCTO>2.0.CO;2

Holloway, C. E., & Neelin, J. D. (2009). Moisture Vertical Structure, Column Water Vapor, and Tropical Deep Convection. *Journal of the Atmospheric Sciences, 66*(6). 1665-1683. https://doi.org/10.1175/2008JAS2806.1

Houze, R. A., Jr., Rasmussen, K. L., Zuluaga, M. D., & Brodzik, S. R. (2015). The variable nature of convection in the tropics and subtropics: A legacy of 16 years of the Tropical Rainfall Measuring Mission satellite. *Review of Geophysics, 53*(3), 994–1021. https://doi.org/10.1002/2015RG000488

Ito, M., & Masunaga, H. (2022). Process-level assessment of the iris effect over tropical oceans. *Geophysical Research Letters*, *49*(7), e2022GL097997. https://doi.org/10.1029/2022GL097997

Jeevanjee, N., & Zhou, L. (2022). On the resolution-dependence of anvil cloud fraction and precipitation efficiency in radiative-convective equilibrium. *Journal of Advances in Modeling Earth Systems, 14*(3), e2021MS002759. https://doi.org/10.1029/2021MS002759

Keil, P., Schmidt, H., Stevens, B., & Bao, J. (2021). Variations of tropical lapse rates in climate models and their implications for upper-tropospheric warming. *Journal of Climate, 34*(24), 9747–9761. https://doi.org/10.1175/JCLI-D-21-0196.1

Klein, S. A., & Hall, A. (2015). Emergent constraints for cloud feedbacks. *Current Climate Change Reports, 1*, 276–287. https://doi.org/10.1007/s40641-015-0027-1

Klein, S. A., Hall, A., J. R. Norris, & Pincus, R. (2017). Low-Cloud Feedbacks from Cloud-Controlling Factors: A Review. *Surveys in Geophysics, 38,* 1307–1329. https://doi.org/10.1007/s10712-017-9433-3

Klein, S. A., & Jakob, C. (1999). Validation and sensitivities of frontal clouds simulated by the ECMWF model. *Monthly Weather Review, 127*, 2514–2531. https://doi.org/10.1175/1520-0493(1999)127<2514

Klein, S. A., Zhang, Y., Zelinka, M. D., Pincus, R., Boyle, J., & Glecker, P. J. (2013). Are climate model simulations of clouds improving? An evaluation using the ISCCP simulator. *Journal of Geophysical Research: Atmospheres, 118(*3). 1329-1342. https://doi.org/10.1002/jgrd.50141

Kubar, T. L., & Jiang, J. H. (2019). Net cloud thinning, low-level cloud diminishment, and Hadley circulation weakening of precipitating clouds with tropical West Pacific SST using MISR and other satellite and reanalysis data. *Remote Sensing, 11*(10), 1250. https://doi.org/10.3390/rs11101250

Kuo, Y., Neelin, J. D., & Mechoso, C. R. (2017). Tropical Convective Transition Statistics and Causality in the Water Vapor-Precipitation Relation. *Journal of the Atmospheric Sciences, 74*(3), 915-931. https://doi.org/10.1175/JAS-D-16-0182.1

Kuo, Y., Schiro, K. A., & Neelin, J. D. (2018). Convective Transition Statistics over Tropical Oceans for Climate Model Diagnostics: Observational Baseline. *Journal of the Atmospheric Sciences, 75*(5), 1553-1570. https://doi.org/10.1175/JAS-D-17-0287.1

Lau, W. K. M., & Kim, K. (2015). Robust Hadley circulation changes and increasing global dryness due to CO_2 warming from CMIP5 model projections. *Proceedings of the National Academy of Sciences of the United States of America, 112*(12), 3630-3635. https://doi.org/10.1073/pnas.1418682112

Li, R. L., Storelvmo, T., Fedorov, A. V., & Choi, Y. (2019). A Positive Iris Feedback: Insights from Climate Simulations with Temperature-Sensitive Cloud–Rain Conversion. *Journal of Climate*, *32*(16), 5305-5324. https://doi.org/10.1175/JCLI-D-18-0845.1

Li, R. L., Studholme, J. H. P., Fedorov, A. V., & Storelvmo, T. (2023). Increasing Precipitation Efficiency Amplifies Climate Sensitivity by Enhancing Tropical Circulation Slowdown and Eastern Pacific Warming Pattern. *Geophysical Research Letters, 50*(2), e2022GL100836. https://doi.org/10.1029/2022GL100836

Li, R. L., Studholme, J. H. P., Fedorov, A. V., & Storelvmo, T. (2022). Precipitation efficiency constraint on climate change. *Nature Climate Change, 12,* 642-648. https://doi.org/10.1038/s41558-022-01400-x

Lindzen, R. S., Chou, M., & Hou, A. Y. (2001). Does the Earth have an adaptive infrared iris? *Bulletin of the American Meteorological Society, 82*(3), 417–432. https://doi.org/10.1175/1520-0477(2001)082<0417:DTEHAA>2.3.CO;2

Liu, R., Liou, K.-N., Su, H., Gu, Y., Zhao, B., Jiang, J. H., & Liu, S. C. (2017). High cloud variations with surface temperature from 2002 to 2015: Contributions to atmospheric radiative cooling rate and precipitation changes. *Journal of Geophysical Research: Atmospheres, 122*(10), 5457–5471. https://doi.org/10.1002/2016JD026303

Lutsko, N. J. & Cronin, T. W. (2018). Increase in precipitation efficiency with surface warming in radiative-convective equilibrium. *Journal of Advances in Modeling Earth Systems*, *10*(11), 2992–3010. https://doi.org/10.1029/2018MS001482

Lutsko, N. J., Popp, M., Nazarian, R. H., & Albright, A. L. (2021). Emergent Constraints on Regional Cloud Feedbacks. *Geophysical Research Letters, 48*(10), e2021GL092934. https://doi.org/10.1029/2021GL092934

Lutsko, N.J., Sherwood, S.C. and Zhao, M. (2023). Precipitation Efficiency and Climate Sensitivity. In Clouds and Their Climatic Impacts (eds S.C. Sullivan and C. Hoose). https://doi.org/10.1002/9781119700357.ch13

Luo, Z., & Rossow, W. B. (2004). Characterizing tropical cirrus life cycle, evolution, and interaction with upper-tropospheric water vapor using Lagrangian trajectory analysis of satellite observations. *Journal of Climate, 17*(23), 4541–4563. https://doi.org/10.1175/3222.1

Mackie, A., & Byrne, M. P. (2023). Effects of circulation on tropical cloud feedbacks in high-resolution simulations. *Journal of Advances in Modeling Earth Systems*, *15*(5), e2022MS003516. https://doi.org/10.1029/2022MS003516

Mamalakis, A., Randerson, J. T., Yu, J.-Y., Pritchard, M. S., Magnusdottir, G., Smyth, P., Levine, P. A., Yu, S., & Foufoula-Georgiou, E. (2021). Zonally contrasting shifts of the tropical rain belt in response to climate change. *Nature Climate Change, 11,* 143-151. https://doi.org/10.1038/s41558-020-00963-x

Mauritsen, T., & Stevens, B. (2015). Missing iris effect as a possible cause of muted hydrological change and high climate sensitivity in models. *Nature Geoscience, 8,* 346-351. https://doi.org/10.1038/NGEO2414

Mauritsen, T., Stevens, B., Roeckner, E., Crueger, T., Esch, M., Giorgetta, M., Haak, H., Jungclaus, J., Klocke, D., Matei, D., Mikolajewicz, U., Notz, D., Pincus, R., Schmidt, H., & Tomassini, L. (2012). Tuning the climate of a global model. *Journal of Advances in Modeling Earth Systems, 4*(3). https://doi.org/10.1029/2012MS000154

McKim, B., Bony, S., & Dufresne, J. L. (2024). Weak anvil cloud area feedback suggested by physical and observational constraints. *Nature Geoscience, 17*, 392-397. https://doi.org/10.1038/s41561-024-01414-4

Meehl, G. A., Senior, C. A., Eyring, V., Flato, G., Lamarque, J., Stouffer, R. J., Taylor, K. E., & Schlund, M. (2020). Context for interpreting equilibrium climate sensitivity and transient climate response from the CMIP6 Earth system models. *Science Advances, 6*(26). https://doi.org/10.1126/sciadv.aba1981

Mitchell, D. M., Lo, E., Seviour, W. J. M., Haimberger, L., & Polvani, L. M. (2020). The vertical profile of recent tropical temperature trends: Persistent model biases in the context of

internal variability. *Environmental Research Letters, 15*, 074034. https://doi.org/10.1088/1748-9326/ab9af7

Muhlbauer, A., E. Berry, J. M. Comstock, and Mace, G. G. (2014). Perturbed physics ensemble simulations of cirrus on the cloud system-resolving scale. *Journal of Geophysical Research: Atmospheres*, *119*(8), 4709–4735. https://doi.org/10.1002/2013JD020709

Murphy, J. M. (1995). Transient Response of the Hadley Centre Coupled Ocean-Atmosphere Model to Increasing Carbon Dioxide. Part III: Analysis of Global-Mean Response Using Simple Models. *Journal of Climate, 8*(3), 496-514. https://doi.org/10.1175/1520-0442(1995)008<0496:TROTHC>2.0.CO;2

Neelin, J. D., Peters, O., & Hales, K. (2009). The Transition to Strong Convection. *Journal of the Atmospheric Sciences, 66*(8). 2367-2384. https://doi.org/10.1175/2009JAS2962.1

Ogura, T., M. J. Webb, & Lock, A. P. (2023). Positive low cloud feedback primarily caused by increasing longwave radiation from the sea surface in two versions of a climate model. *Geophysical Research Letters*, *50*(20), https://doi.org/10.1029/2023GL104786

Ohno, T., Satoh, M., & Noda, A. (2019). Fine vertical resolution radiative–convective equilibrium experiments: Roles of turbulent mixing on the high-cloud response to sea surface temperatures. *Journal of Advances in Modeling Earth Systems, 11*(6), 1637–1654. https://doi.org/10.1029/2019MS001704

Peters, O., & Neelin, J. D. (2006). Critical phenomena in atmospheric precipitation. *Nature Physics, 2.* 393-396. https://doi.org/10.1038/nphys314

Pincus, R., Forster, P. M., & Stevens, B. (2016). The Radiative Forcing Model Intercomparison Project (RFMIP): Experimental protocol for CMIP6. *Geoscientific Model Development, 9*(9), 3447–3460. https://doi.org/10.5194/gmd-9-3447-2016

Pincus, R., Platnick, S., Ackerman, S. A., Hemler, R. S., & Hofmann, R. J. (2012). Reconciling simulated and observed views of clouds: MODIS, ISCCP, and the limits of instrument simulators. *Journal of Climate, 25*(13), 4699–4720. https://doi.org/10.1175/JCLI-D-11-00267.1

Plesca, E., Grützun, V., & Buehler, S. A. (2018). How Robust Is the Weakening of the Pacific Walker Circulation in CMIP5 Idealized Transient Climate Simulations? *Journal of Climate*, *31*(1), 81-97. https://doi.org/10.1175/JCLI-D-17-0151.1

Po-Chedley, S., Zelinka, M. D., Jeevanjee, N., Thorsen, T. J., & Santer, B. D. (2019). Climatology explains intermodel spread in tropical upper tropospheric cloud and relative humidity response to greenhouse warming. *Geophysical Research Letters, 46*(22), 13399–13409. https://doi.org/10.1029/2019GL084786

Pope, K. N., Holloway, C. E., Jones, T. R., Stein, T. H. M. (2021). Cloud-Radiation Interactions and Their Contributions to Convective Self-Aggregation. *Journal of Advances in Modeling Earth Systems, 13*(9). https://doi.org/10.1029/2021MS002535

Proske, U., Ferrachat, S., Neubauer, D., Staab, M., & Lohmann, U. (2022). Assessing the potential for simplification in global climate model cloud microphysics. *Atmospheric Chemistry and Physics, 22*(7), 4737–4762. https://doi.org/10.5194/acp-22-4737-2022

Qian, Y., Yan, H., Hou, Z., Johannesson, G., Klein, S., Lucas, D., Neale, R., Rasch, P., Swiler, L., Tannahill, J., Wang, H., Wang, M., & Zhao, C. (2015). *Journal of Advances in Modeling Earth Systems, 7*(2), 382-411. https://doi.org/10.1002/2014MS000354

Qu, X., Hall, A., S. A. Klein, & DeAngelis, A. M. (2015). Positive tropical marine low-cloud cover feedback inferred from cloud-controlling factors. *Geophysical Research Letters*, *42*(18), 7767–7775. https://doi.org/10.1002/2015GL065627

Raghuraman, S. P., Medeiros, B., & Gettelman, A. (2024). Observational quantification of tropical high cloud changes and feedbacks. *Journal of Geophysical Research: Atmospheres, 129*(7). https://doi.org/10.1029/2023JD039364

Ramaswamy, V., Chanin, M.-L., Angell, J., Barnett, J., Gaffen, D., Gelman, M., Keckhut, P., Koshelkov, Y., Labitzke, K., Lin, J.-J. R., O'Neill, A., Nash, J., Randel, W., Rood, R., Shine, K., Shiotani, M., & Swinbank, R. (2001). Stratospheric Temperature Trends: Observations and Model Simulations. *Reviews of Geophysics, 39*(1), 71-122. https://doi.org/10.1029/1999RG000065

Retsch, M. H., Jakob, C., & Singh, M. S. (2020). Assessing convective organization in tropical radar observations. *Journal of Geophysical Research: Atmospheres*, *125*(7), e2019JD031801. https://doi.org/10.1029/2019JD031801

Richardson, M. T., Roy, R. J., & Lebsock, M. D. (2022). Satellites suggest rising tropical high cloud altitude: 2002–2021. *Geophysical Research Letters, 49*(10). https://doi.org/10.1029/2022GL098160

Roe, G. H., & Armour, K. C. (2011). How sensitive is climate sensitivity? *Geophysical Research Letters, 38*(14), L14708. https://doi.org/10.1029/2011GL047913

Rugenstein, M., Bloch-Johnson, J., Abe-Ouchi, A., Andrews, T., Beyerle, U., Cao, L., Chadha, T., Danabasoglu, G., Dufresne, J.-L., Duan, L., Foujols, M.-A., Frölicher, T., Geoffroy, O., Gregory, J., Knutti, R., Li, C., Marzocchi, A., Mauritsen, T., Menary, … Yang, S (2019). LongRunMIP Motivation and Design for a Large Collection of Millennial-Length AOGCM Simulations. *Bulletin of the American Meteorological Society, 100*(12), 2551-2570. https://doi.org/10.1175/BAMS-D-19-0068.1

Saint-Lu, M., Bony, S., & Dufresne, J. L. (2020). Observational evidence for a stability iris effect in the tropics. *Geophysical Research Letters, 47*(14), e2020GL089059. https://doi.org/10.1029/2020GL089059

Saint-Lu, M., Bony, S., & Dufresne, J.-L. (2022). Clear-sky control of anvils in response to increased CO_2 or surface warming or volcanic eruptions. *npj Climate and Atmospheric Science, 5*. https://doi.org/10.1038/s41612-022-00304-z

Sassen, K., Wang, Z., & Liu, D. (2009). Cirrus clouds and deep convection in the tropics: Insights from CALIPSO and CloudSat. *Journal of Geophysical Research: Atmospheres, 114*(D4). https://doi.org/10.1029/2009JD011916

Schiro, K. A., Ahmed, F., Giangrande, S. E., & Neelin, J. D. (2018). The GoAmazon2014/5 campaign points to a deep-inflow approach to deep convection across scales. *Proceedings of the National Academy of Sciences of the United States of America, 115*(18), 4577–4582. https://doi.org/10.1073/pnas.1719842115

Schiro, K. A., Neelin, J. D., Adams, D. K., & Litner, B. R. (2016). Deep Convection and Column Water Vapor over Tropical Land versus Tropical Ocean: A Comparison between the Amazon and the Tropical Western Pacific. *Journal of the Atmospheric Sciences, 73*(10), 4043-4063. https://doi.org/10.1175/JAS-D-16-0119.1

Schiro, K. A., Su, H., Wang, Y., Langenbrunner, B., Jiang, J. H., & Neelin, J. D. (2019). Relationships between tropical ascent and high cloud fraction changes with warming revealed by perturbation physics experiments in CESM. *Geophysical Research Letters, 46*(16), 10112–10121. https://doi.org/10.1029/2019GL083026

Schiro, K. A., Su, H., Ahmed, F., Dai, N., Singer, C. E., Gentine, P., Elsaesser, G. S., Jiang, J. H., Choi, Y.-S., & Neelin, J. D. (2022). Model spread in tropical low cloud feedback tied

to overturning circulation response to warming. *Nature Communications, 13*. https://doi.org/10.1038/s41467-022-34787-4

Seeley, J. T., Jeevanjee, N., Langhans, W., & Romps, D. M. (2019). Formation of tropical anvil clouds by slow evaporation. *Geophysical Research Letters, 46*(1), 492–501. https://doi.org/10.1029/2018GL080747

Shell, K. M., Kiehl, J. T., & Shields, C. A. (2008). Using the Radiative Kernel Technique to Calculate Climate Feedbacks in NCAR's Community Atmospheric Model. *Journal of Climate*, *21*(10), 2269-2282. https://doi.org/10.1175/2007JCLI2044.1

Sherwood, S. C., Webb, M. J., Annan, J. D., Armour, K. C., Forster, P. M., Hargreaves, J. C., Hegerl, G., Klein, S. A., Marvel, K. D., Rohling, E. J., Watanabe, M., Andrews, T., Braconnot, P., Bretherton, C. S., Foster, G. L., Hausfather, Z., von der Heydt, A. S., Knutti, R., & Mauritsen, T., … Zelinka, M. D. (2020). An assessment of Earth's climate sensitivity using multiple lines of evidence. *Reviews of Geophysics, 58*(4). https://doi.org/10.1029/2019RG000678

Siler, N., Po-Chedley, S., & Bretherton, C. S. (2018). Variability in modeled cloud feedback tied to differences in the climatological spatial pattern of clouds. *Climate Dynamics, 50*, 1209–1220. https://doi.org/10.1007/s00382-017-3673-2

Silvers, L. G., Reed, K. A., & Wing, A. A. (2023). The response of the large-scale tropical circulation to warming. *Journal of Advances in Modeling Earth Systems*, *15*(3), e2021MS002966. https://doi.org/10.1029/2021MS002966

Silvers, L. G., & Robinson, T. (2021). Clouds and radiation in a mock-Walker circulation. *Journal of Advances in Modeling Earth Systems*, *13*(2), e2020MS002196. https://doi.org/10.1029/2020MS002196

Sokol, A. B., Wall, C. J., & Hartmann, D. L. (2024). Anvil cloud thinning implies greater climate sensitivity. *Nature Geoscience, 17,* 398-403. https://doi.org/10.1038/s41561-024-01420-6

Stauffer, C. L., & Wing, A. A. (2022). Properties, changes, and controls of deep-convecting clouds in radiative-convective equilibrium. *Journal of Advances in Modeling Earth Systems*, *14*(6), e2021MS002917. https://doi.org/10.1029/2021MS002917

Stein, T. H. M., Holloway, C. E., Tobin, I., & Bony, S. (2017). Observed Relationships between Cloud Vertical Structure and Convective Aggregation over Tropical Ocean. *Journal of Climate*, *30*(6), 2187-2207. https://doi.org/10.1175/JCLI-D-16-0125.1

Stevens, B., Sherwood, S. C., Bony, S., & Webb, M. J. (2016). Prospects for narrowing bounds on Earth's equilibrium climate sensitivity. *Earth's Future, 4*(11), 512-522. https://doi.org/10.1002/2016EF000376

Su, H., Jiang, J. H., Neelin, J. D., Shen, T. J., Zhai, C., Yue, Q., Wang, Z., Huang, L., Choi, Y.-S., Stephens, G. L., & Yung, Y. L. (2017). Tightening of tropical ascent and high clouds key to precipitation change in a warmer climate. *Nature Communications, 8*. https://doi.org/10.1038/ncomms15771

Su, H., Jiang, J. H., Zhai, C., Shen, T. J., Neelin, J. D., Stephens, G. L., & Yung, Y. L. (2014). Weakening and strengthening structures in the Hadley circulation change under global warming and implications for cloud response and climate sensitivity. *Journal of Geophysical Research: Atmospheres, 119*(10), 5787–5805. https://doi.org/10.1002/2014JD021642

Su, H., Wu, L., Zhai, C., Jiang, J. H., Neelin, J. D., & Yung, Y. L. (2020). Observed tightening of tropical ascent in recent decades and linkage to regional precipitation changes.

Geophysical Research Letters, 47(3), e2019GL085809. https://doi.org/10.1029/2019GL085809

Su, H., Zhai, C., Jiang, J. H., Wu, L., Neelin, J. D., & Yung, Y. L. (2019). A dichotomy between model responses of tropical ascent and descent to surface warming. *npj Climate and Atmospheric Science, 2*. https://doi.org/10.1038/s41612-019-0066-8

Taylor, K. E., Stouffer, R. J., & Meehl, G. A. (2012). An Overview of CMIP5 and the Experiment Design. *Bulletin of the American Meteorological Society*, *93*(4), 485-498. https://doi.org/10.1175/BAMS-D-11-00094.1

Tobin, I., Bony, S., & Roca, R. (2012). Observational Evidence for Relationships between the Degree of Aggregation of Deep Convection, Water Vapor, Surface Fluxes, and Radiation. *Journal of Climate, 25*(20). 6885-6904. https://doi.org/10.1175/JCLI-D-11-00258.1

Tsushima, Y., S. Iga, H. Tomita, M. Satoh, A. T. Noda, and M. J. Webb (2014), High cloud increase in a perturbed SST experiment with a global nonhydrostatic model including explicit convective processes, *Journal of Advances in Modeling Earth Systems*, *6*(3), 571–585, https://doi.org/10.1002/2013MS000301

Tsushima, Y., Ringer, M. A., Martin, G. M., Rostron, J. W., & Sexton, D. M. H. (2020). Investigating physical constraints on climate feedbacks using a perturbed parameter ensemble. *Climate Dynamics, 55*, 1159–1185. https://doi.org/10.1007/s00382-020-05318-y

Turbeville, S. M., Nugent, J. M., Ackerman, T. P., Bretherton, C. S., & Blossey, P. N. (2022). Tropical cirrus in global storm-resolving models: 2. Cirrus life cycle and top-of-

atmosphere radiative fluxes. *Earth and Space Science, 9*(2), e2021EA001978. https://doi.org/10.1029/2021EA001978

Vecchi, G. A., & Soden, B. J. (2007). Global Warming and the Weakening of the Tropical Circulation. *Journal of Climate*, *20*(17), 4316-4340. https://doi.org/10.1175/JCLI4258.1

Vial, J., Dufresne, J. L., & Bony, S. (2013). On the interpretation of intermodel spread in CMIP5 climate sensitivity estimates. *Climate Dynamics, 41*, 3339–3362. https://doi.org/10.1007/s00382-013-1725-9

Volodin, E. M. (2008). Relation between temperature sensitivity to doubled carbon dioxide and the distribution of clouds in current climate models. *Izvestiya, Atmospheric and Oceanic Physics, 44*, 288-299. https://doi.org/10.1134/S0001433808030043

Wall, C. J., & Hartmann, D. L. (2018). Balanced cloud radiative effects across a range of dynamical conditions over the tropical West Pacific. *Geophysical Research Letters, 45*(20), 11490–11498. https://doi.org/10.1029/2018GL080046

Wall, C. J., Hartmann, D. L., & Norris, J. R. (2019). Is the net cloud radiative effect constrained to be uniform over the tropical warm pools? *Geophysical Research Letters, 46*, 12495–12503. https://doi.org/10.1029/2019GL083642

Wang, C., Soden, B. J., Yang, W., & Vecchi, G. A. (2021). Compensation between cloud feedback and aerosol-cloud interaction in CMIP6 models. *Geophysical Research Letters*, *48*(4), e2020GL091024. https://doi.org/10.1029/2020GL091024

Wang, Y., Su, H., Jiang, J. H., Xu, F., & Yung, Y. L. (2020). Impact of cloud ice particle size uncertainty in a climate model and implications for future satellite missions. *Journal of Geophysical Research: Atmospheres, 125*(6), e2019JD032119. https://doi.org/10.1029/2019JD032119

Webb, M. J., Lambert, F. H., & Gregory, J. M. (2013). Origins of differences in climate sensitivity, forcing and feedback in climate models. *Climate Dynamics, 40*. 677-707. https://doi.org/10.1007/s00382-012-1336-x

Wilson Kemsley, S., Ceppi, P., Andersen, H., Cermak, J., Stier, P., & Nowack, P. (2024). A systematic evaluation of high-cloud controlling factors. *Atmospheric Chemistry and Physics, 24*, 8295–8316. https://doi.org/10.5194/acp-24-8295-2024

Wing, A. A., & Emanuel, K. A. (2014). Physical mechanisms controlling self-aggregation of convection in idealized numerical modeling simulations. *Journal of Advances in Modeling Earth Systems, 6*(1). 59-74. https://doi.org/10.1002/2013MS000269

Wing, A. A., Emanuel, K., Holloway, C. E., & Muller, C. (2017). Convective Self-Aggregation in Numerical Simulations: A Review. *Surveys in Geophysics, 38*. 1173–1197. https://doi.org/10.1007/s10712-017-9408-4

Wing, A. A., Stauffer, C. L., Becker, T., Reed, K. A., Ahn, M.-S., Arnold, N. P., Bony, S., Branson, M., Bryan, G. H., Chaboureau, J.-P., De Roode, S. R., Gayatri, K., Hohenegger, C., Hu, I.-K., Jansson, F., Jones, T. R., Khairoutdinov, M., Kim, D., Martin, Z. K., … Zhao, M. (2020). Clouds and convective self-aggregation in a multimodel ensemble of radiative-convective equilibrium simulations. *Journal of Advances in Modeling Earth Systems, 12*(9), e2020MS002138. https://doi.org/10.1029/2020MS002138

Wing, A. A., & Cronin, T. W. (2016). Self-aggregation of convection in long channel geometry. *Quarterly Journal of the Royal Meteorological Society, 142*(694), 1-15. https://doi.org/10.1002/qj.2628

Wing, A. A., Silvers, L. G., & Reed, K. A. (2024). RCEMIP-II: Mock-Walker simulations as phase II of the radiative–convective equilibrium model intercomparison project.

Geoscientific Model Development, 17(16), 6195–6225. https://doi.org/10.5194/gmd-17-6195-2024

Wodzicki, K. R., & Rapp, A. D. (2016). Long-term characterization of the Pacific ITCZ using TRMM, GPCP, and ERA-Interim. *Journal of Geophysical Research: Atmospheres, 121*(7), 3153–3170. https://doi.org/10.1002/2015JD024458

Wodzicki, K. R., & Rapp, A. D. (2022). More intense, organized deep convection with shrinking tropical ascent regions. *Geophysical Research Letters*, *49*(15), e2022GL098615. https://doi.org/10.1029/2022GL098615

Xu, K.-M., Wong, T., Wielicki, B. A., Parker, L., Lin, B., Eitzen, Z. A., & Branson, M. (2007). Statistical analyses of satellite cloud object data from CERES. Part II: Tropical convective cloud objects during 1998 El Niño and evidence for supporting the fixed anvil temperature hypothesis. *Journal of Climate, 20*(5), 819–842. https://doi.org/10.1175/jcli4069.1

Zelinka, M. D., & Hartmann, D. L. (2010). Why is longwave cloud feedback positive? *Journal of Geophysical Research, 115*(D16). https://doi.org/10.1029/2010JD013817

Zelinka, M. D., & Hartmann, D. L. (2011). The observed sensitivity of high clouds to mean surface temperature anomalies in the tropics. *Journal of Geophysical Research, 116*(D23). https://doi.org/10.1029/2011JD016459

Zelinka, M. D., Myers, T. A., McCoy, D. T., Po-Chedley, S., Caldwell, P. M., Ceppi, P., Klein, S. A., & Taylor, K. E. (2020). Causes of higher climate sensitivity in CMIP6 models. *Geophysical Research Letters, 47*(1), e2019GL085782. https://doi.org/10.1029/2019GL085782

Zelinka, M. D., Klein, S. A., & Hartmann, D. L. (2012a). Computing and partitioning cloud feedbacks using cloud property histograms. Part I: Cloud radiative kernels. *Journal of Climate, 25*(11), 3715–3735. https://doi.org/10.1175/JCLI-D-11-00248.1

Zelinka, M. D., Klein, S. A., & Hartmann, D. L. (2012b). Computing and partitioning cloud feedbacks using cloud property histograms. Part II: Attribution to changes in cloud amount, altitude, and optical depth. *Journal of Climate, 25*(11), 3736–3754. https://doi.org/10.1175/JCLI-D-11-00249.1

Zelinka, M. D., Klein, S. A., Taylor, K. E., Andrews, T., Webb, M. J., Gregory, J. M., & Forster, P. M. (2013). Contributions of different cloud types to feedbacks and rapid adjustments in CMIP5. *Journal of Climate, 26*(14), 5007-5027. https://doi.org/10.1175/JCLI-D-12-00555.1

Zelinka, M. D., Klein, S. A., Qin, Y., & Myers, T. A. (2022). Evaluating climate models' cloud feedbacks against expert judgment. *Journal of Geophysical Research, 127*(2), e2021JD035198. https://doi.org/10.1029/2021JD035198

Zelinka, M. D., Randall, D. A., & Webb, M. J. (2017). Clearing clouds of uncertainty. *Nature Climate Change, 7*, 674–678. https://doi.org/10.1038/nclimate3402

Zelinka, M. D., Zhou, C., & Klein, S. A. (2016). Insights from a refined decomposition of cloud feedbacks. *Geophysical Research Letters, 43*(17), 9259-9269. https://doi.org/10.1002/2016GL069917

Zhai, C., Jiang, J. H., & Su, H. (2015). Long-term cloud change imprinted in seasonal cloud variation: More evidence of high climate sensitivity. *Geophysical Research Letters, 42*(20), 8729-8737. https://doi.org/10.1002/2015GL065911

Zhang, G. J., & McFarlane, N. A. (1995). Sensitivity of climate simulations to the parameterization of cumulus convection in the Canadian climate centre general circulation model. *Atmosphere-Ocean*, *33*(3), 407–446. https://doi.org/10.1080/07055900.1995.9649539

Zhang, Y., Xie, S., Covey, C., Lucas, D. D., Glecker, P, Klein, S. A., Tannahill, J., Doutriaux, C., & Klein, R. (2012). Regional assessment of the parameter-dependent performance of CAM4 in simulating tropical clouds. *Geophysical Research Letters, 39*(14). https://doi.org/10.1029/2012GL052184

Zhao, M. (2014). An investigation of the connections among convection, clouds, and climate sensitivity in a global climate model. *Journal of Climate, 27*(5), 1845–1862. https://doi.org/10.1175/JCLI-D-13-00145.1

Zhou, C., Dessler, A. E., Zelinka, M. D., Yang, P., & Wang, T. (2014). Cirrus feedback on interannual climate fluctuations. *Geophysical Research Letters, 41*(24), 9166-9173. https://doi.org/10.1002/2014GL062095

Zhou, C., Zelinka, M. D., & Klein, S. A. (2017). Analyzing the dependence of global cloud feedback on the spatial pattern of sea surface temperature change with a Green's function approach. *Journal of Advances in Modeling Earth Systems, 9*(5). 2174-2189. https://doi.org/10.1002/2017MS001096